Development of the Zero-Heat-Flux Wearable Deep Body Thermometer for Using in Hot Environments

doi: https://doi.org/10.3390/s23041970

博　　士　　論　　文

Development of the Zero-Heat-Flux Wearable Deep Body Thermometer for Using in Hot Environments

高温環境下で使用可能な熱流補償型深部体温計の開発研究

金沢大学大学院自然科学研究科
機械科学専攻

学　籍　番　号　2024032007
氏　　名　陸　　晗子
主任指導教員名　田中　志信
提　出　年　月　2023.01.04

CONTENT

1. Introduction

The core body temperature (CBT), compared to skin temperature, which is easily affected by external temperature, is a key indicator for thermal strain[1] and personal thermal comfort in a high-temperature environment. It has been pointed out that at-risk populations of heatstroke, including athletes[2][3], outdoor workers[4], and firefighters[5], require non-invasive CBT thermometers for health management and to monitor the thermal strain. This study aims to develop a non-invasive CBT thermometer with reasonable accuracy available at wider ambient temperatures.

Conventional direct measurements of CBT involve probes inserted into body orifices such as the rectum or esophagus for accurate measurements. Still, it is difficult for the subject to tolerate prolonged measurements while awake[6]. As alternative methods, infrared scanning thermometers can quickly read the tympanic temperature in a few seconds. Still, some studies[7][8][9] claim that its accuracy remains questionable due to the complex structure of the auditory canal. Ingestible thermometry capsules were used to measure the temperature of the gastrointestinal tract from the inside of the body[10]. Still, its position in the body was uncontrollable, and the result may be easily influenced by the intake of food or fluid[11][12]. Patch-type temperature probes[13] and wrist-type thermometers[14] have been developed. However, the effectiveness of these probes for actual measurements of humans and their performance in high-temperature environments have not been thoroughly investigated.

The Zero-Heat-Flow (ZHF) method was developed by Fox et al. as a non-invasive method to measure CBT continuously[15]. Its measurement accuracy was improved by Togawa[16] and has been widely used for perioperative temperature management. In this method, the skin's surface is covered by a heat insulator with a heater to compensate for the outward heat dissipation. The thermistors are placed above and below the insulator layer to measure heater temperature T_{heater} and skin temperature $T_{skin,}$ respectively. Then the heater is controlled so as to keep the T_{heater} equal to T_{skin}. When the state of thermal equilibrium is maintained, CBT could be measured indirectly and continuously from the skin surface.

The Zero-Heat-Flow method has proven to have excellent clinical performance[17], but it cannot work in a high-temperature environment. The heater only works when T_{heater} is lower than T_{skin}, which means that

when the ambient temperature of the probe is higher than CBT, the heater will be turned off. In such a situation, a temperature gradient from outside to inside will result, leading to significant measurement errors. This problem limits the use of this method so far only in stable clinical settings[18].

However, our co-author (T. T.)has demonstrated that a ZHF probe was possible to maintain the heat equilibrium and measure in a high-temperature environment if a Peltier module and radiator were placed instead of a heater [19]. In this study, we redesigned and constructed a ZHF probe with the Peltier module and insulator, investigated its behavior in detail, and discussed its performance and wearability in practical applications.

References

1. Epstein, Y.; Yanovich, R. Heatstroke. *N. Engl. J. Med.* **2019**, *380*, 2449–2459, doi:10.1056/NEJMra1810762.
2. Fang, Z.; Xu, X.; Zhou, X.; Deng, S.; Wu, H.; Liu, J.; Lin, Z. Investigation into the Thermal Comfort of University Students Conducting Outdoor Training. *Build. Environ.* **2019**, *149*, 26–38, doi:10.1016/j.buildenv.2018.12.003.
3. Hollander, K.; Klöwer, M.; Richardson, A.; Navarro, L.; Racinais, S.; Scheer, V.; Murray, A.; Branco, P.; Timpka, T.; Junge, A.; et al. Apparent Temperature and Heat-Related Illnesses during International Athletic Championships: A Prospective Cohort Study. *Scand. J. Med. Sci. Sport.* **2021**, *31*, 2092–2102, doi:10.1111/sms.14029.
4. Lee, J.; Lee, Y.H.; Choi, W.J.; Ham, S.; Kang, S.K.; Yoon, J.H.; Yoon, M.J.; Kang, M.Y.; Lee, W. Heat Exposure and Workers' Health: A Systematic Review. *Rev. Environ. Health* **2022**, *37*, 45–59, doi:10.1515/reveh-2020-0158.
5. Kim, S.; Kim, D.H.; Lee, H.H.; Lee, J.Y. Frequency of Firefighters' Heat-Related Illness and Its Association with Removing Personal Protective Equipment and Working Hours. *Ind. Health* **2019**, *57*, 370–380, doi:10.2486/indhealth.2018-0063.
6. Hymczak, H.; Gołąb, A.; Mendrala, K.; Plicner, D.; Darocha, T.; Podsiadło, P.; Hudziak, D.; Gocoł, R.; Kosiński, S. Core Temperature Measurement—Principles of Correct Measurement, Problems, and Complications. *Int. J. Environ. Res. Public Health* 2021, *18*.
7. Berksoy, E.A.; Anıl, M.; Bıcılıoğlu, Y.; Gökalp, G.; Bal, A. Comparison of Infrared Tympanic, Non-Contact Infrared Skin, and Axillary Thermometer to Rectal Temperature Measurements in a Pediatric Emergency Observation Unit. *Int. J. Clin. Exp. Med.* **2018**, *11*, 567–573.
8. Zhen, C.; Xia, Z.; Long, L.; Pu, Y. Accuracy of Infrared Ear Thermometry in Children: A Meta-Analysis and Systematic Review. *Clin. Pediatr. (Phila).* **2014**, *53*, 1158–1165, doi:10.1177/0009922814536774.
9. Mogensen, C.B.; Wittenhoff, L.; Fruerhøj, G.; Hansen, S. Forehead or Ear Temperature Measurement Cannot Replace Rectal Measurements, except for Screening Purposes. *BMC Pediatr.* **2018**, *18*, 1–6, doi:10.1186/s12887-018-0994-1.
10. Bongers, C.C.W.G.; Hopman, M.T.E.; Eijsvogels, T.M.H. Validity and Reliability of the MyTemp Ingestible Temperature Capsule. *J. Sci. Med. Sport* **2018**, *21*, 322–326, doi:10.1016/j.jsams.2017.06.006.
11. Monnard, C.R.; Fares, E.J.; Calonne, J.; Miles-Chan, J.L.; Montani,

J.P.; Durrer, D.; Schutz, Y.; Dulloo, A.G. Issues in Continuous 24-h Core Body Temperature Monitoring in Humans Using an Ingestible Capsule Telemetric Sensor. *Front. Endocrinol. (Lausanne).* **2017**, *8*, 1–13, doi:10.3389/fendo.2017.00130.

12. Byrne, C.; Lim, C.L. The Ingestible Telemetric Body Core Temperature Sensor: A Review of Validity and Exercise Applications. *Br. J. Sports Med.* **2007**, *41*, 126–133, doi:10.1136/bjsm.2006.026344.
13. Popovic, Z.; Momenroodaki, P.; Scheeler, R. Toward Wearable Wireless Thermometers for Internal Body Temperature Measurements. *IEEE Commun. Mag.* **2014**, *52*, 118–125, doi:10.1109/MCOM.2014.6917412.
14. Yeh, C.Y.; Chung, Y.T.; Chuang, K.T.; Shu, Y.C.; Kao, H.Y.; Chen, P.L.; Ko, W.C.; Ko, N.Y. An Innovative Wearable Device for Monitoring Continuous Body Surface Temperature (HEARThermo): Instrument Validation Study. *JMIR mHealth uHealth* **2021**, *9*, 1–10, doi:10.2196/19210.
15. Fox, R.H.; Solman, A.J.; Isaacs, R.; Fry, A.J.; MacDonald, I.C. A New Method for Monitoring Deep Body Temperature from the Skin Surface. *Clin. Sci.* **1973**, *44*, 81–86, doi:10.1042/cs0440081.
16. Togwa, T.; Nemoto, T.; Yamazaki, T.; Kobayashi, T. A Modified Internal Temperature Measurement Device. *Med. Biol. Eng.* **1976**, *14*, 361–364, doi:10.1007/BF02478138.
17. Dahyot-Fizelier, C.; Lamarche, S.; Kerforne, T.; Bénard, T.; Giraud, B.; Bellier, R.; Carise, E.; Frasca, D.; Mimoz, O. Accuracy of Zero-Heat-Flux Cutaneous Temperature in Intensive Care Adults. *Crit. Care Med.* **2017**, doi:10.1097/CCM.0000000000002317.
18. Tamura, T.; Huang, M.; Togawa, T. Current Developments in Wearable Thermometers. *Adv. Biomed. Eng.* **2018**, *7*, 88–99, doi:10.14326/abe.7.88.
19. Tamura, T.; Nemoto, T.; Togawa, T. A Zero-Heat-Flow Transducer for Monitoring Perfusion Blood Temperature. *IEEE Trans. Biomed. Eng.* **1979**, *BME-26*, 644–646, doi:10.1109/TBME.1979.326548.

2. Body temperature

Body temperature is one of the vital signs of our body's metabolism, and most of the biochemistry processes speed depend on body temperature. This chapter will introduce the type of body temperature, how we keep our heat balance and the abnormality of body temperature.

2.1. Type of body temperature

2.1.1. Core Temperature & Skin Temperature

The skin surface's temperature, known as *skin temperature* or *shell temperature*, increases and decreases significantly in the surrounding area (**Figure 2-1**).

On the other side, the temperature in the deep part of the body, such as the brain and organs, maintains an almost constant temperature within ±0.6°C even though the body was exposed to different temperatures. It was called *core temperature* or *deep body temperature*.

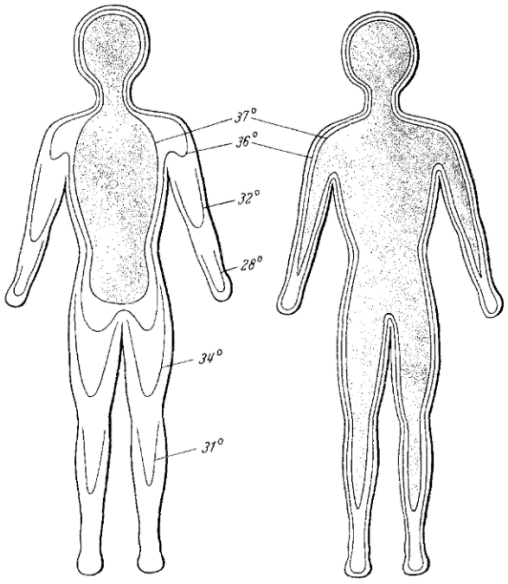

(a)

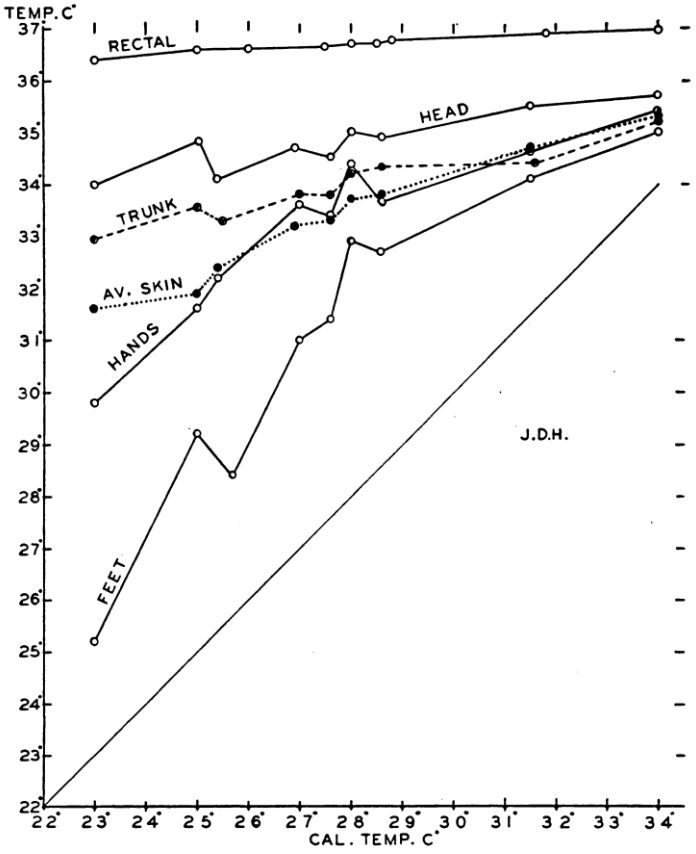

(b)

Figure 2-1 (a) Difference in body temperatures. The temperature of different body parts at environmental temperatures of 20°C and 35 °C[1]. (b) Rectal and skin temperatures of humans at different environmental temperatures.[2]

The core temperature varies when measured from different sites (**Figure 2-2**), but the rectal temperature was the most useful conference core temperature in clinical settings.

Axilla, sublingual and auditory canal temperature is the most useful position for skin body temperature in daily life since they could be seen as the core temperature in some ways. However, it also indicates that they have lower measurement results than through the rectum.

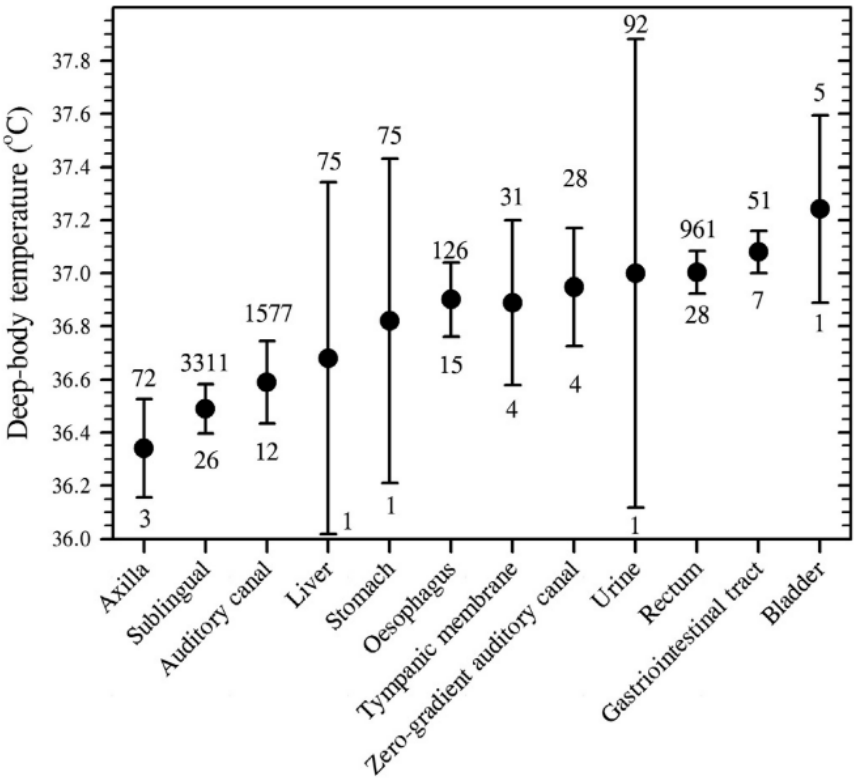

Figure 2-2 Variations in resting, deep-body temperature among twelve measurement sites [3]

Core temperature monitoring is adopted for perioperative care since surgery, and general anesthesia may break the normal balance between heat generation and heat loss. Even mild perioperative hypothermia can cause abnormalities and consequences like infection, pressure ulcers, and morbid cardiac events. [4]

2.1.2. Basal Body Temperature

The body temperature, such as gastrointestinal temperature, may even fall under 36.4 °C when sleeping in the early morning, but it will raise to over 37.3 °C in the daytime (**Figure 2-3**). The changing of the body temperature was called the *circadian rhythm* of the body temperature. For healthy adults, the circadian rhythm of body temperature may be controlled within 1°C, but for children, the difference may be over 2°C.

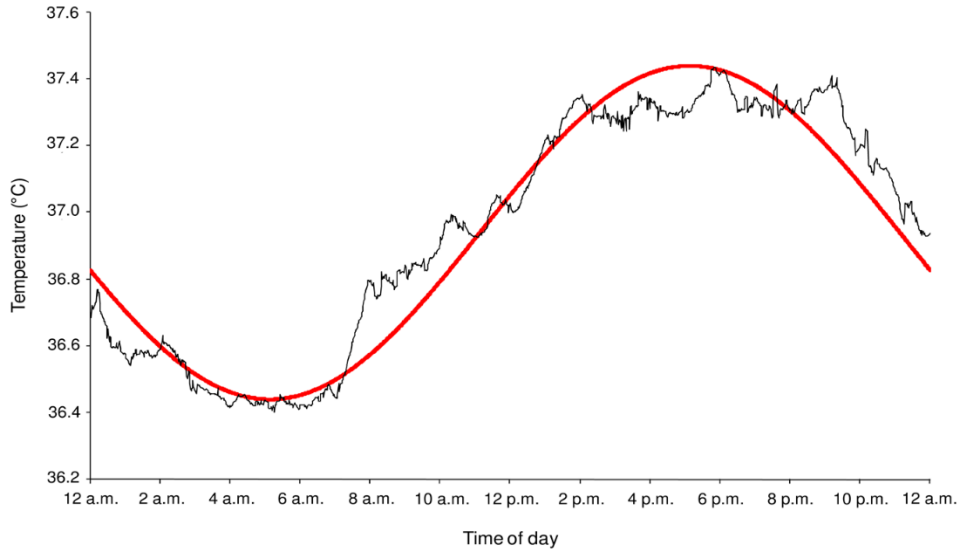

Figure 2-3 Circadian rhythm of gastrointestinal temperature[5]

The body temperature measured every morning after wakeup was called the *basal body temperature*.

The basal body temperature was noticed as a biphasic change in women during the normal menstrual cycle. The change was caused by progesterone. From the beginning of menstruation to ovulation, the basal body temperature remains lower than 36.45°C since progesterone remains low during the follicular phase. After ovulation, the amount of progesterone generated by the corpus luteum will increase. Progesterone was noticed to raise the metabolic rate, which will keep the basal body temperature high. Progesterone levels will decrease in the late luteal phase if unpregnant, and so as the basal body temperature.

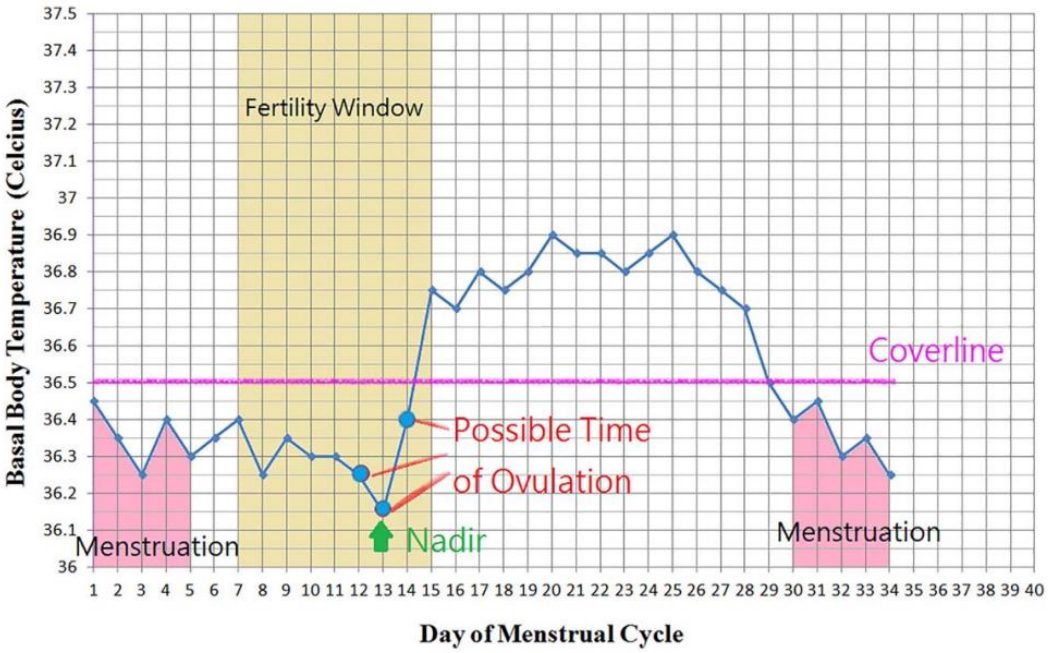

Figure 2-4 The basal body temperature during the menstrual cycle[6]

Although basal body temperature could be influenced by factors like fever, alcohol, drugs, and sleep disturbance, monitoring basal body temperature is still used to seek pregnancy since it is one of the most convenient ways to detect ovulation.

2.2. Heat balance

The balance of heat production and heat loss controls the body temperature. When the heat production exceeds the heat loss, the core temperature will rise. On the contrary, the heat loss becomes greater, the body heat will decrease, and the core temperature will fall.

2.2.1. Heat Production

The metabolic rate of the body is affected by factors that:

(a) Basal metabolism rate (BMR). It is the minimum energy required to perform all the body's biochemical reactions, and it varies from age, height, and sex.

(b) Extra metabolism rate caused by muscle activity, including shivering.

(c) Extra metabolism is caused by hormones, like thyroxine, catecholamine, progesterone, etc.

(d) Higher body temperature may result in extra metabolism

since most biochemical processes are more effective when the cell temperature is higher than usual.

(e) The digestion, absorption, and storage of food make specific dynamic effects.

2.2.2. Heat Loss

The heat generated by the deep organs transfers to the skin surface and is lost to the outside.

Fat is the main actor of the insulator system, and it helps the heat in the deep body transfer too fast to the skin surface. The venous plexus is also important since it controls the blood flow to the skin, which means it controls the heat transfer speed.

The main ways of how the heat loss from the skin is shown in **Figure 2-5**.

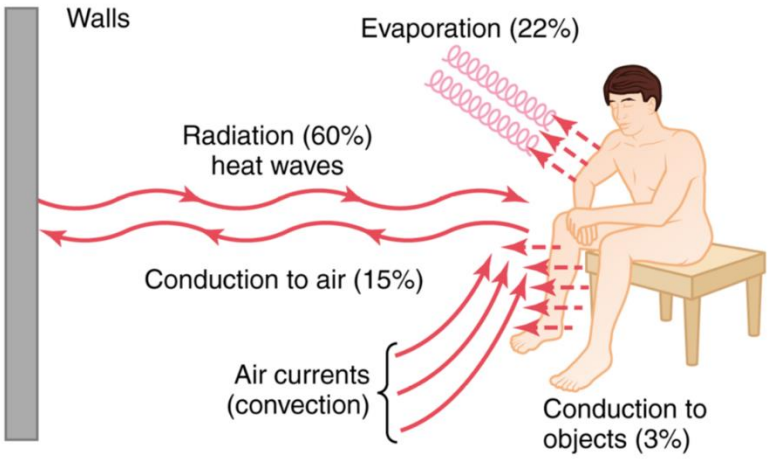

Figure 2-5 mechanisms of heat loss from the body[7]

The methods include:

(a) Radiation. The heat from the skin is lost in all directions by a type of electromagnetic wave named infrared heat rays. In this condition, radiation contains about 60% heat loss.

(b) Conduction. When a project is conducted at a lower temperature, the heat will transfer from the warm project. So as the body, and when a nude man seat on the chair, his body heat will transfer to air and the chair.

(c) Convection. When there are wind or liquid currents to wash

over the body, the heat conducted to the surrounding will be taken away by the removal of the warmed air or liquid.

(d) Evaporation. Each gram of evaporated water will make 0.58 kcal of heat loss. A person is always evaporating water, no matter whether he is sweating or not. Heat loss of this part can be controlled by regulating the sweating rate.

2.3. Body temperature regulation mechanism

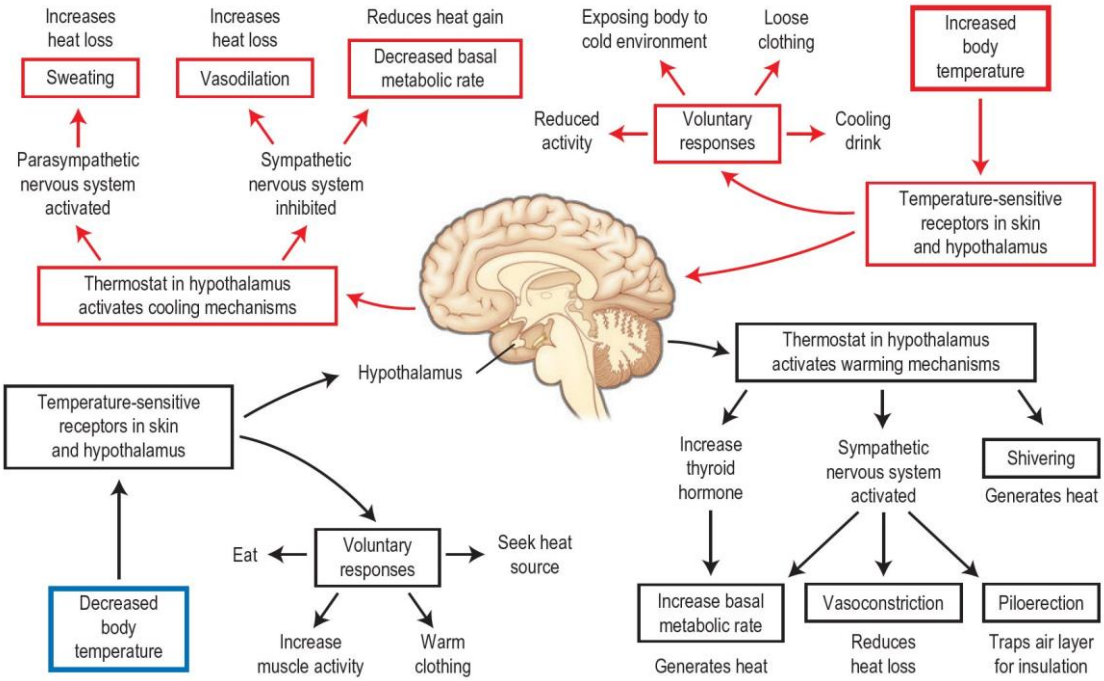

Figure 2-6 Regulation of core body temperature [8]

Thermal receptors are used to detect the temperature. They are on the skin, in the organs, and even in the hypothalamus. They could be divided into cold receptors, warmth receptors, and even pain receptors since the burning hot and freezing cold will make humans feel pain. The amounts of cold receptors are generous, like 10 times the amount of warm receptors.

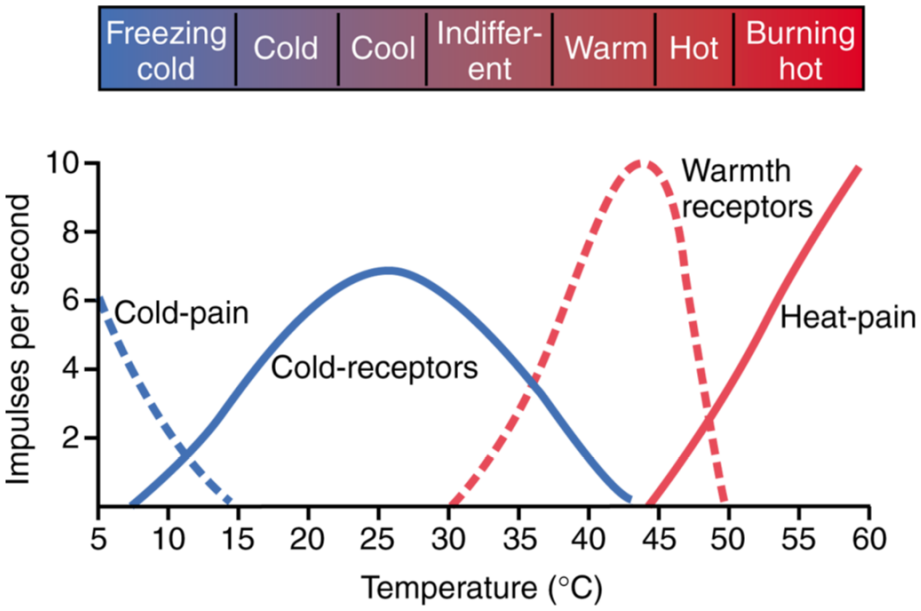

Figure 2-7 Thermal receptors in different temperatures. [7]

The body temperature regulation contains behavioral thermoregulation and autonomic thermoregulation.

Behavioral thermoregulation is when the person who feels uncomfortable with the temperature will put on or take off clothes, open the air conditioner or walk into places with a nice temperature. This is the most effective way to maintain body temperature in an extremely hot or cold environment.

Autonomic thermoregulation is a well-designed control system.

Signals from skin and organs or the hypothalamus will be integrated by the posterior hypothalamus. When the hypothalamic temperature centers find out the body temperature is too high or too low, it will go on a few mechanisms to decrease or increase the body temperature.

There are three essential ways to decrease the temperature when the body are in hot condition:

(a) Skin blood vessels vasodilation: inhibition of the sympathetic nervous centers will cause vasodilation. Heat could be transferred from the organs to the surface quicker than usual, and heat radiation from the skin could be enhanced.

(b) Sweating. Sweat glands will be activated since the parasympathetic centers are active, and sweat evaporation will help increase heat loss.

(c) Decrease of metabolic rate: this will reduce heat production.

Three important mechanisms are token to increase the core temperature:

(a) Skin vasoconstriction throughout the body. Stimulation of the sympathetic nervous centers helps the blood not to transfer to the exterior layer of the body and decreases heat loss.

(b) Piloerection. It will help the air layer on the skin surface to be thicker so that the heat loss can be decreased.

(c) Increase in the rate of metabolic. Shivering will produce more heat in the skeletal muscles, and increased catecholamine or other hormone output will produce more heat in the organs.

2.4. Abnormal body temperature

Environmental conditions like bacterial diseases and brain tumors may cause abnormal body temperature. **Figure 2-8** shows the different regulation results of our body under various conditions.

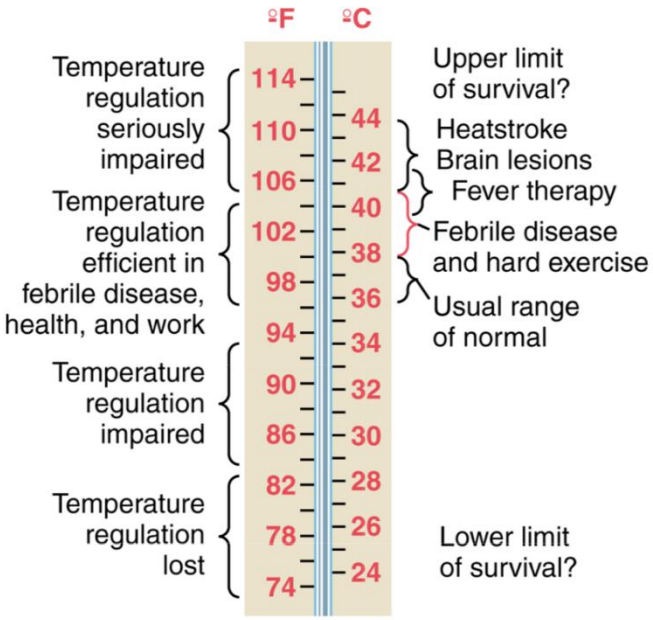

Figure 2-8 Different body temperatures under different conditions.

2.4.1. Heatstroke

A heatstroke is a form of hyperthermia, and it is a true medical emergency that is often fatal if not properly treated. It happens not only in extremely hot conditions but also in somewhere that is not too hot but with high humidity.

Heatstroke is sometimes classified as exertional heat stroke (EHS, which is due to overexertion in hot weather) or non-exertional heat stroke (NEHS, which occurs in climactic extremes and affects the elderly, infants and chronically ill. Heatwave blankets Japan in the summer of 2019, with 71,319 hospitalized. 52% of the patients are elders over 65 years old, and most of heatstroke happens at home. [9]

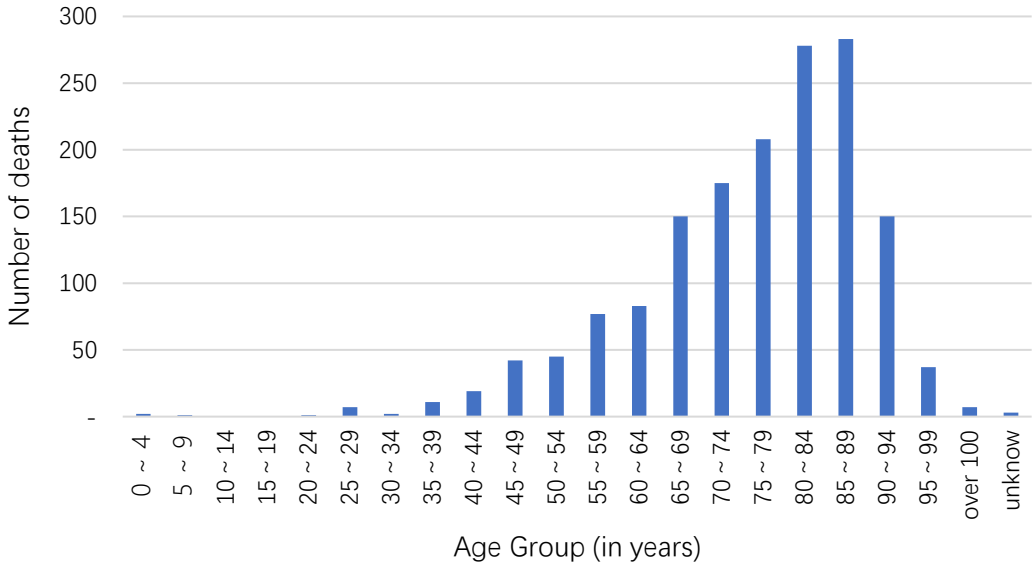

Figure 2-9 Number of deaths in 2018 due to heatstroke by age group [10]

In a 2018 report by the Ministry of Health, Labor and Welfare (MHLW) of Japan on the actual age groups with deaths due to heatstroke, 81.5% of total heatstroke deaths were elders over 65 years old (**Figure2-9**). Health management of seniors has become a serious problem in Japan.

The pathway to heatstroke is shown in **Figure 2-10**. It is indicated that it is also vital to measure the core temperature for heatstroke prevention and health management of the elderly living alone since the increased core temperature is one of the signs of heatstroke.

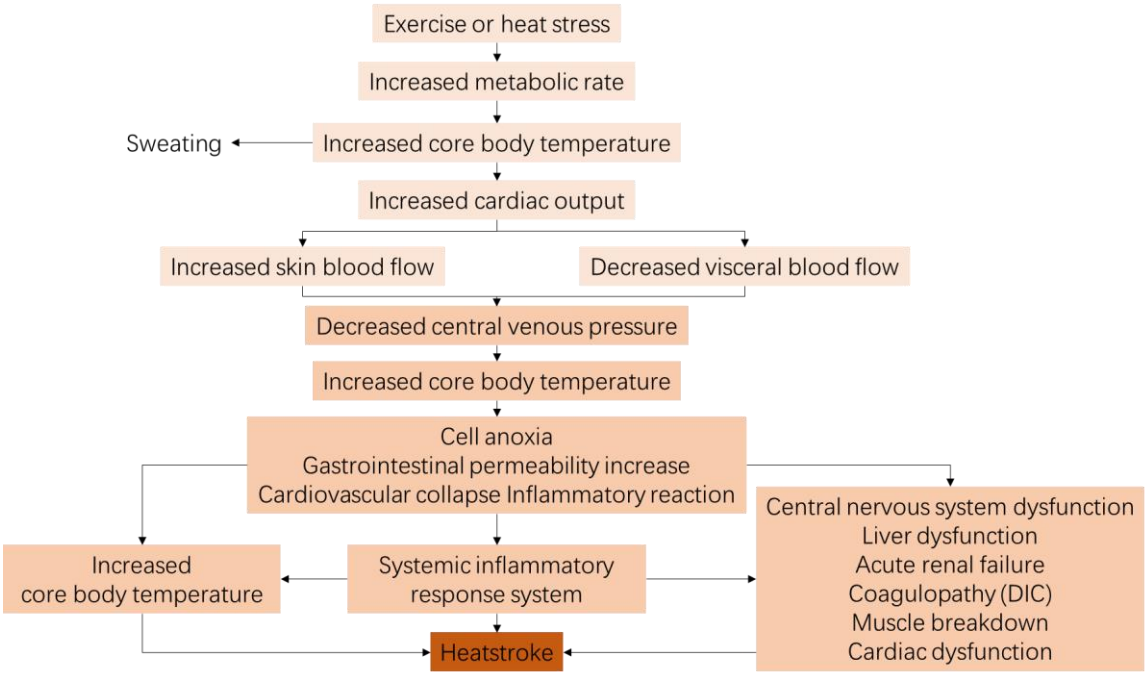

Figure 2-10 pathophysiological pathway leading to Heatstroke [11]

2.4.2. Hypothermia

Hypothermia is someone's core temperature lower than 35.0 °C. When our body is exposed to somewhere freezing, our body temperature will have high heat loss, and the core temperature may not be regulated in time. Low body temperature will cause low biomedical reaction speed, and when the core temperature is lower than 29.4 °C, the hypothalamus will lose the ability to thermoregulation.

2.4.3. Fever

Our temperature regulation is controlling our temperature at a special temperature around 36-37degree, which is named the setpoint, or thermostat.

Proteins, breakdown products of proteins, and other substances may change the set point of core temperature.

Just after the set point is raised, the hypothalamus finds out that the core temperature is lower than the set point, and the regulation will be carried out to raise the body temperature. That is why we feel cold at the beginning process of the fever. When the setpoint suddenly reduces back to a lower value, sweating and vasodilation will help the heat to transfer to the outside as soon as possible.

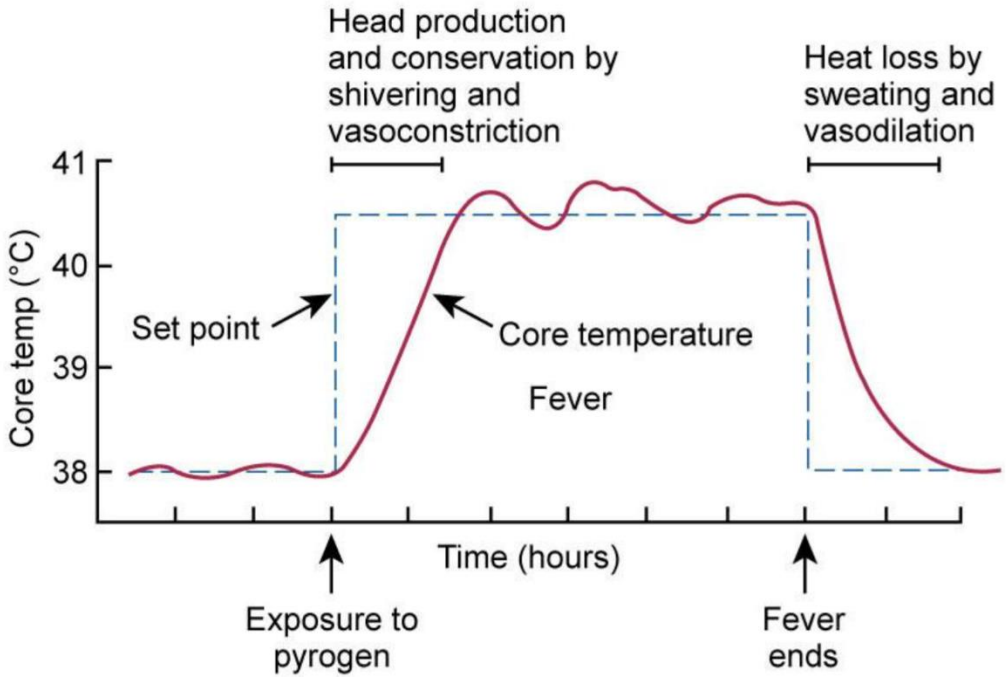

Figure 2-11 A change in the setpoint for temperature regulation

References

[1] J. Aschoff and R. Wever, "Kern und Schale im Wärmehaushalt des Menschen," Naturwissenschaften, vol. 45, pp. 477-485, 1958, doi: 10.1007/BF00635546.

[2] J. D. Hardy, E. F. Du Bois, and G. F. Soderstrom, "Basal Metabolism, Radiation, Convection and Vaporization at Temperatures of 22 to 35°C.: Six Figures," The Journal of Nutrition, vol. 15, pp. 477-497, 1938, doi: 10.1093/jn/15.5.477.

[3] N. A. S. Taylor, M. J. Tipton, and G. P. Kenny, "Considerations for the measurement of core, skin and mean body temperatures," Journal of Thermal Biology, vol. 46, pp. 72-101, 2014, doi: 10.1016/j.jtherbio.2014.10.006.

[4] S. R. Insler and D. I. Sessler, "Perioperative Thermoregulation and Temperature Monitoring," Anesthesiology Clinics of North America, vol. 24, no. 4, pp. 823-837, 2006, doi: 10.1016/j.atc.2006.09.001.

[5] R. Lericollais, A. Gauthier, N. Bessot, A. Zouabi, and D. Davenne, "Morning Anaerobic Performance Is Not Altered by Vigilance Impairment," PLOS ONE, vol. 8, p. e58638, 2013.

[6] H.-W. Su, Y.-C. Yi, T.-Y. Wei, T.-C. Chang, and C.-M. Cheng, "Detection of ovulation, a review of currently available methods," Bioengineering & Translational Medicine, vol. 2, pp. 238-246, 2017, doi: 10.1002/btm2.10058.

[7] J. E. Hall, "Guyton and Hall Textbook of Medical Physiology," 2015.

[8] M. Swash and R. Hutchison, Hutchison's clinical methods. Saunders, 2002.

[9] 消防庁, "2019 年（5 月から 9 月）の熱中症による救急搬送状況," 2019.

[10] 日本厚生労働省政策統括官付参事官付人口動態・保健社会統計室, "年齢（5 歳階級）別にみた熱中症による死亡数の年次推移（平成 7 年～30 年） " 2019. [Online]. Available: https://www.mhlw.go.jp/toukei/saikin/hw/jinkou/tokusyu/necchusho18/index.html.

[11] Y. Epstein and R. Yanovich, "Heatstroke," New England Journal of Medicine, vol. 380, pp. 2449-2459, 2019, doi: 10.1056/NEJMra1810762.

3. The measurement of core temperature

3.1. Invasive measurement

3.1.1. Direct measurement

The direct measurement required invasively inserting a transducer head inside the body. Needle type (**Figure 3-1 (a)**) and Catheter type (**Figure 3-2 (b)**) transducer heads are the most useful type in clinical settings.

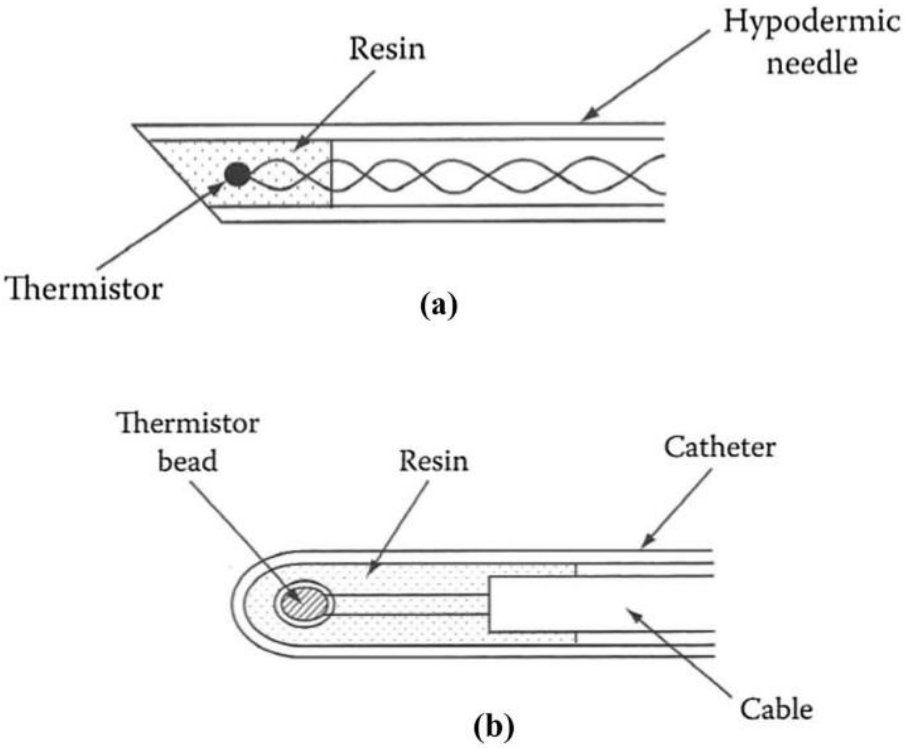

Figure 3-1 Transducer heads (a) Needle-type (b) Catheter-type [1]

Rectal is the most useful position for core temperature direct measurement, especially for children and babies. It was considered the hottest part of our body in the early years and was used as the standard position of core body temperature. The disadvantage of rectum measurement is that response may delay when the core temperature changes rapidly.

The esophagus is preferred since measurements in this position respond quickly and close to the aorta, and the blood flow toward the hypothalamus.

3.1.2. Ingestible capsule thermometer

In the 1980s, the Johns Hopkins University Applied Physics Laboratory worked closely with Goddard Space Flight Center to develop the Ingestible Thermal Monitoring System. These days CoreTemp® developed the commercially available thermometer, as shown in **Figure 3-2**.

The capsule was coated with silicone, and it has a silver oxide battery, circuit board, and sensing quartz crystal inside. After the capsule is ingested, the crystal sensor vibrates at a frequency nearly to the core temperature, produces the magnetic flux, and the circuits will transmit the signal at a low frequency harmlessly through the body. This capsule will last in the body for 24-36 hours.

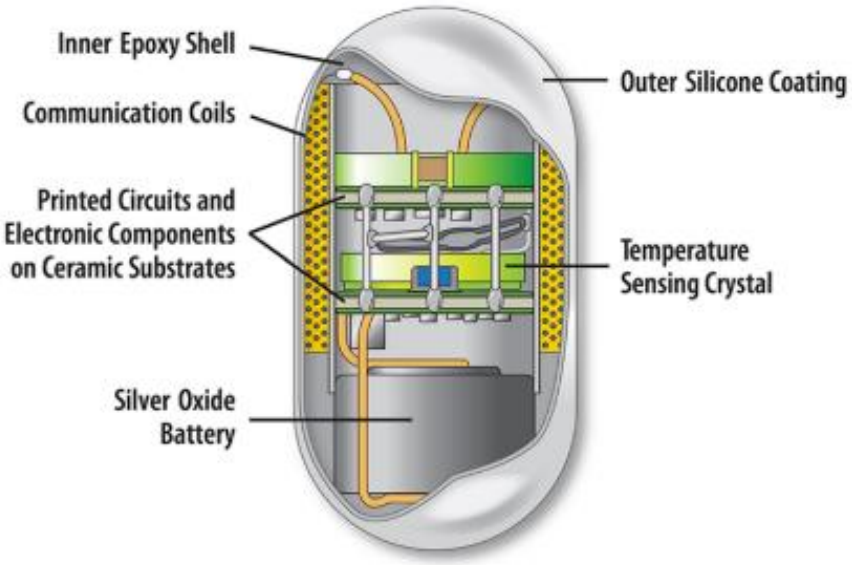

Figure 3-2 Ingestible capsule thermometer (CorTemp®)

However, this capsule is a one-use device at a high price. Now it is used for keeping athletes from overheating, monitoring the core body temperatures of firefighters as they work in the extremely hot position, and divers as they work in deep, freezing water.

3.2. Non-invasive measurement

3.2.1. The Zero-Heat-Flux method

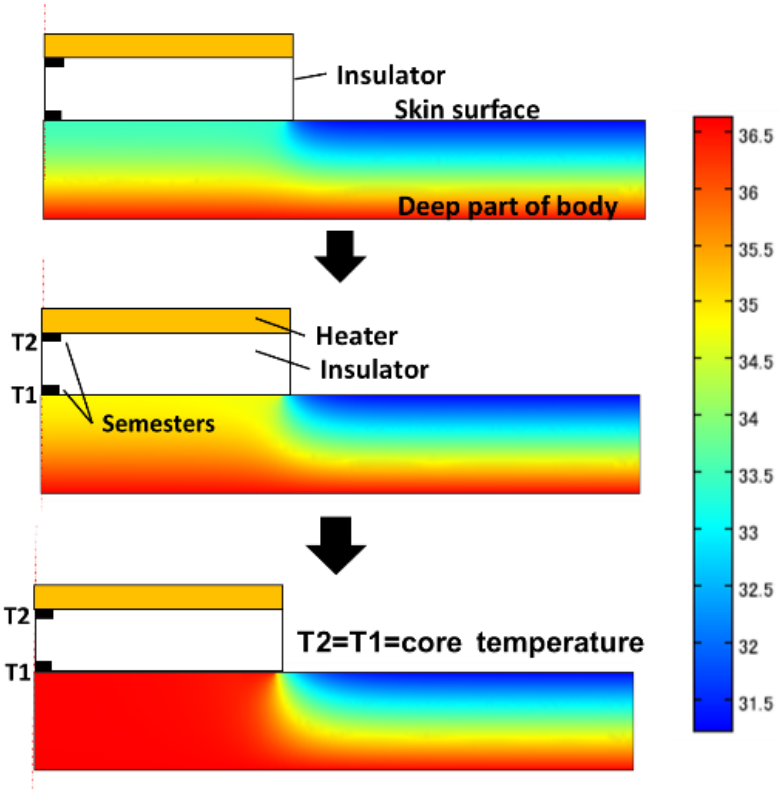

Figure 3-3 The Principle of Zero-Heat-Flux method

The zero-heat-flux method was devised by R. h. Fox and A. J. Solman in 1970[2], and it can measure the core temperature non-invasively from the surface of the body.

As shown in **Figure 3-3**, an insulator is applied to the skin surface to measure the core temperature from the skin surface to prevent the heat from losing to the air. To decrease the surface convection, a heater is used to heat the insulator and make the temperature of T1 equal to T2, compensating for the convection heat Flux. When the T2 is equal to T1, the probe can be conserved as an ideal heat insulator, and the core temperature can be measured from thermistor T2. It was called Zero-Heat -Flux method or the Zero-Heat-Flow method.

The measurement accuracy was improved by Togawa[3], and it was commercialized as a medical device and was widely used in hospitals. For example, CoreTemp CM-210 (**Figure 3-4**) is widely used for continuous monitoring of core temperature in the intensive care unit, as Bair Hugger (**Figure 3-5**) from 3M company provides softer probes made by grade foam and flexible circuits for the forehead measurement.

Figure 3-4 CoreTemp® CM-210, Terumo

Figure 3-5 Bair Hugger ™ Temperature Monitoring System.3M ™

Although zero-heat-flux thermometry can get results of high measurement accuracy, the core thermometer using this method has a few weaknesses, as follow:

- The heater layer consumes considerable power, so it is not feasible for wearable yet.
- It needs a preparation time of 10-30 mins to reach equilibrium (depending on the measurement position).
- The results may become unreliable when the surrounding temperature is cold or extremely hot.

3.2.2. The Dual-Heat-Flux method

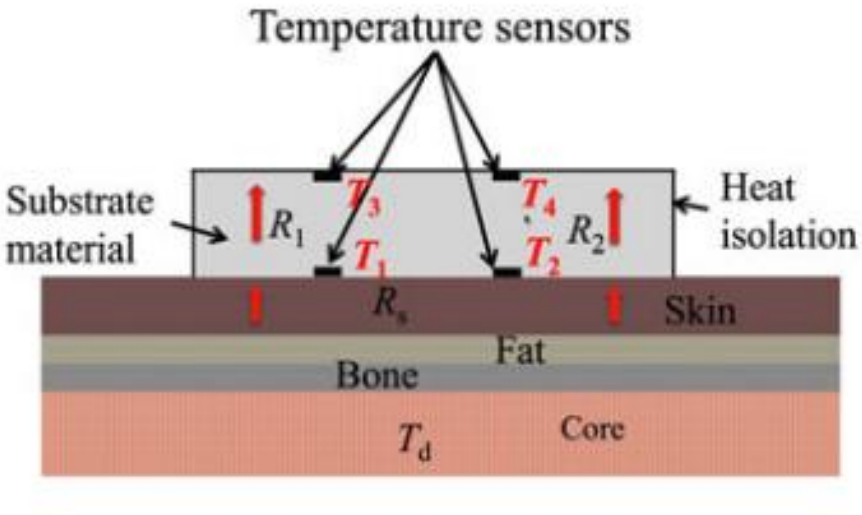

Figure 3-6 Illustration of DHFM thermometry

The Dual-heat-flux method is a passive non-invasive method requiring no AC power. Kitamura proposed this method, and M. Huang improved it. [4]

Heat conduction will build up a temperature gradient. When a material attaches to the skin surface, the heat flow from the core to the skin will also pass through the material. The core temperature could be calculated by

$$\frac{(T_d - T_1)}{R_{s1}} = \frac{(T_1 - T_3)}{R_1}$$

or

$$\frac{(T_d - T_2)}{R_{s2}} = \frac{(T_2 - T_4)}{R_2}$$

R_{s1} and R_{s2} are the heat resistances of the skin and the subcutaneous tissues for each path. R_1 and R_2 are the corresponding resistances of the material.

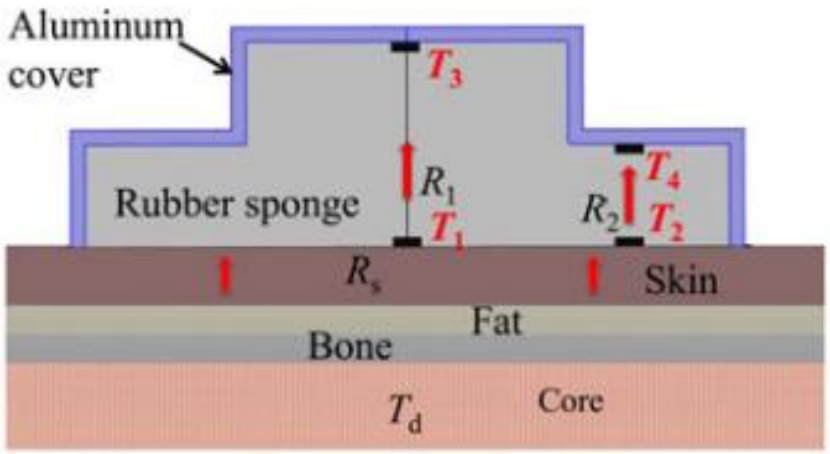

Figure 3-7 Implementation of DHFM thermometry

The improved DHFM thermometry is shown in **Figure 3-7**. A double cylinder design to generate two heat paths at the same substrate material condition and the core temperature could be shown as

$$T_d = T_1 + \frac{(T_1 - T_2)(T_1 - T_3)}{k(T_2 - T_4) - (T_1 - T_2)}$$

k (=R_1/R_2) is the ratio of heat resistance of the two heat paths.

However, the DHFM thermometer also has disadvantages like less accuracy than the Zero-Heat-Flux method, minor lag, and the presence of artifacts.

3.2.3. The Infrared scanner

The infrared scanner is a new non-invasive core temperature assessment method that can be used in the clinic and at home. The main advantage of this method is that it is easy to use and can get results in a few seconds. The method used an infrared scanner to detect the highest temperature of the tympanum or the forehead skin from the temporal artery. Based on this value, the device uses a proprietary algorithm to estimate the core temperature.

Figure 3-8 Infrared scanner MC-510 (OMRON, Japan)

However, some research found that the infrared scanner did not accurately monitor the core temperature, especially when it was

raised by passive heating [5]. It is indicated that the distance to the forehead and the differences in the ear structure will influence the monitor's accuracy.

3.3. Predictions of core temperature

Scientists are trying to estimate core temperature non-invasively using models, sensors, and algorithms.

Xu et al. described a linear relationship between skin temperature, heat flux, and core temperature, suggesting that applying a Kalman Filter (KF) may be a viable approach. Alexander P. Welles [6] used the Kalman filter to estimate the core temperature from skin temperature, heat flux, and heart rate.

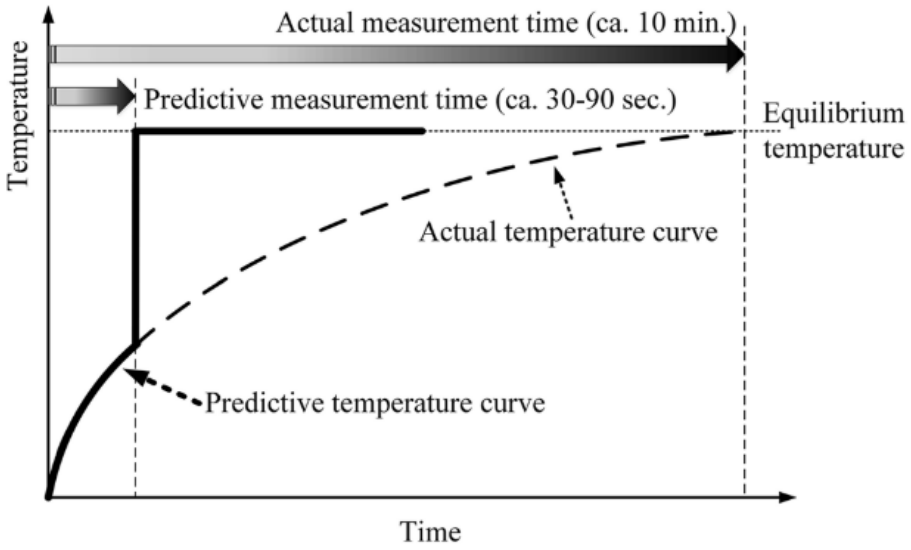

Figure 3-9 The predictive method

Terumo also used a previously calibrated curve of temperature-time course and the actual measurement of the first 30~90 s to predict the final temperature value. It could reduce the preparation time.

However, the estimation results are not always so reliable since the clothes, measurement positions, metabolic activity, and other factors could influence them.

References

[1] W. Chen, "Thermometry and interpretation of body temperature," Biomedical Engineering Letters, vol. 9, pp. 3-17, 2019, doi: 10.1007/s13534-019-00102-2.

[2] R. H. Fox, A. J. Solman, R. Isaacs, A. J. Fry, and I. C. MacDonald, "A new method for monitoring deep body temperature from the skin surface.," Clinical science, vol. 44, pp. 81-86, 1973, doi: 10.1042/cs0440081.

[3] T. Nemoto and T. Togawa, "Improved probe for a deep body thermometer," Medical & Biological Engineering & Computing, vol. 26, pp. 456-459, 1988, doi: 10.1007/BF02442312.

[4] M. Huang, T. Tamura, Z. Tang, W. Chen, and S. Kanaya, "A Wearable Thermometry for Core Body Temperature Measurement and Its Experimental Verification," IEEE Journal of Biomedical and Health Informatics, vol. 21, no. 3, pp. 708-714, 2017, doi: 10.1109/JBHI.2016.2532933.

[5] D. A. LOW et al., "Temporal Thermometry Fails to Track Body Core Temperature during Heat Stress," Medicine & Science in Sports & Exercise, vol. 39, no. 7, pp. 1029-1035, 2007, doi: 10.1249/mss.0b013e318050ca3e.

[6] A. P. Welles et al., "Estimation of core body temperature from skin temperature, heat flux, and heart rate using a Kalman filter," Computers in Biology and Medicine, vol. 99, pp. 1-6, 2018, doi: 10.1016/j.compbiomed.2018.05.021.

4. Reducing the power consumption of the ZHF method

4.1. Simulation in COMSOL

An adiabatic material is covered on the probe and surrounding skin surface to prevent heat radiation and reduce power consumption. Simulation experiments were taken before we made the real prototype probe to determine whether this method is effective.

4.1.1. Simulation settings and model

We made an axisymmetric two-dimensional model of three elements (probe, adiabatic and skin tissue) as shown in **Figure 4-1**. The finite element method simulated and analyzed the relationship between the heat insulation radius and the heater power consumption. COMSOL is used as the simulation software.

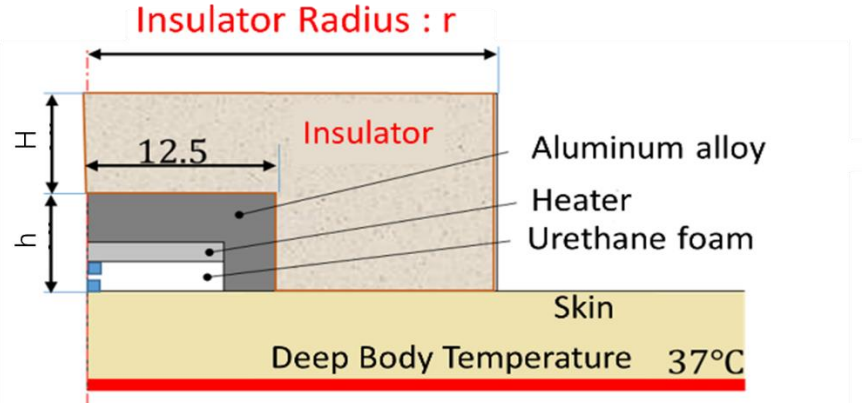

Figure4-1 Simulation model showing axis-symmetric view of the prototype probe

We changed the radius of the insulator r, the height of the insulator H and the height of the insulator h to see the skin temperature at the equilibrium.
The equation and properties of tissues and materials are as follows:

Heat equation: $\rho C \frac{\partial T}{\partial t} - k\nabla^2 T = Q_m + Q_b$

Boundary conditions for body surface: $h[T - T_a]$

The metabolic heat of tissues and the heat transfer by blood was

ignored since it changed when the measurement position changed.

Table4-1 Thermal properties of tissue used for simulation

Density of tissues : ρ [kg/m^3]	1000
Specific Heat Capacity : C [J/(kg·K)]	3000
Thermal conductivity of tissue : k [W/(m·K)]	0.4
Metabolic heat of tissues : Qm[W/m^3]	
Heat transfer by blood : Qb[W/m^3]	
Deep body temperature : Tc [deg]	37
Atmospheric temperature : Ta [deg]	25
Heat transfer coefficient : h [W/(m^2·K)]	28.5

Table 4-2 Thermal properties used for simulation

	Aluminum alloy	Urethane foam	Foamed Plastics
Density [kg/m^3]	2700	300	1090
Thermal conductivity [W/(m·k)]	256	0.06	0.1
Specific heat[J/kg·K]	913	30	1340

4.1.2. Simulation results

(a) Results of different insulator radius r and insulator height H

Figure 4-2 shows how the height H and the radius r influenced the skin temperature at the measurement. When the core temperature is set to 37 degrees, skin temperatures closer to 37 will provide more accuracy. We can see from the result that the height H didn't cause too many changes to the temperature, but when the insulator radius increases, the measurement will get results much closer to 37 degrees. The height of the probe was set to 12mm.

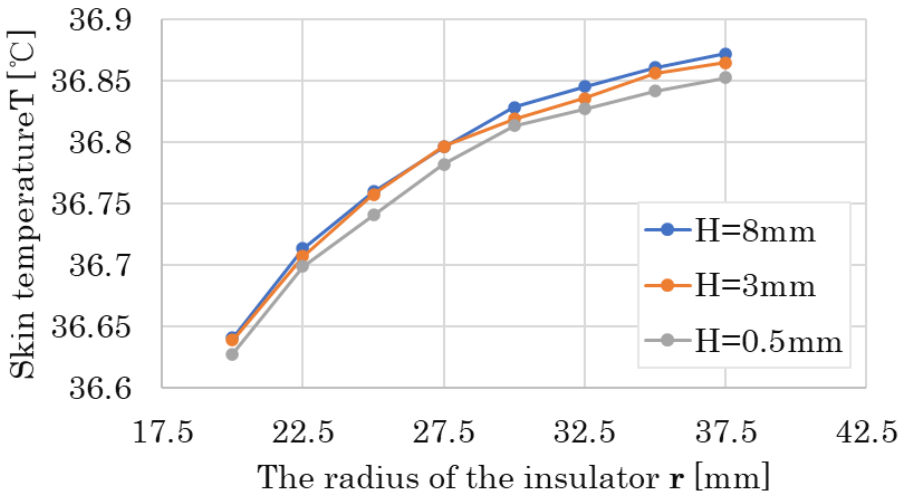

Figure 4-2 Skin temperature results with different insulator height H

(b) Results of different probe height h

We changed the probe's height; the data is shown in **Figure 4-3**. The skin temperature didn't change obviously when the height varied. Also, when the probe is higher, the time for preparation becomes longer. The insulator radius was set to 32.5mm, and the height H was set to 0.8mm.

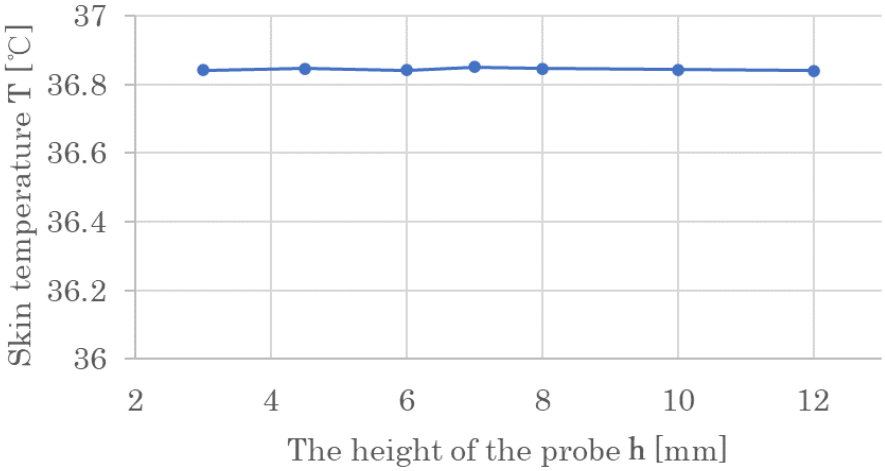

Figure 4-3 Skin temperature result of different probe height

(c) Results of the standard models and fit models

From the results, we can find out that the thickness of the probe did not cause too much influence on accuracy. So we made normal type models (H=17.5mm, h=12.5mm) and fit type models (H=3mm, h=7mm) and changed the radius of the insulator r to see how the skin temperature and the power consumption would vary.

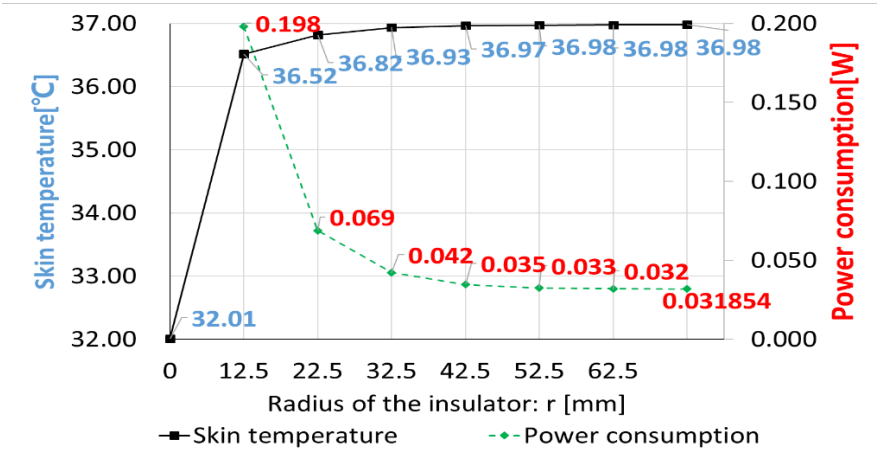

Figure 4-4 Normal-type model simulation results

Results show that the insulation of the probe and the surrounding surface will effectively decrease the power consumption. When the insulator radius increases, the skin temperature will be closer to 37 degrees, which means that the measurement will get better accuracy.

We got low power consumption and highly accurate results when the radius is over 32.5mm for the standard type.

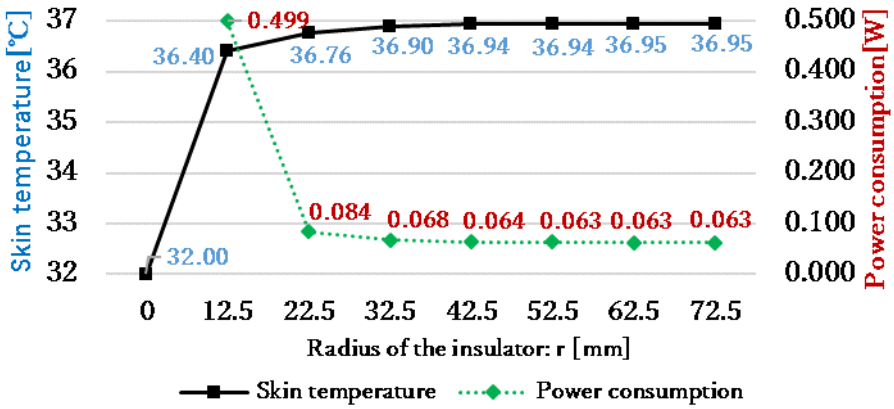

Figure 4-5 Fit-type model simulation results

For the fit type model, when the radius goes up to 26mm, most of the power was reduced, and we also got better results.

4.2. The wearable prototype thermometer

The prototype core temperature measurement system was made of the prototype probe and the electric system.

4.2.1. Prototype probes

The prototype probe is shown in **Figure 4-6**.

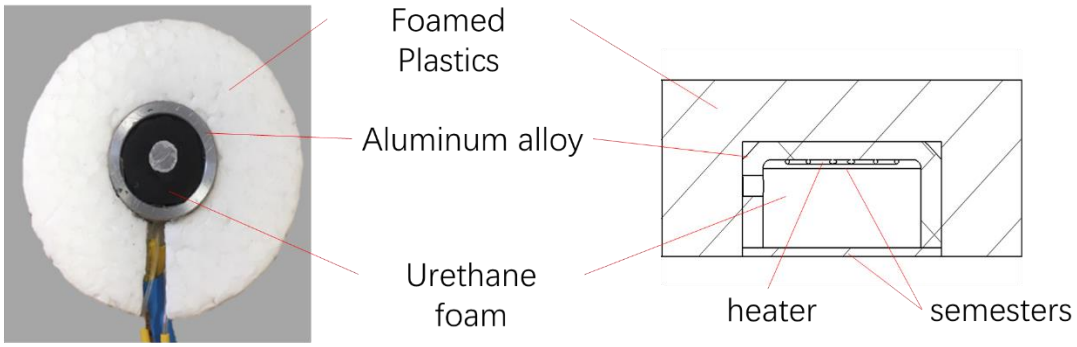

Figure 4-6 The structure of the prototype probe

Thermistors are commonly used in body temperature measurement since they have good linearity in the physiological range of the body temperature. Two thermistors (PB7-43, Shibaura Electronics, Japan) were used to measure the temperature of the heater layer and the skin surface because of their micro size[1].

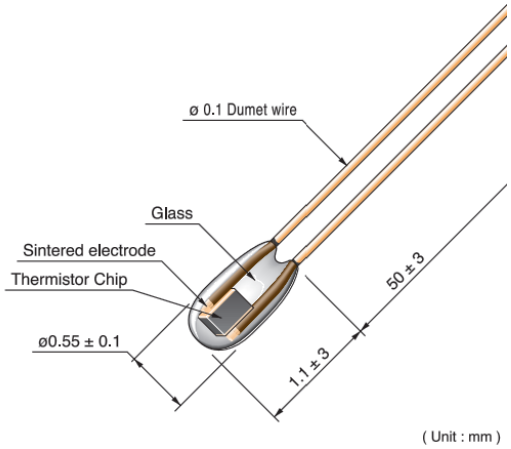

Figure 4-7 The PB7-43 thermistor[1]

Urethane foam was used as the insulator between the two thermistors, and the heater layer used the Nichrome conductive wire to generate heat on time. An aluminum alloy was covered on them to make them stable, and the heat could be transferred to the surrounding skin surface. Six conductive wires connect from the probe to the electric part, four for the two thermistors and two for the heater layer.

The theoretical analysis and simulation result suggested that the radius of the foamed plastics outside the probe would influence its accuracy and power consumption. Based on the simulation result, we made three types of probes, the standard type, the fit type, the sucker type.

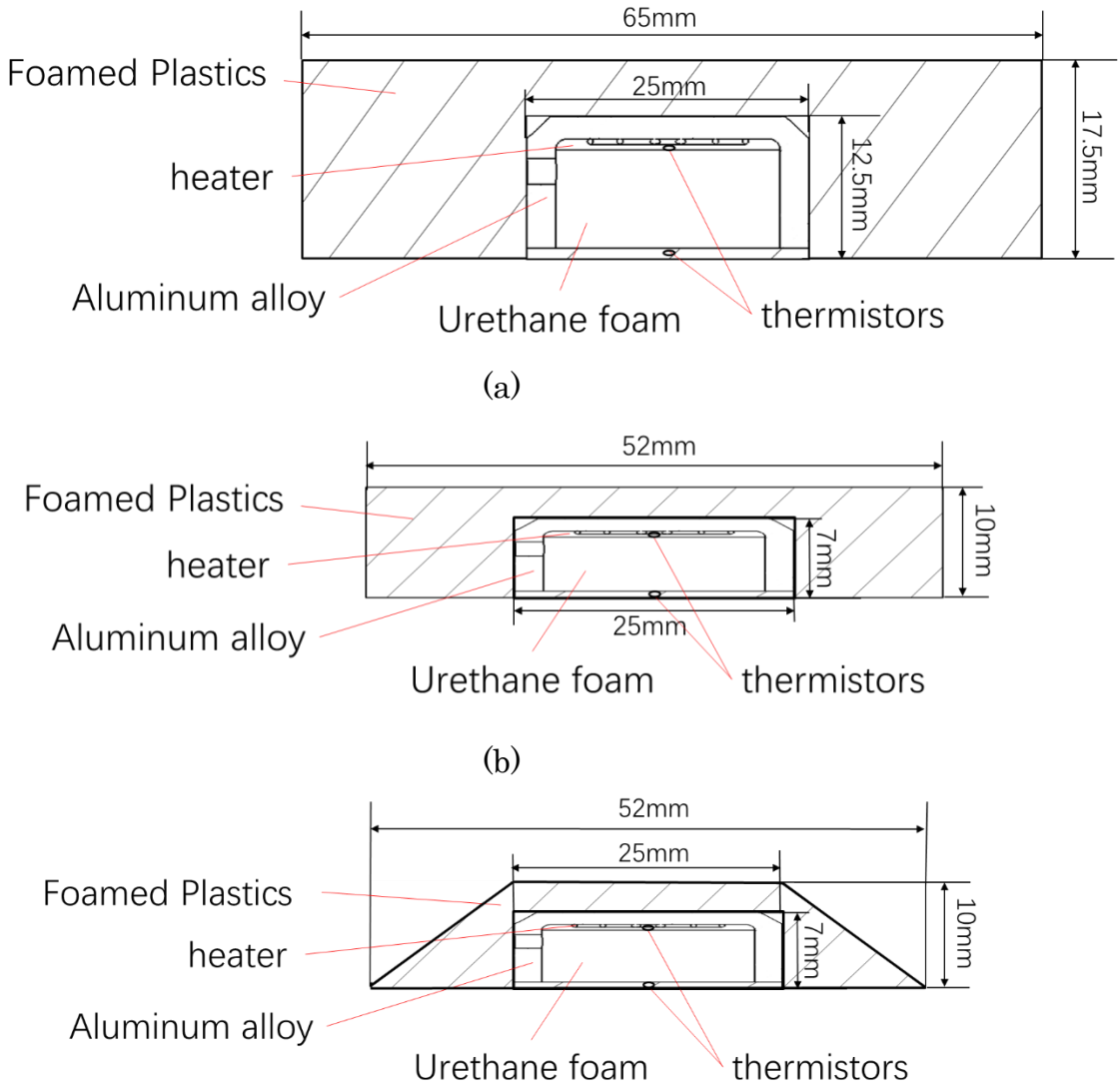

Figure 4-8 Three Prototype probes. (a) The standard type. (b) The fit type. (c) The sucker type.

4.2.2. The electric system

The electric system mainly contains the signal amplification circuit, Arduino Uno and the heater control circuit.

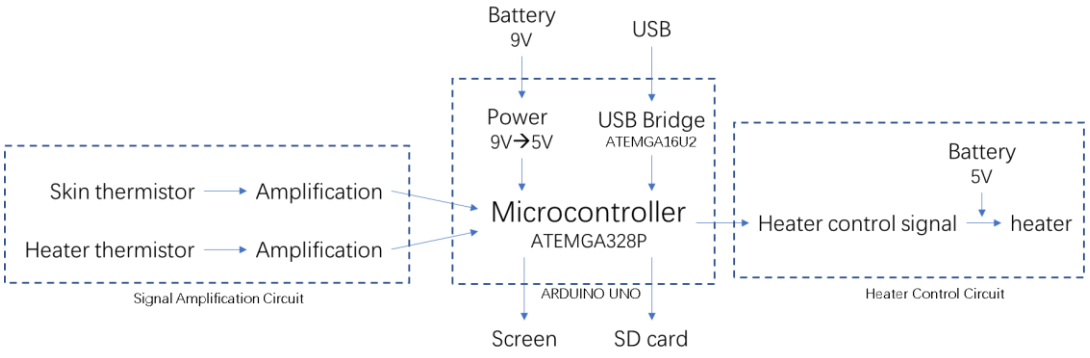

Figure 4-9 The electric system

The signal amplification circuit (**Figure 4-10**) amplified the variation of signal for 16 times and transfer it to the Arduino Uno part.

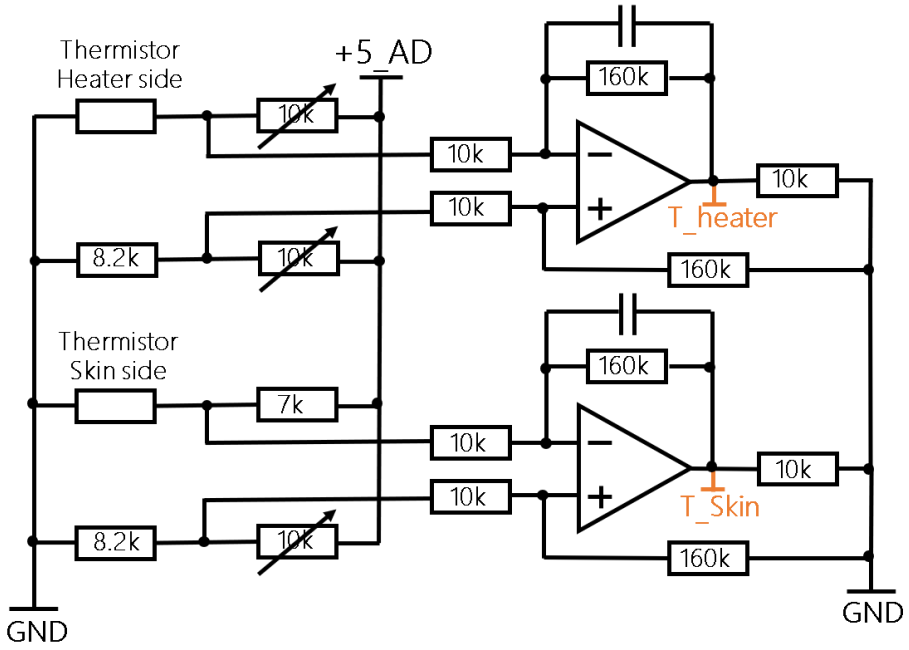

Figure 4-10 The signal amplification circuit

9V Alkaline battery was adopted to motivate the Arduino Uno, and the 5V regulator inside the Arduino will change it to a stable electricity supply for the amplification circuit and Arduino itself.

The microcontroller in Arduino is ATEMGA 328P, and it will help to record the data in the SD card and displaying it on a small LCD screen as shown in Figure 4-11. It could also connect itself with a computer using the USB.

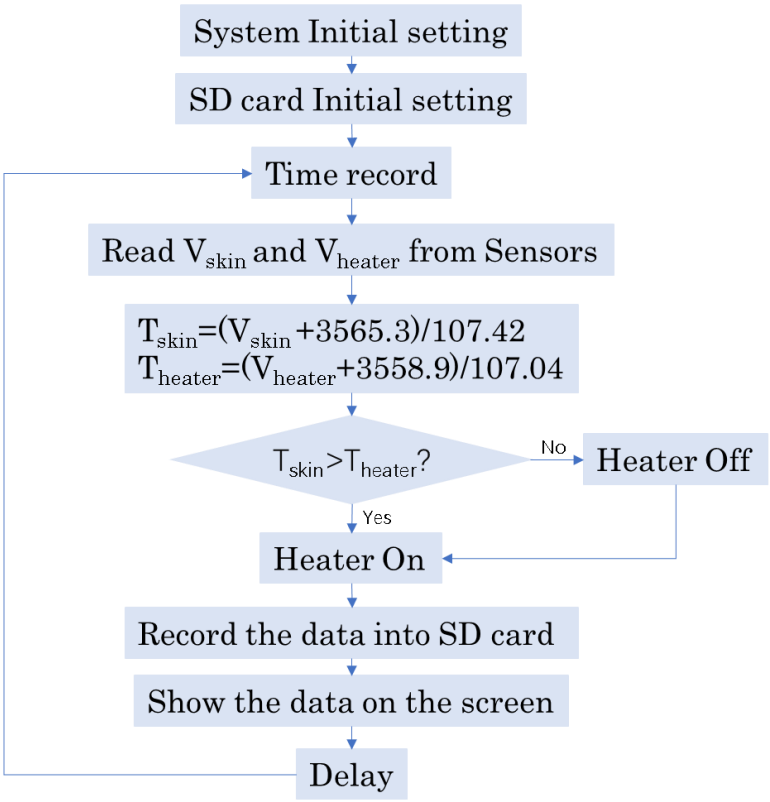

Figure 4-11 The programing of Arduino

The microcontroller will also decide the heater to generate heat or not, and Arduino will provide the heater control circuit (**Figure 4-12**) a PWM output for the heater.

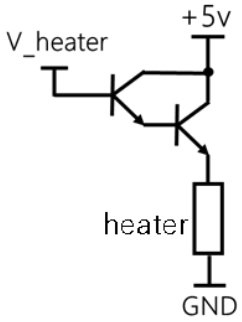

Figure 4-12 Heater control circuit

To amplify the power of the PWM wave for the heater, two transistors were adopted in the heater circuit. They will also provide the Arduino from the large current of the heater.

4.3. Fast-Changing Measurement of the wearable thermometers

4.3.1. Standard type thermometer

(a) Method

- Room temperature is set to 25±1℃
- A female subject (24 years old) participated in the experiment.
- Lithium polymer battery (3200mAh, DC 5.07V, 1A max) was used as the power supply.
- The standard prototype probe and the CTM-205 probe are secured to the forehead with elastics.
- The experiment consisted of 40 minutes acclimation phase, a 10 minutes squatting phase, and another 40 minutes recovery phase.

(b) Results

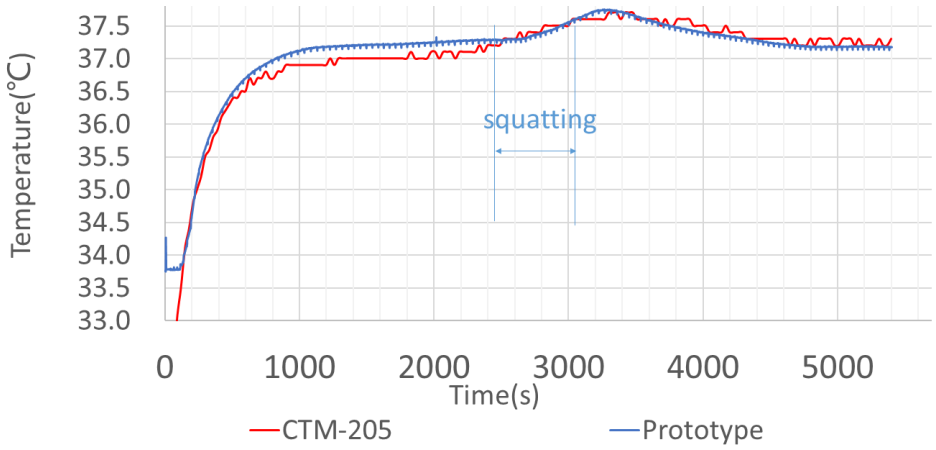

(a)

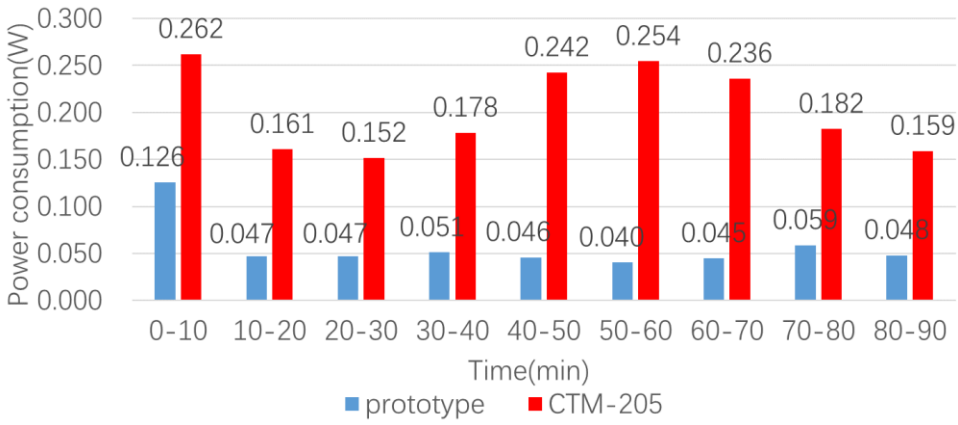

(b)

Figure 4-13 (a) Temperature comparison result of the standard prototype (b) Power consumption comparison result of the standard prototype

Figure 4-13 (a) shows the time-varying results of CTM-205 and prototype thermometer. The changes in core temperature can be caught by the standard prototype thermometer.

On the other hand, **Figure 4-13 (b)** shows the cumulative power consumption per 10 minutes. Except for the initial 10 minutes, the power consumption of the prototype thermometer is reduced to about one-fourth of CTM-205.

4.3.2. Fit type thermometer

(a) Method

- Room temperature was set to 25±1℃
- A male subject (23 years old) participated in the experiment.
- Lithium polymer battery (3200mAh, DC 5.07V, 1A max) was used as the power supply.
- The fit prototype probe and the CTM-205 probe are secured to forehead with elastics.
- The experiment consisted of 40 minutes acclimation phase, a 10 minutes cycling phase, and another 40 minutes recovery phase.
- During the acclimation phase, the subject seat on a chair quietly for 40 minutes. The first 20 minutes was the preparation time for the measurement. Zero-Heat-Flux measurements need time to transfer the heat from the heater layer to the tissue under the skin surface.
- In the cycling phase (**Figure 4-15**), the subject cycling to keep the heart rate at 140 bpm.
- After the cycling, the subject returns to seat and rest for another 40 minutes.

Figure 4-15 The cycling phase

(b) Results

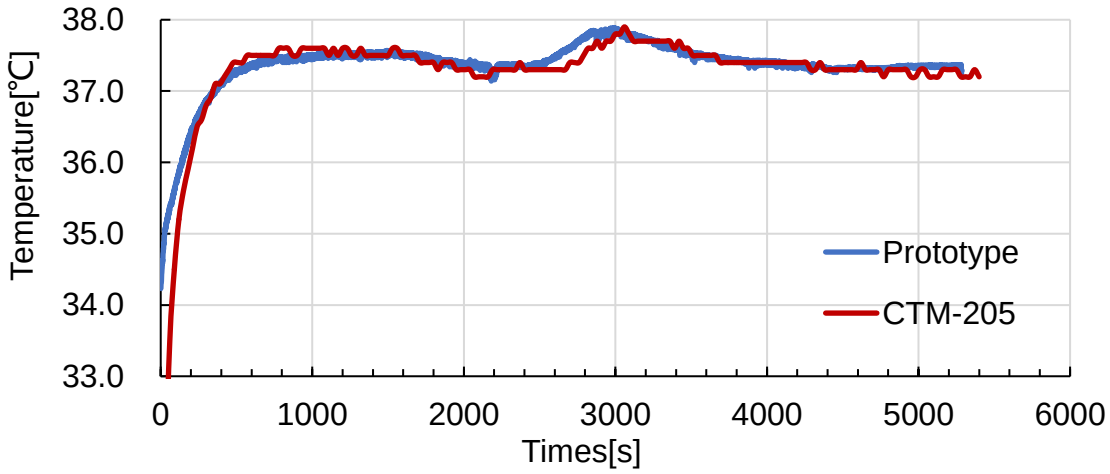

(a)

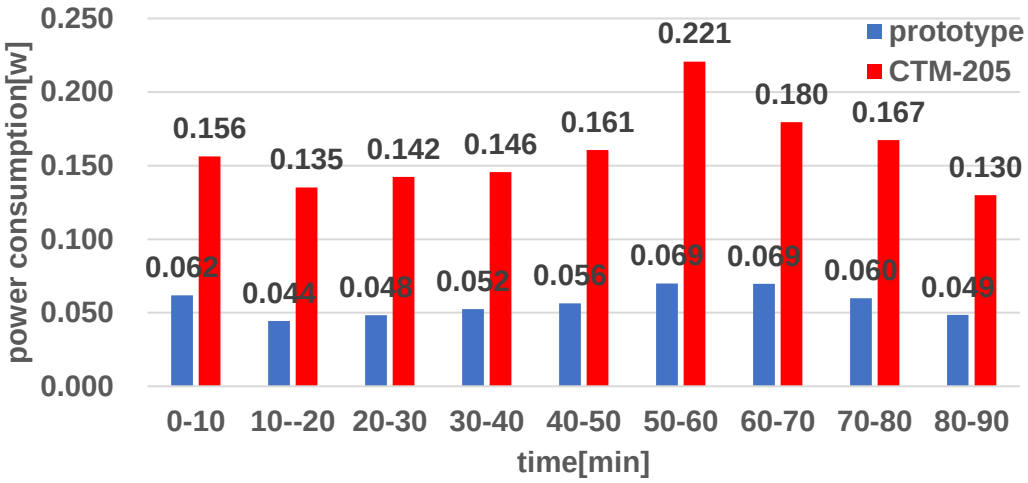

(b)

Figure 4-16 (a)Temperature comparison result of the fit prototype (b) Power consumption comparison result of the standard prototype

Figure 4-16 shows that the fast-changing core temperature could also be caught by the fit prototype thermometer. The power consumption of fit type was higher than the standard type, but it was much easier to be wear and more fit to the shape of our forehead.

4.3.3. Sucker type thermometer

(a) Methods

- Room temperature was set to 25±1˚C
- Male subjects (24 ±1years old) participated in the experiment.
- Lithium polymer battery (3200mAh, DC 5.07V, 1A max) was used as the power supply.
- The sucker prototype probe and the CTM-205 probe are secured to forehead with elastics.
- The experiment consisted of 30 minutes acclimation phase, a 10 minutes cycling phase, and another 20 minutes recovery phase.

(b) Results

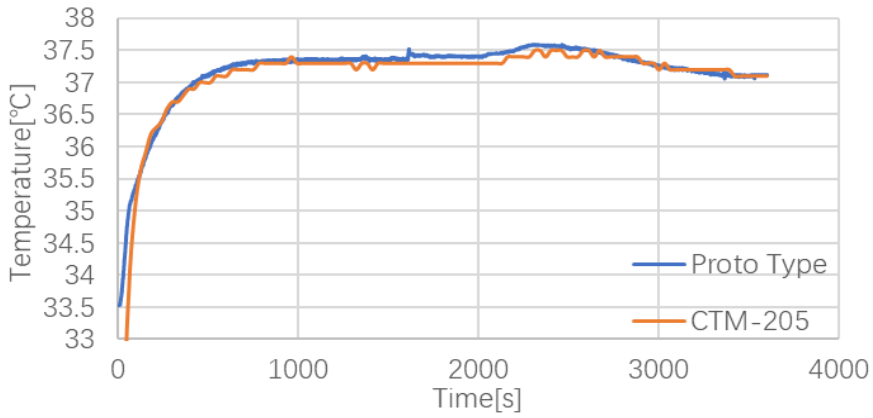

(a)

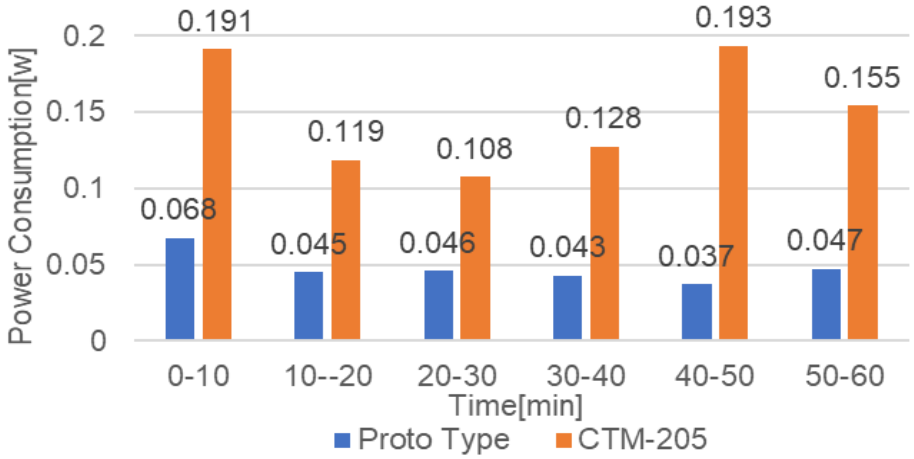

(b)

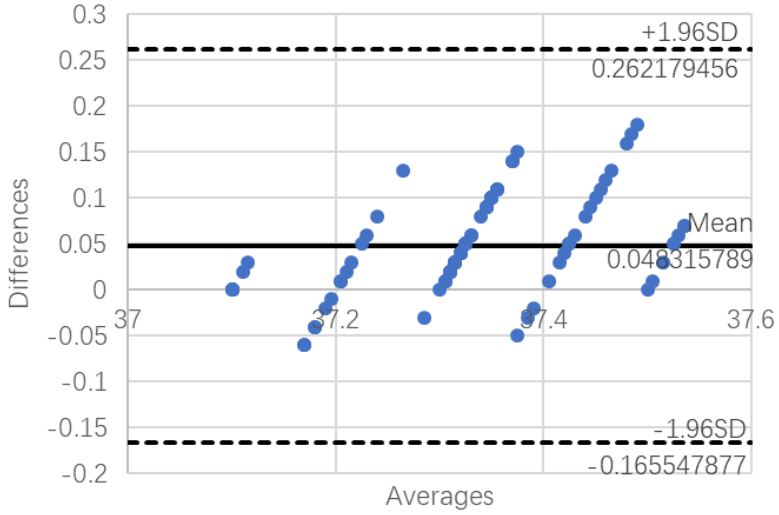

(c)

Figure 4-17 The measurement result of subject A (a) Temperature comparison result; (b) power consumption comparison. (c) Bland-Altman plots showing the difference between the sucker prototype and CTM205

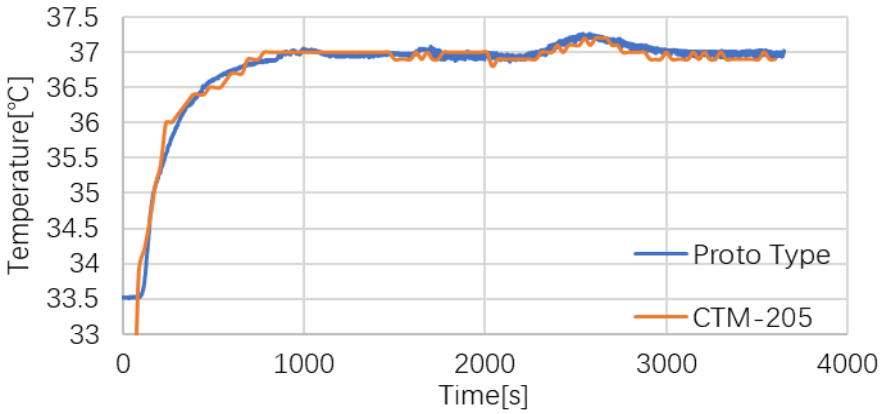

(a)

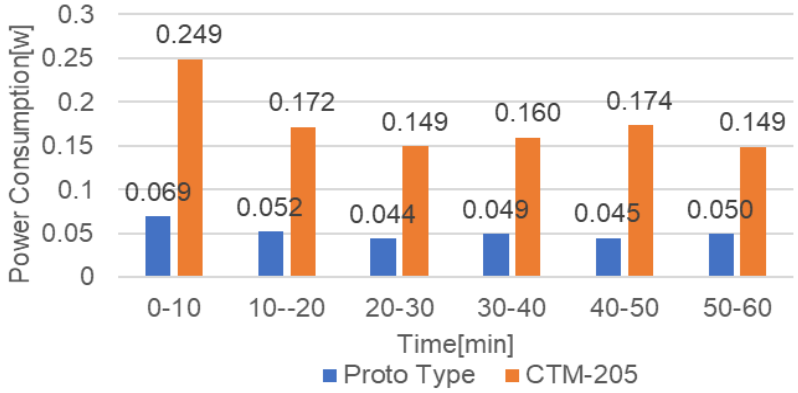

(b)

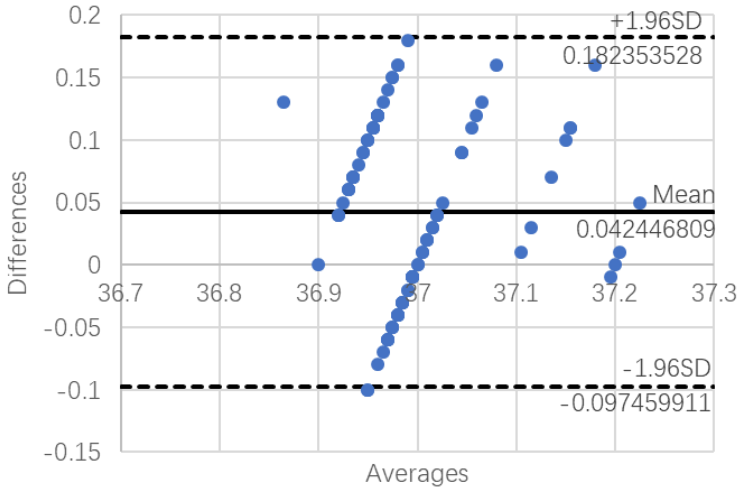

(c)

Figure 4-18 The measurement result of subject B (a) Temperature comparison result; (b) power consumption comparison. (c) Bland-Altman plots showing the difference between the sucker prototype and CTM205

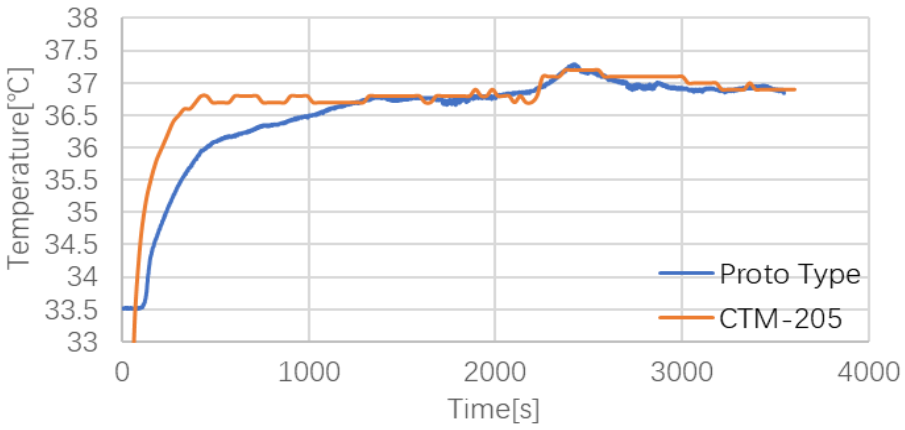

(a)

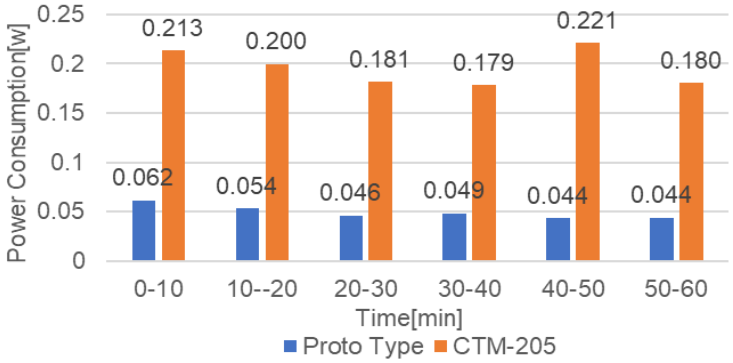

(b)

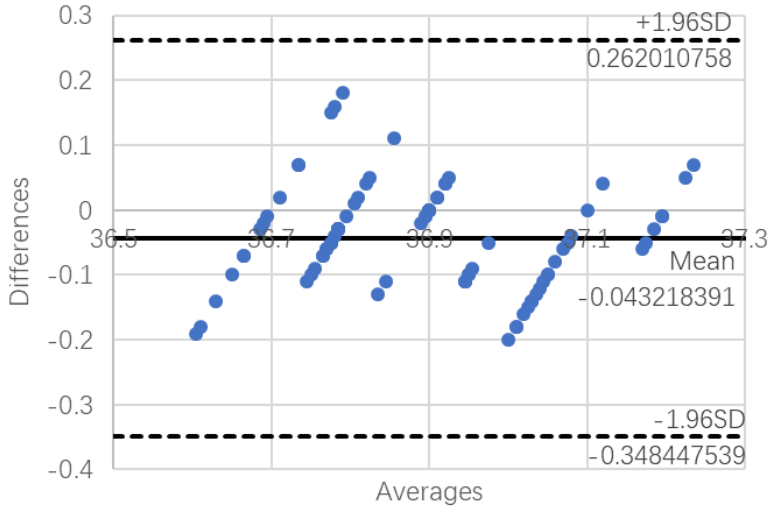

(c)

Figure 4-19 The measurement result of subject C (a) Temperature comparison result; (b) power consumption comparison. (c) Bland-Altman plots showing the difference between the sucker prototype and CTM205

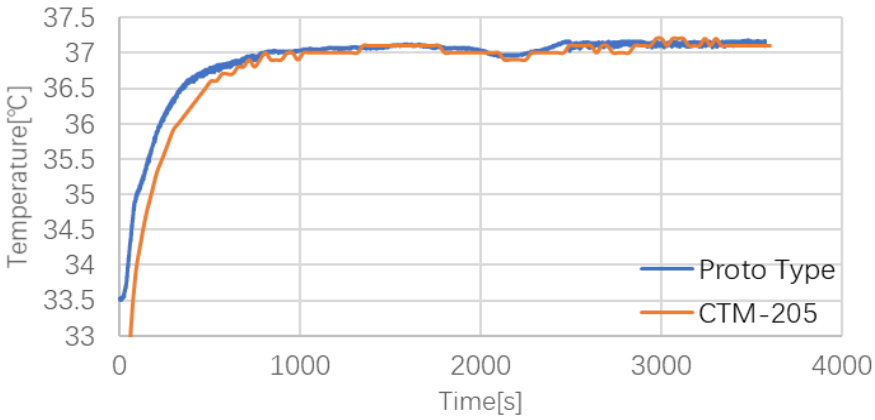

(a)

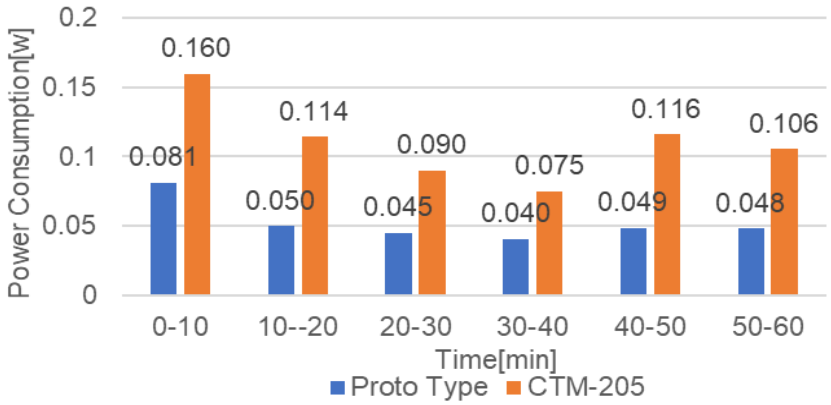

(b)

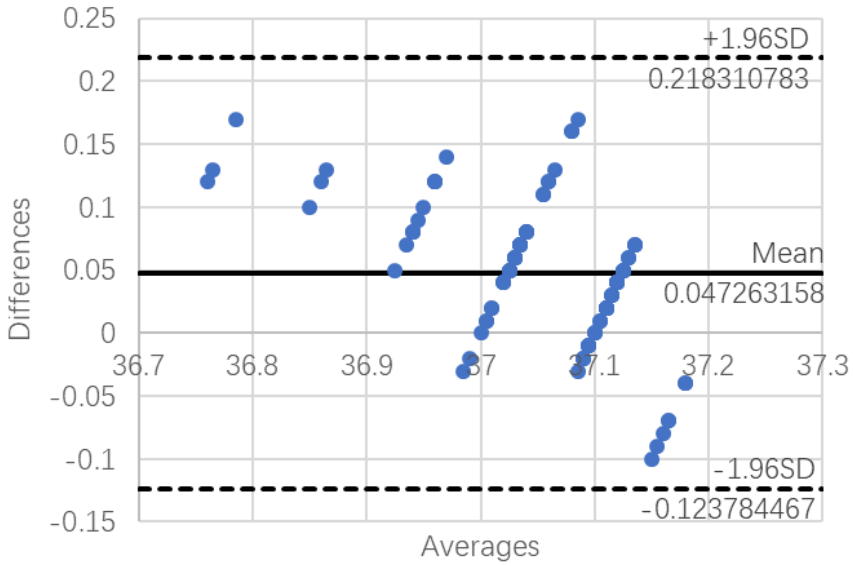

(c)

Figure 4-20 The measurement result of subject D (a) Temperature comparison result; (b) power consumption comparison. (c) Bland-Altman plots showing the difference between the sucker prototype and CTM205

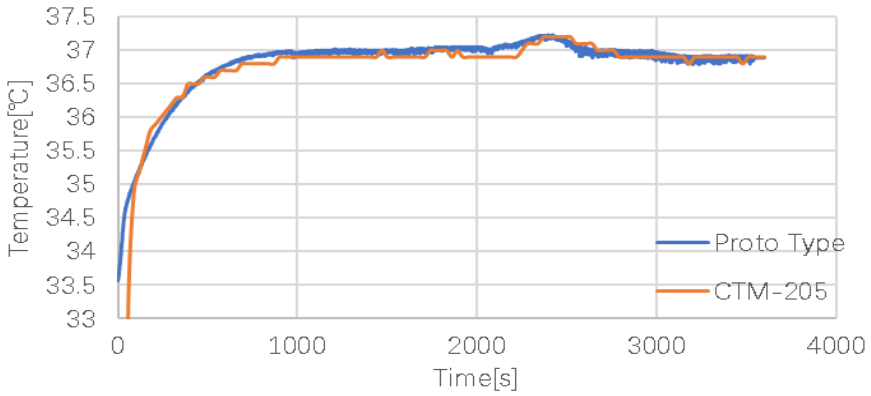

(a)

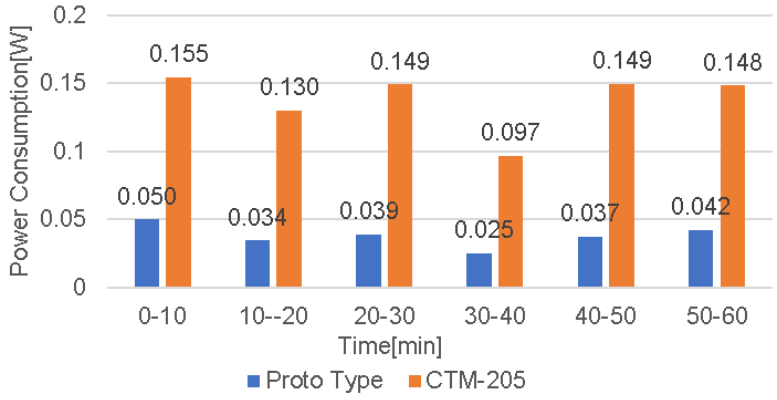

(b)

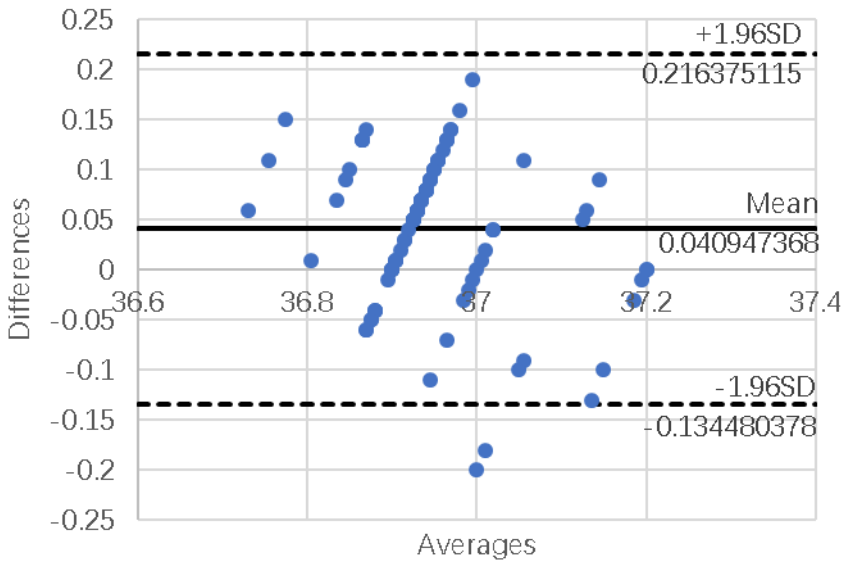

(c)

Figure 4-21 The measurement result of subject E (a) Temperature comparison result; (b) power consumption comparison. (c) Bland-Altman plots showing the difference between the sucker prototype and CTM205

Figure 4-17~ Figure 4-21 shows the results of the measurement. Subjects show nice accuracy in catching the fast-changing core temperature. Subject C had a head size smaller than other subjects, the unfit may be the reason for the inaccuracy of the first 20 mins.

All the power consumption comparison results show that sucker shape insulation of probe and surrounding skin are effective at reducing the power consumption.

4.4. Long term Measurement for wearable thermometer

4.4.1. Method

A young male subject participated in a prolonged measurement experiment. The experiment was conducted in a room with a room temperature of 25 degrees, and the subject would sleep and eat three times over 24 hours and record their exact timing. The experiment started at 13:30 on the first day and the trial device was used to record the depth temperature changes over 24 hours. The first 30 minutes of measurements with the device were the preparation time. The prototype probe was set to the forehead with an elastic hair band, and the data was stored on the SD card. The power consumed in the long-term measurement is also calculated from the voltage and resistance applied by the probe.

We expected the device to complete long measurements and capture the deep temperature changes due to feeding and sleeping. The experiment was approved by the ethics committee of Kanazawa University.

4.4.2. Results

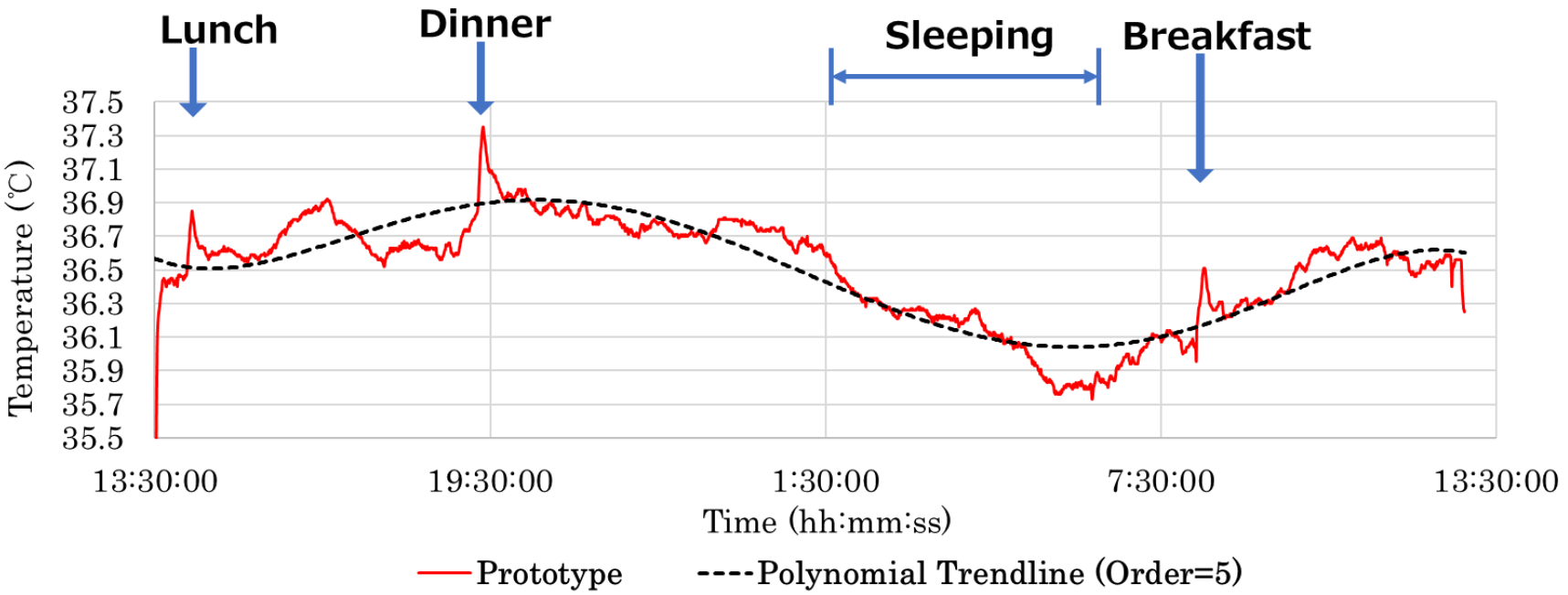

Figure 4-22 Temperature results of the long-term Experiment

Figure 4-22 shows the temperature results of the long-term measurement. The Polynomial Trendline with order=5 shows that the approximate temperature variation of this result is consistent with the body rhythm variation of high daytime and low nighttime sleep time; and there is a metabolism-induced temperature increase after food intake.

4.5. Discussion

We compared the actual temperature measurement error and power reduction during their movement by means of a rapid change test for three probes. We found in our tests that the fit-type probe was able to balance both power reduction and miniaturization, while maintaining a certain level of measurement accuracy.

In theory, the Standard type probe may be more power reduction; but in practice we found that the fit type, because of the thin edge, has a certain deformation ability, can more closely contact the forehead with the curvature of the skin. And this will reduce the temperature loss due to sweat evaporation, thus achieving a reduction in power consumption.

The long time measurement shows that our probe can complete long time measurement; and in this we found that the screen display actually consumes more heat than the probe itself. This can be improved by waking up the screen with a button, and in fact does not require the screen to be on display all the time.

References

1. SHIBAURA ELECTRONICS Co., L. SHIBAURA THERMISTORS: ELEMENTS & SENSORS 2018, 25.

5. Extending the high-temperature performance

5.1. Problem of the ZHF method in high temperature

The Zero-Heat-Flow method has proven excellent clinical performance[1], but it cannot work in a high-temperature environment.

The heater only works when T_{heater} is lower than T_{skin}, which means that when the ambient temperature of the probe is higher than CBT, the heater will be turned off. In such a situation, a temperature gradient from outside to inside will result in significant measurement errors.

This problem limits the use of this method so far only in stable clinical settings[2].

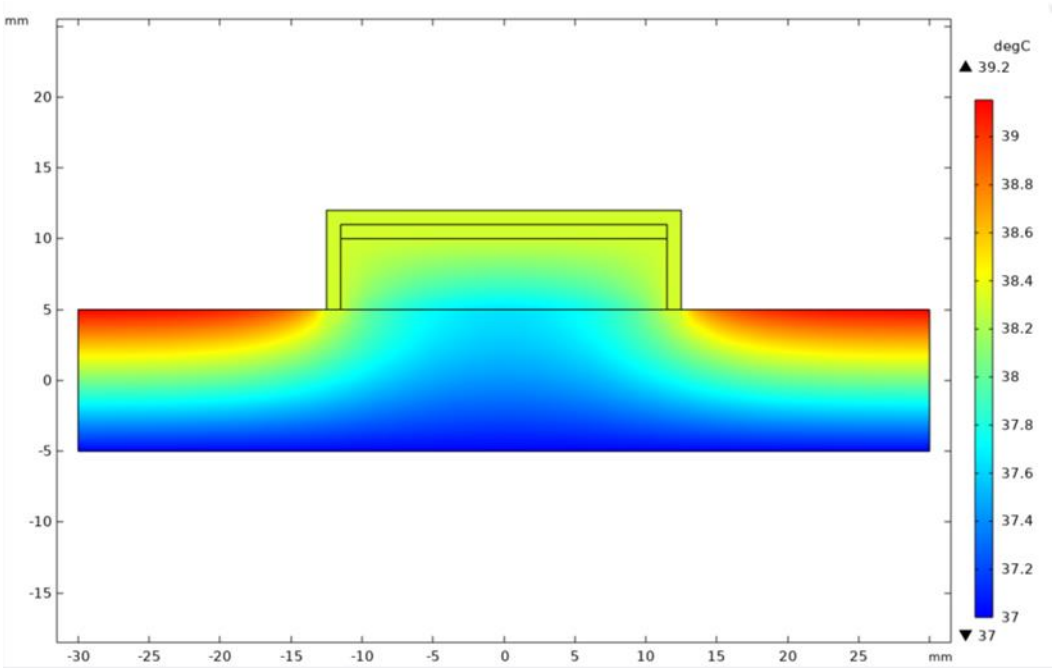

Figure5-1 The ZHF-type thermometer in a high-temperature environment

5.2. Proposal

Our co-author (T. T.)has demonstrated that a ZHF probe could maintain the heat equilibrium and measure in a high-temperature environment if a Peltier module and radiator were placed instead of a heater [3].

5.2.1. Peltier Module

Peltier modules take advantage of the Peltier effect: heat is absorbed or dissipated at the junction of two different conductors when an electric current passes through. This phenomenon was first discovered by the French scientist Peltier in 1834. He formed a closed circuit of the metals Bi and Sb, and by simply changing the direction of the current, he was able to achieve heating or cooling at the junction of the two conductors, with heat being transferred from one point to the other.

The internal structure of the Peltier module consists of semiconductor chips made of N-type and P-type bismuth telluride materials. These chips are connected in series by electrical connections but in a parallel thermodynamic arrangement. A highly thermally conductive ceramic plate is used as the thermal and cold contact surfaces to achieve the best heat transfer performance between the module's high and low-temperature ceramic surfaces.

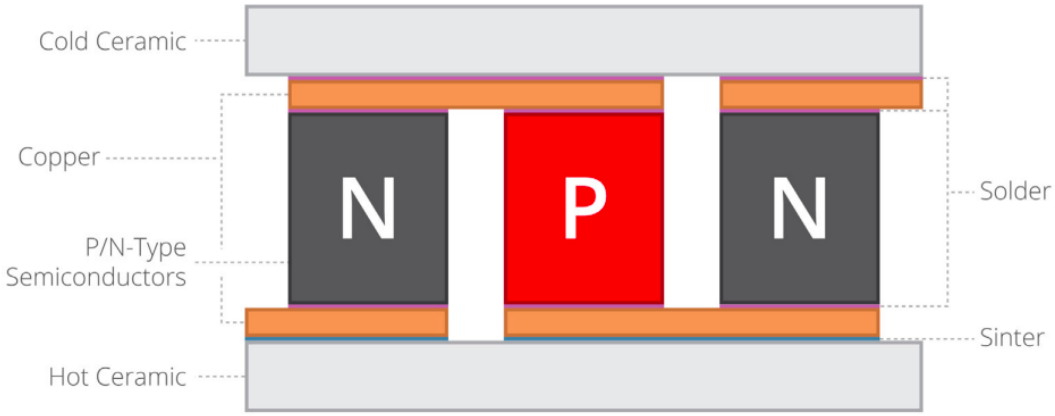

Figure 5-2 Cross Section of Peltier Module

5.2.2. Design with the Peltier module

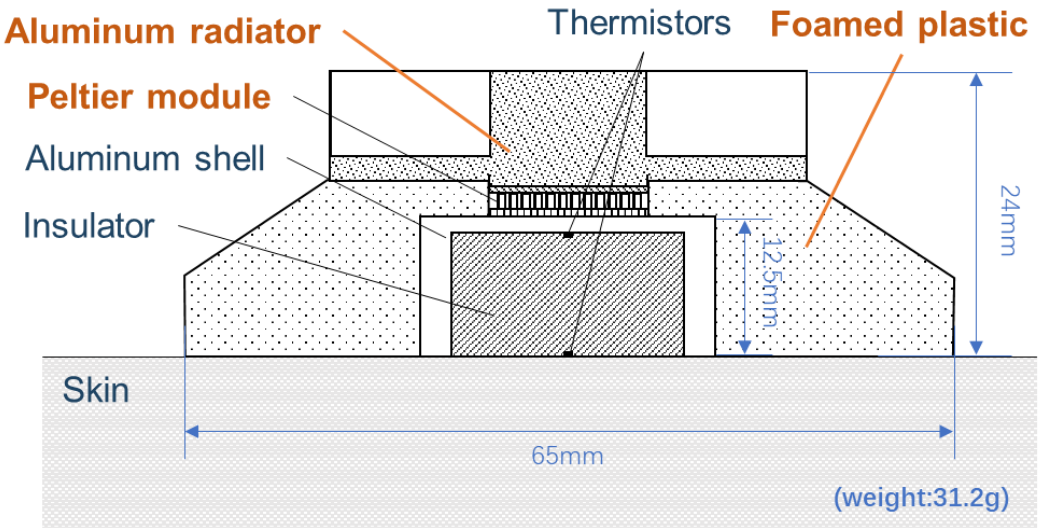

Figure5-3 Cross-section of the prototype probe

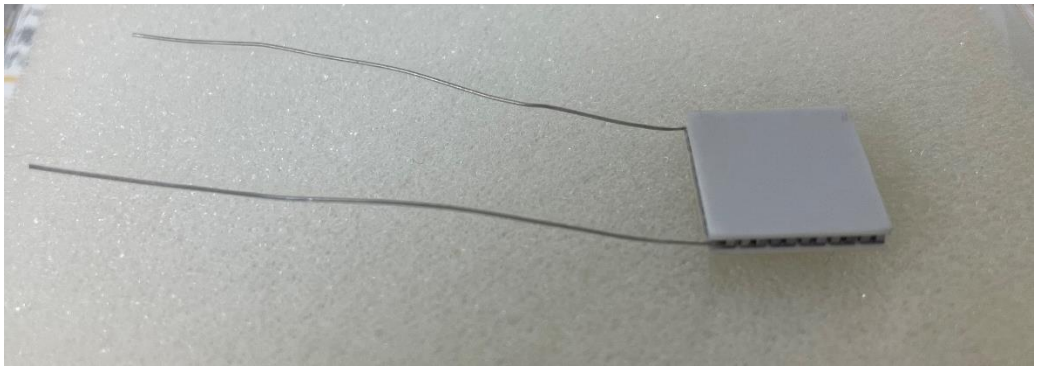

Figure 5-4 The Peltier module used in the probe (NL1023T-03AC, Marlow Industries, Inc.)

Based on the results of the previous study, a prototype Zero-Heat-Flux probe using a Peltier element was designed, as shown in **Figure 5-3**. The figure shows the cross-section of the prototype probe, which consists of a radiator, a Peltier module (NL1023T-03AC, Marlow Industries, Inc., **Figure 5-4**), thermistors (PSB-S7, SHIBAURA Electronics Co., Ltd.), an aluminum shell, and insulation material (foamed plastic). According to our previous study[4], the peripheral skin surface around the aluminum shell is covered by an insulator in order to reduce heat dissipation from the skin near the shell son that to reduce power consumption and improving the wearability of the probe. The **Figure 5-5** shows the appearance of the prototype probe, which weighs 31.2g.

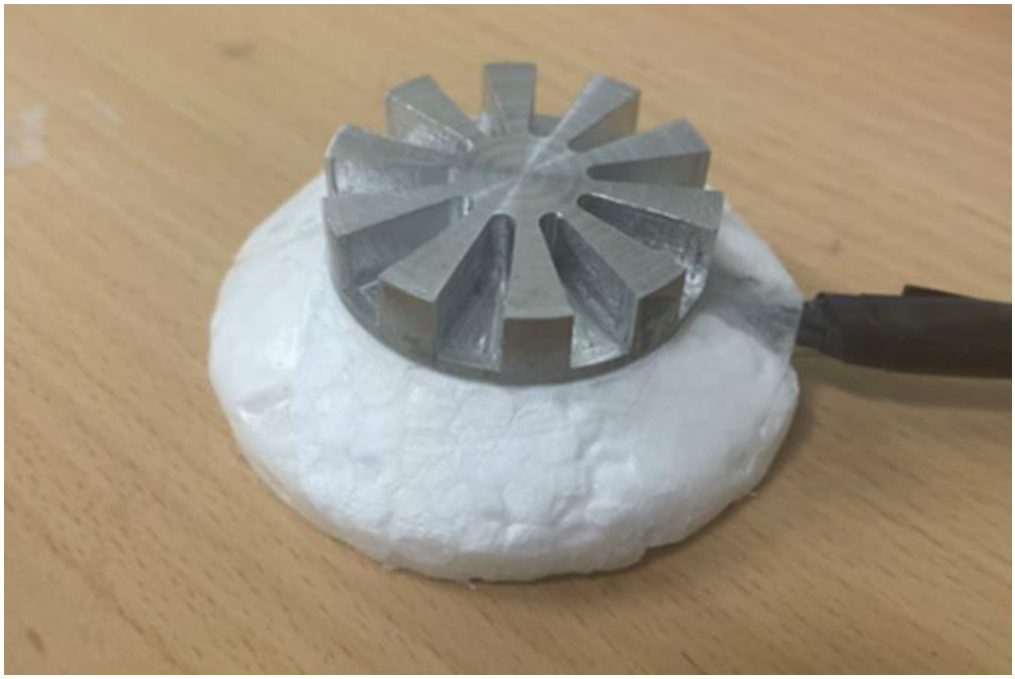

Figure5-5 Cross-section of the prototype probe

5.2.3. The Prototype thermometer with Peltier Module

The block diagram of the control system is shown in **Figure 5-6**.

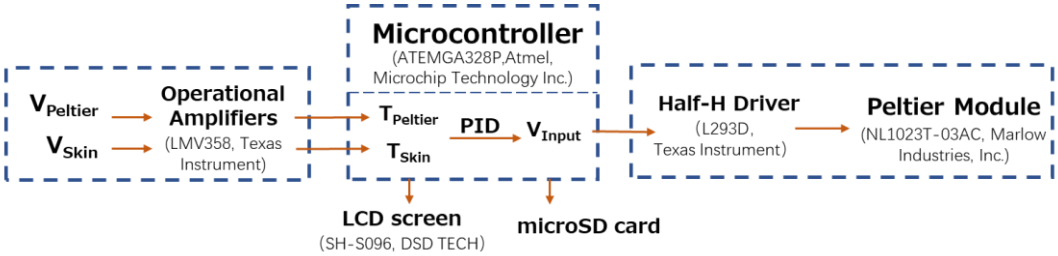

Figure 5-6. Block diagram of the control system

The operation of the control system is to control the current drain of the Peltier Module so as to maintain the Peltier side temperature at the same temperature as the skin surface temperature. The potential differences of the thermistors on the skin side and the Peltier side (V_{skin} and $V_{peltier}$) in constant current operation are amplified by operational amplifiers and sent to the microcontroller unit (ATmega328P, Atmel, Microchip Technology Inc (MCU)). The MCU reads the voltages and uses a correction formula to obtain the temperatures on the skin and Peltier element sides (T_{skin}, $T_{peltier}$). Based on these two temperatures, MCU uses a PID algorithm to get the voltage added to the Peltier element (V_{input}) and passes it to the half-H driver.

The Half-H Driver (L293D, Texas Instrument) capable of supplying high voltage and high current (max. 36 V, 600 mA) and

reversing the polarity was used to power the Peltier module.

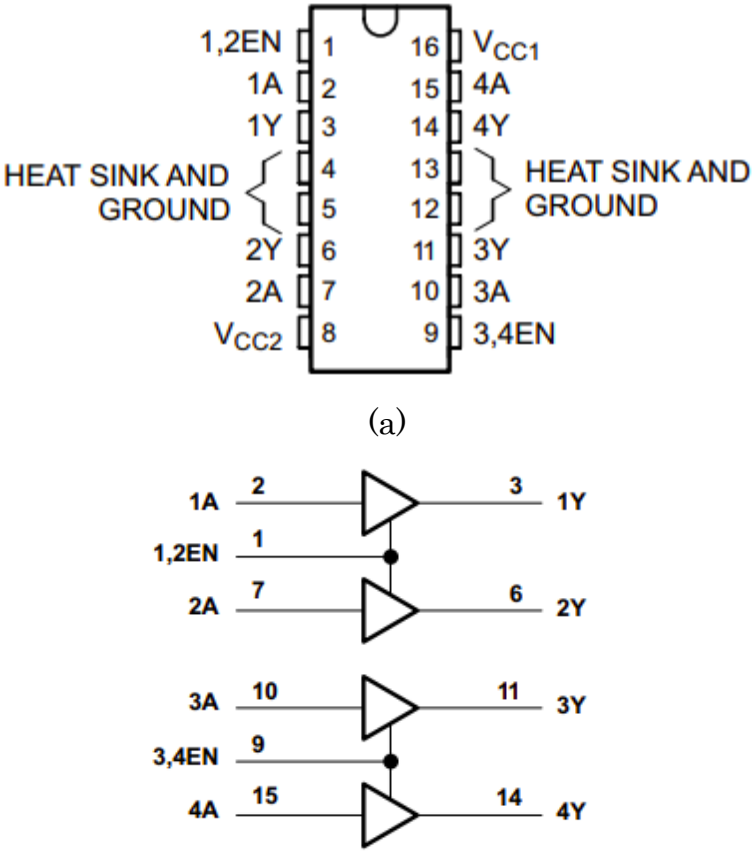

Figure 5-7 (a) Pin Configuration of L293D (b)Logic Diagram of L293D

The servo control loop gains of proportional, integral, and differential operation (Kp, Ki, and Kt) were determined based on the finite element analysis results described below, using the values shown in Table 2. So that when the outside temperature is lower than the skin temperature, heat flow is compensated for by heating the body surface as in conventional core body thermometers. When the ambient temperature is higher than the skin temperature, the heat flow can still be compensated by changing the current direction, cooling the body surface, and maintaining regular measurements.

For data collection, the results (T_{skin}, $T_{Peltier}$, and U_{input}) were recorded with a 16GB micro-SD card and were displayed on a 0.9-inch LCD screen (SH-S096, DSD TECH).

Reference

1. Dahyot-Fizelier, C.; Lamarche, S.; Kerforne, T.; Bénard, T.; Giraud, B.; Bellier, R.; Carise, E.; Frasca, D.; Mimoz, O. Accuracy of Zero-Heat-Flux Cutaneous Temperature in Intensive Care Adults. *Crit. Care Med.* **2017**, doi:10.1097/CCM.0000000000002317.
2. Tamura, T.; Huang, M.; Togawa, T. Current Developments in Wearable Thermometers. *Adv. Biomed. Eng.* **2018**, *7*, 88–99, doi:10.14326/abe.7.88.
3. Tamura, T.; Nemoto, T.; Togawa, T. A Zero-Heat-Flow Transducer for Monitoring Perfusion Blood Temperature. *IEEE Trans. Biomed. Eng.* **1979**, *BME-26*, 644–646, doi:10.1109/TBME.1979.326548.
4. S. Muto, N. Sakai, M. Nogawa, H. Naito, S. Tanaka, T. Nemoto, T. Togawa Development of a Wearable Body Core Temperature Monitor -Preliminary Study for Reduction of Power Consumption-. In Proceedings of the Proceedings of the Joint International Conference of BDAHI2016 and u-Healthcare2016 (BigHealth-2016); 2016; p. 33.

6. Finite Element Model Analysis

Before the actual fabrication of the probe, we performed a finite element model analysis to verify whether our design could compensate for heat flow and accurately detect core body temperature at different external temperatures. We built a 3D model based on COMSOL Multiphysics' LiveLink™ for SOLIDWORKS®.

6.1. Models

6.1.1. Peltier Module Models

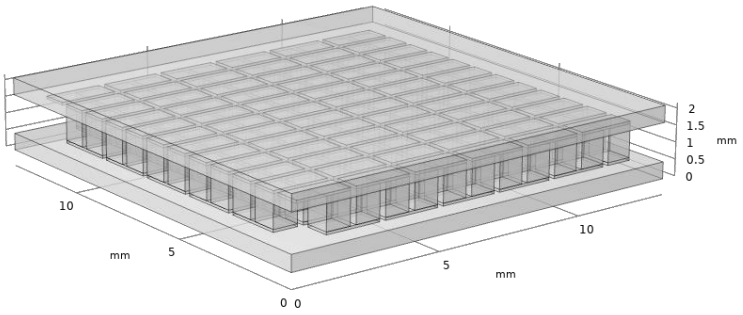

Figure 6-1 The Outlooking of Peltier Module Model

First, we made the Peltier Module Model, and verify the accuracy of the model in Comsol. Heat Transfer Module and AC/DC Module from COMSOL 5.6a were used to make the Peltier Module Models. We have taken reference from the official COMSOL webpage for a tutorial on how to make the model, and we have taken the dimensions of the actual Peltier and made an equivalent model of the actual Peltier to ensure that the simulation works properly.

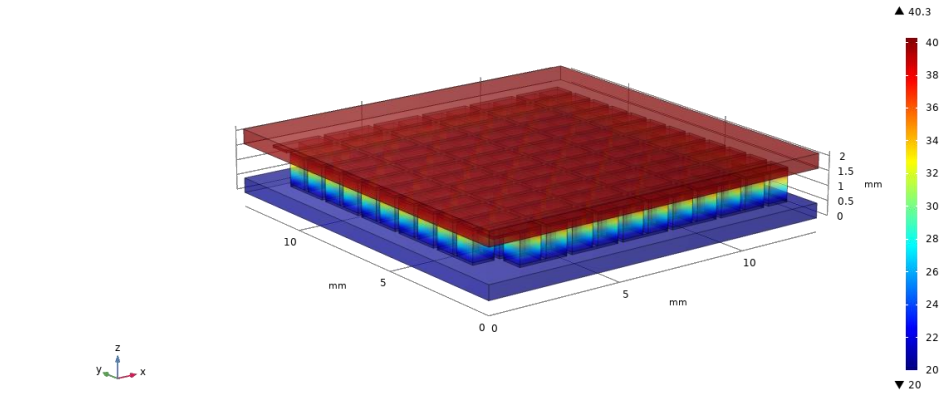

(a)

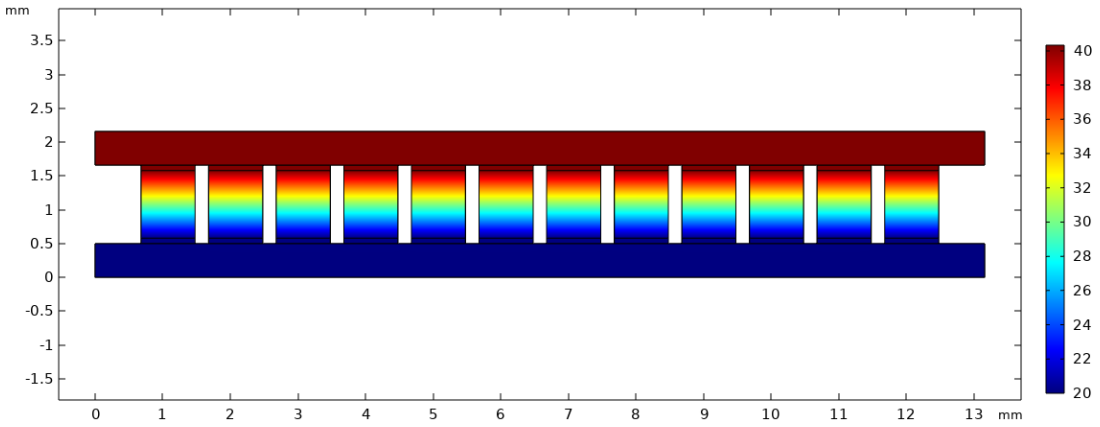

(b)

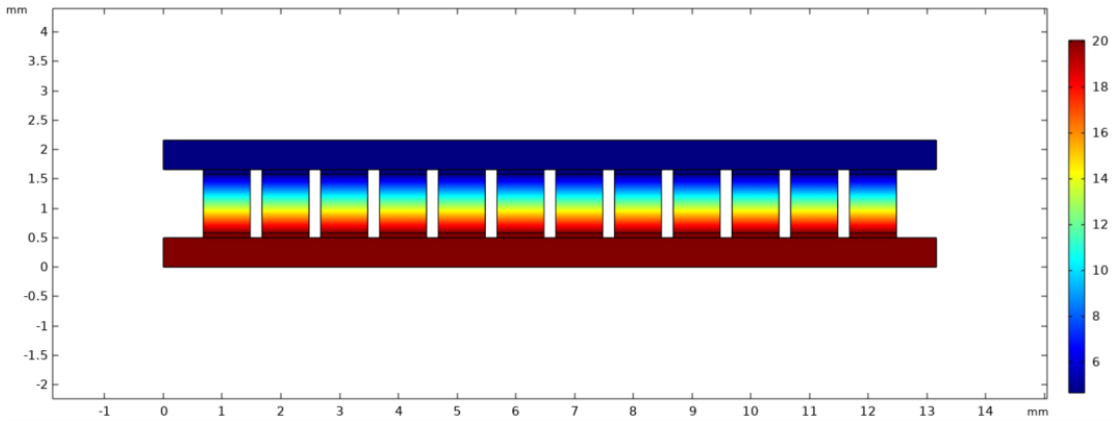

(c)

Figure 6-2 The temperature results of the Peltier Module Model. (a) The 3D result(I=0.3A). (b) The 2D result (x=6.3mm,I=0.3A) (c) The 2D result (x=6.3mm, I=-0.3A)

We set the current through the Peltier to 0.3 A and observed whether the temperature results were as expected. The results show that when current is applied to the Peltier in our model, the heat on

one side flows to the other side by the action of the current, with one side being hot and the other cold as shown in Figure 6-2 (b). When the direction of the current switched, the high-temperature side switched accordingly (Figure 6-2(c)).

6.1.2. Prototype Models

In this Prototype model, the prototype probe is placed on a thermally homogeneous cylindrical skin tissue with a radius of 80 mm and a thickness of 10 mm. The components in the probe are also thermally homogeneous.

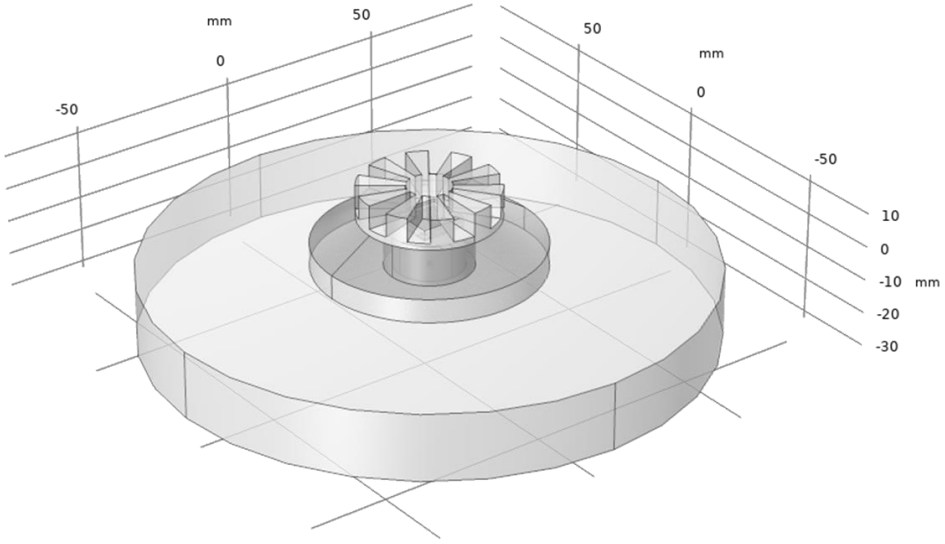

Figure 6-3 The Peltier Module Model.

6.2. Analysis settings

The physical property parameters in Table 6-1 are referenced from the COMSOL v5.6 material library.

Table 6-1. The assumed values of the probe materials

Component	Thermal Conductivity	Density	Specific heat	Electrical Conductivity	Seebeck Coefficient
	W/(mK)	kg/m3	J/(kg·K)	S/m	V/K
Skin	0.37	$1.1x10^3$	$3.4x10^3$	/	/
Aluminum	240	$2.7x10^3$	900	/	/
Closed-cell foam	0.04	210	16	/	/
Foam	0.04	24	2.2	/	/
Alumina	27	$3.9x10^3$	900	/	/
Copper	400	$9.0x10^3$	390	$6x10^7$	/
P-Bi2Te3	1.6	$7.7x10^3$	150	$8.70x10^4$	$2.1x10^{-4}$
N-Bi2Te4	1.6	$7.7x10^3$	150	$8.70x10^4$	$-2.1x10^{-4}$

For the boundary conditions, the contact surfaces of the skin and the probe with the outside air are set up for natural thermal convection. The convective heat transfer coefficient (free convection and gas) was set to 5 W/(m2·K) to be consistent with skin (Table 6-2), ignoring the effect of probe geometry on this coefficient [1]. In addition, the lateral borders of the skin are set to be thermally insulated.

Table 6-2. The assumed values in the finite element analysis

Quantity	Notation	Assumed Value
External temperature	T_{EXT}	25/42℃
Core body temperature	T_{CBT}	37℃
Convection heat transfer coefficient (Free convection, gases)	h	5 W/(m^2·K)
Proportional gain	K_p	3
Integral gain	K_i	1
Derivative gain	K_d	1

As listed in Table 6-2, we simulated the measurements that the prototype probe could achieve after a certain measurement duration and the time required to reach a steady-state measurement under two external temperature conditions (25/42 °C). During this process, the PID algorithm is used to calculate the input voltage Vinput applied to the Peltier Module, while its PID parameters are listed in Table 6-2.

6.3. The initial conditions

For the initial condition setting, the bottom surface of the skin was set to a deep temperature (37 °C). The initial temperature of the entire probe was set to 25 °C.

In the initial stage of the experiment, we did not initialize the skin.

However, during the temperature change we found that setting the whole skin tissue to 25 degrees without skin initialization leads to a large amount of heat transfer in the premeasurement period, compromising the prediction of measurement preparation time that we value (Figure 6-4).

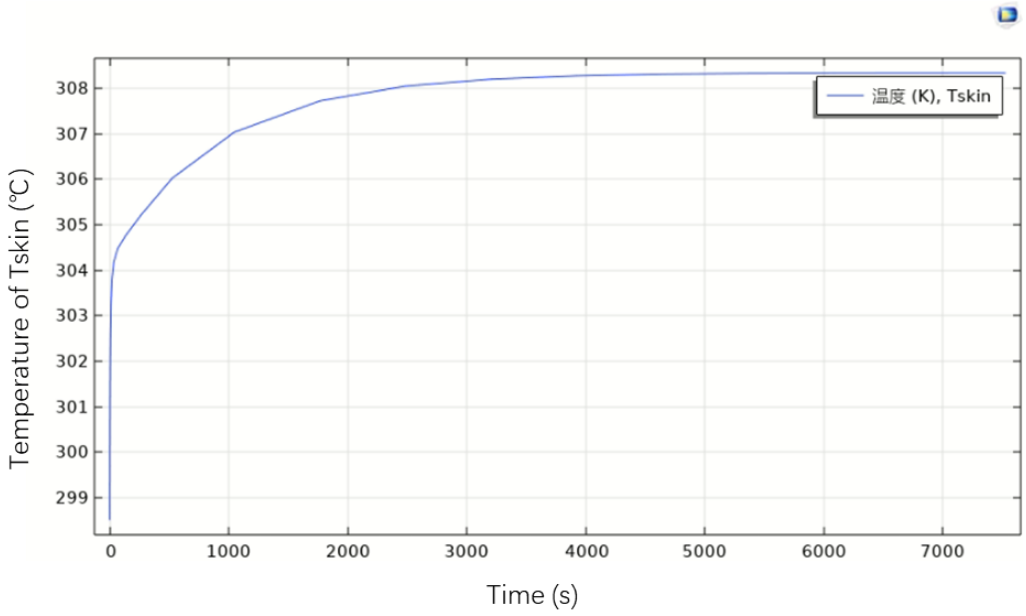

(a)

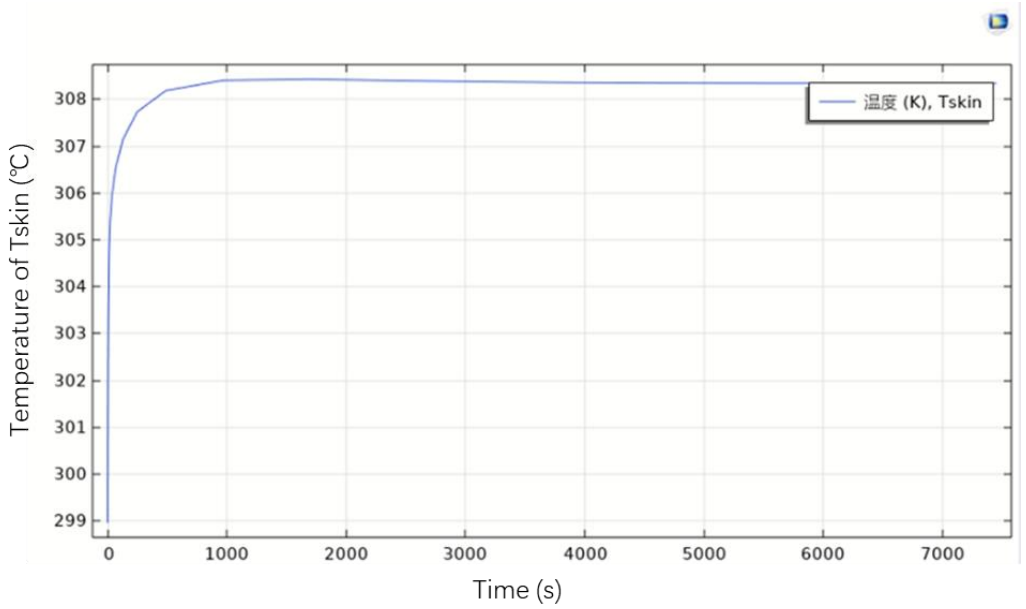

(b)

Figure 6-4 The temperature results without initialization (a) and with the initialization(b).

We therefore initialized the skin, i.e., set the skin and room temperature for the same condition, so that it was left until the temperature no longer changed.

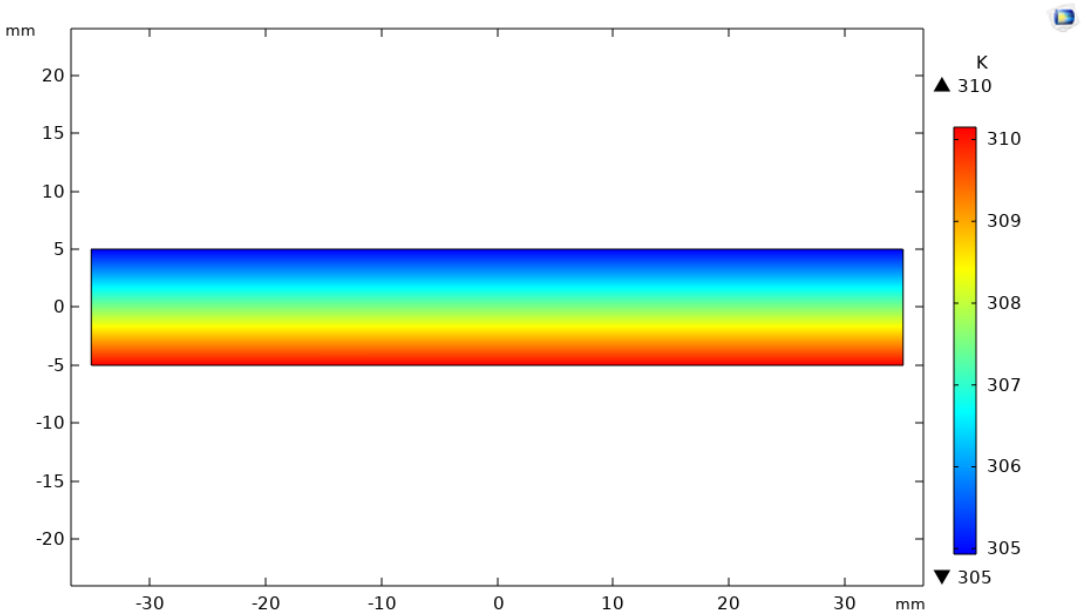

Figure 6-4 Initialization temperature of the skin (Room temperature: 25 degrees)

We placed a homogeneous skin tissue (y=10mm) in the same condition at an external temperature of 25 degrees for 3000 s and obtained the temperature results as in Figure 6-4. We selected several points at different depths in Figure 6-4 (Table 6-3) and read their temperatures to produce a calibration form (Figure6-5).

Table 6-3 Sampling in skin temperature results

Y [mm]	Y [m]	Distance from the CBT [mm]	Temperature [degreeC]
-4.7012	-0.0047	0.2988	309.99
-3.0836	-0.00308	1.9164	309.15
-1.7693	-0.00177	3.2307	308.46
-0.05055	-5.1E-05	4.94945	307.57
2.0726	0.002073	7.0726	306.46
3.6902	0.00369	8.6902	305.61
4.1957	0.004196	9.1957	305.35

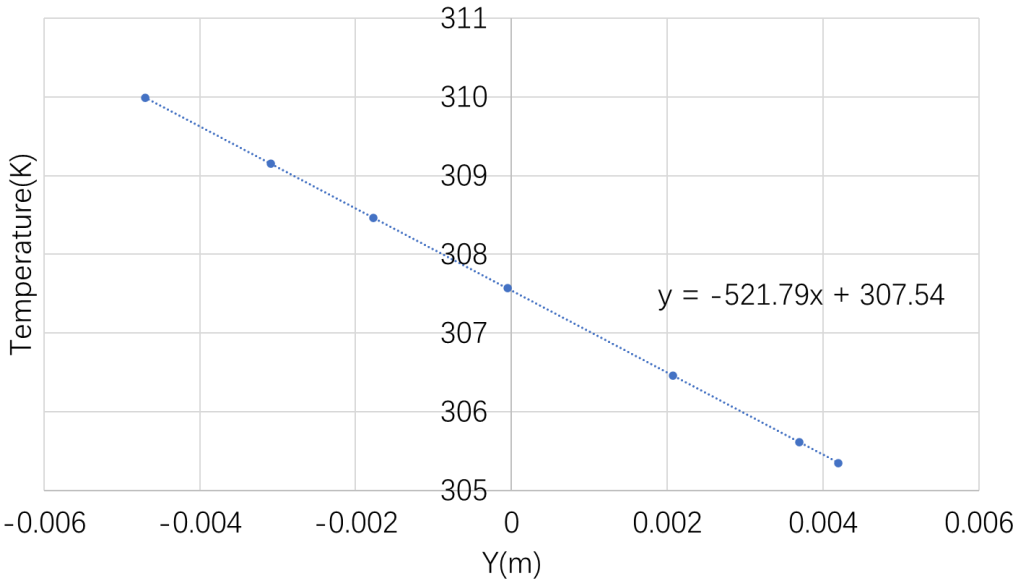

Figure 6-5 Calibration of the skin initial temperature (T_{air}=25degrees, Y_{max}=10mm).

The calibration forms were applied to the initialization of the deep temperature in the overall model

6.4. Analysis results

6.4.1. In Room Temperature

The temperature results (Figure 6-6) show that the Peltier can replace the heater as a means of heating the inside of the probe and maintaining measurements in a room temperature environment, and that our PID algorithm can accurately follow the changes between temperatures and control the voltage applied to the Peltier.

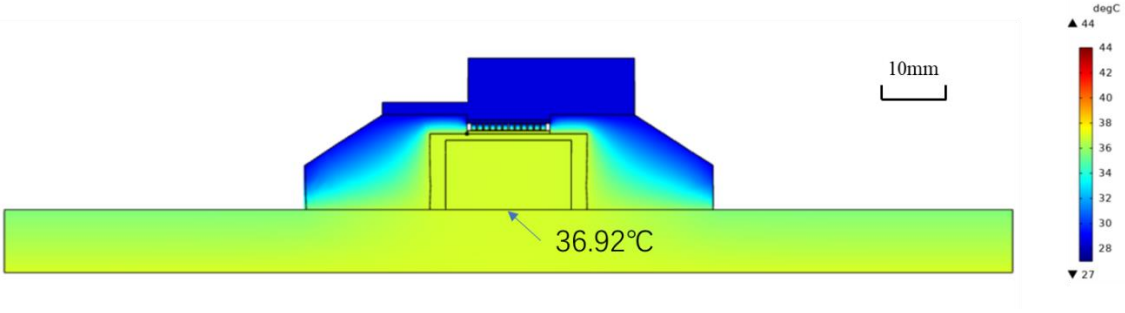

(a)

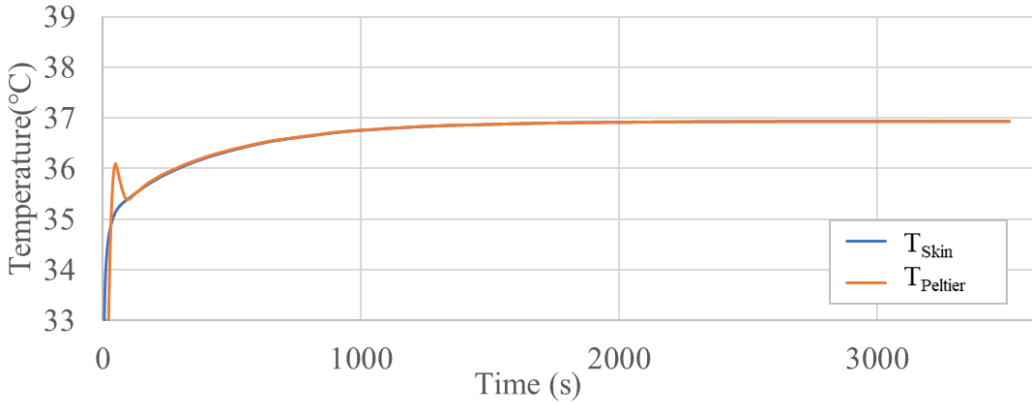

(b)

Figure 6-6 Results of finite element analysis (TAir = 25°C, t = 3600 s) (a)Temperature results (b) Thermistor temperature results from finite element analysis

6.4.2. In High Temperature

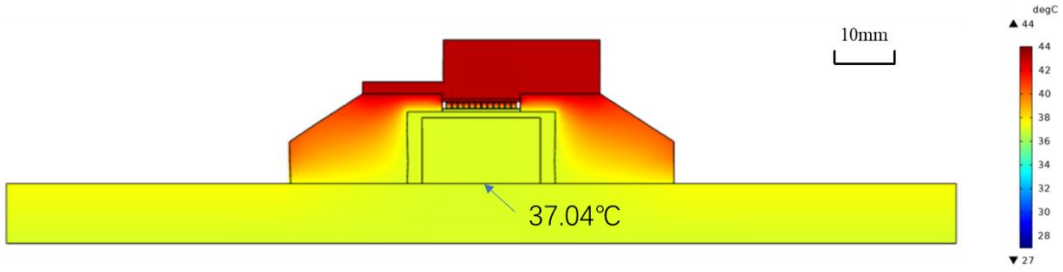

(a)

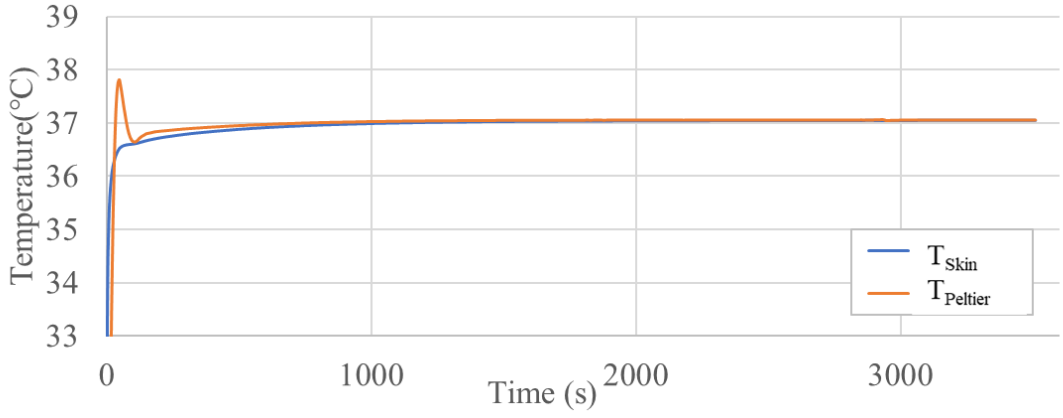

(b)

Figure 6-7 Results of finite element analysis (T_{Air} = 42°C, t = 3600 s) (a)Temperature results (b) Thermistor temperature results from finite element analysis

As shown in Figure 6-7, the temperature results show that the Peltier can cooling the inside of the probe and maintaining measurements in a room temperature environment, and that our PID algorithm can accurately follow the changes between temperatures and control the voltage applied to the Peltier.

6.5. Analysis with a different probe radius

Simulations were performed to determine the relationship between the probe radius and the error in the measured results of the probe. The cross-sectional temperature results are shown in Figure 6-8. Here, we selected a higher subcutaneous tissue thickness (15mm) for a more obvious observation of the relationship between the probe radius and the measurement results. The convective heat transfer coefficient was set to 28.5 W/(m2·K).

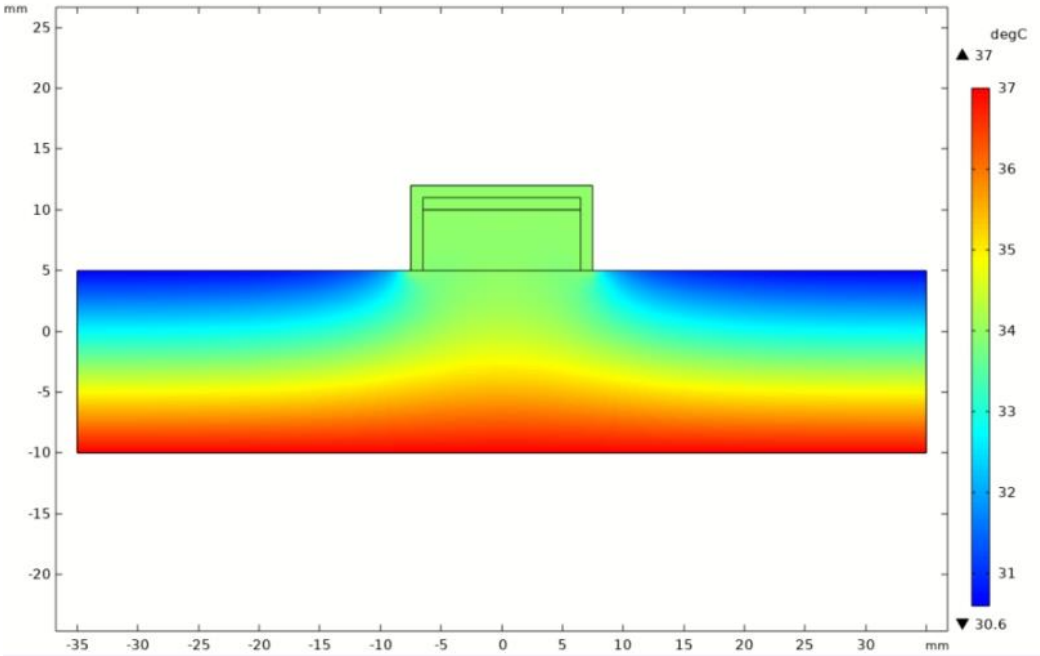

(a)

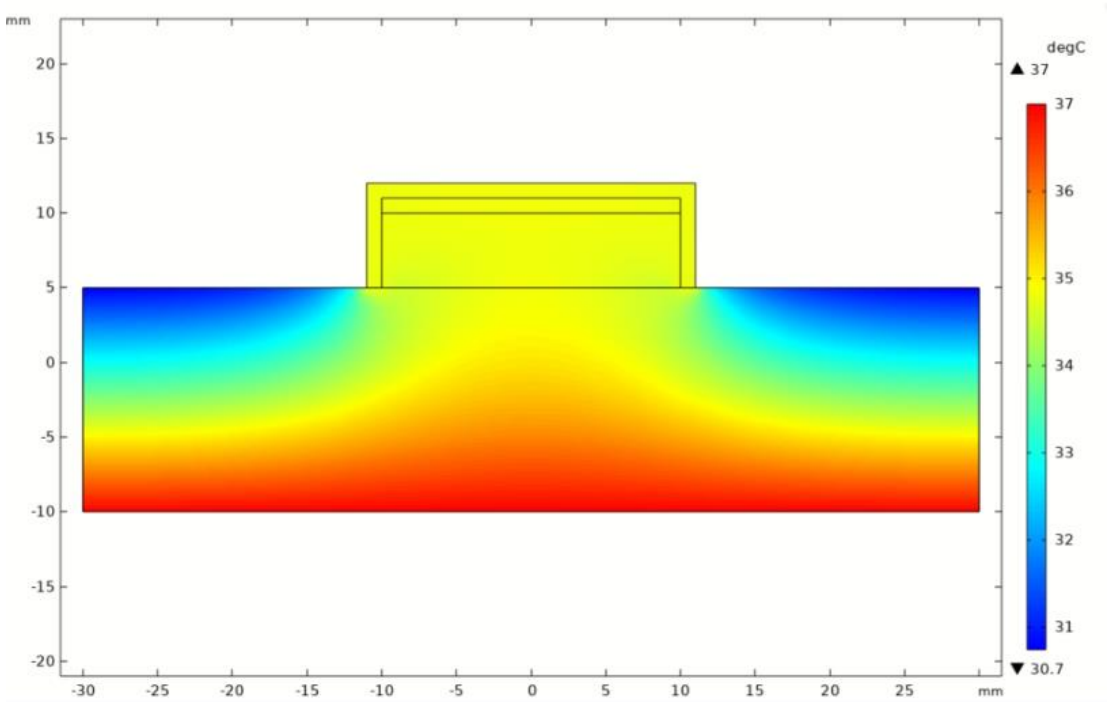
mm
20
15
10
5
0
-5
-10
-15
-20
-30
-25
-20
-15
-10
-5
0
5
10
15
20
25
mm
degC
▲ 37
37
36
35
34
33
32
31
▼ 30.7

(b)

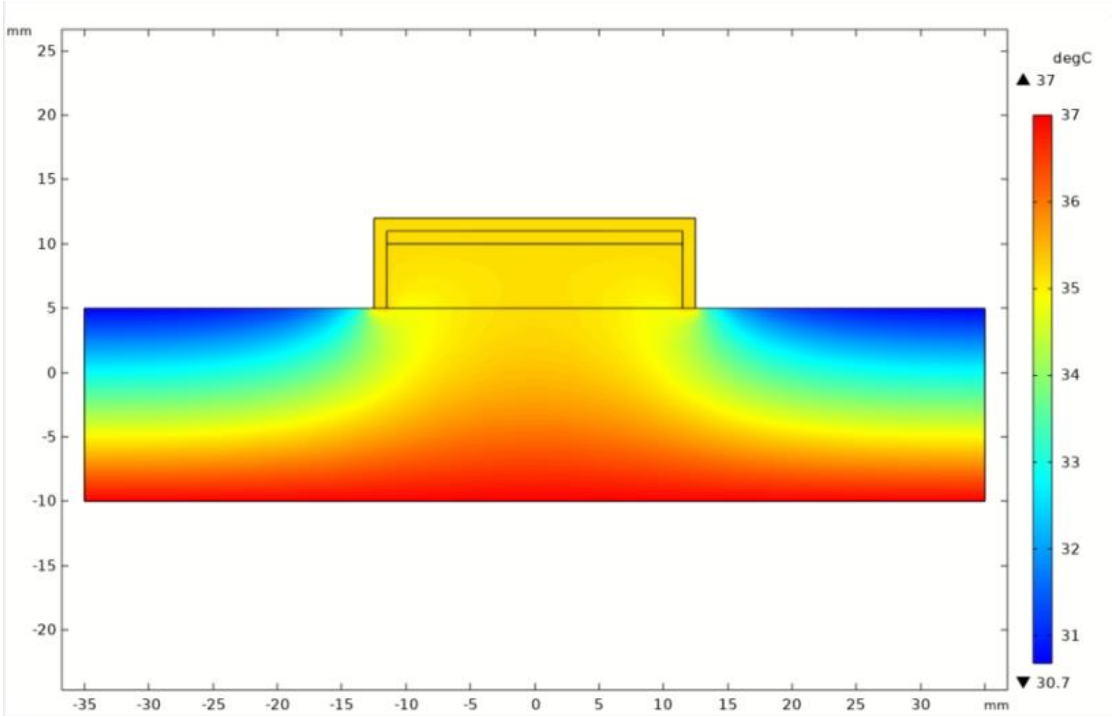
mm
25
20
15
10
5
0
-5
-10
-15
-20
-35
-30
-25
-20
-15
-10
-5
0
5
10
15
20
25
30
mm
degC
▲ 37
37
36
35
34
33
32
31
▼ 30.7

(c)

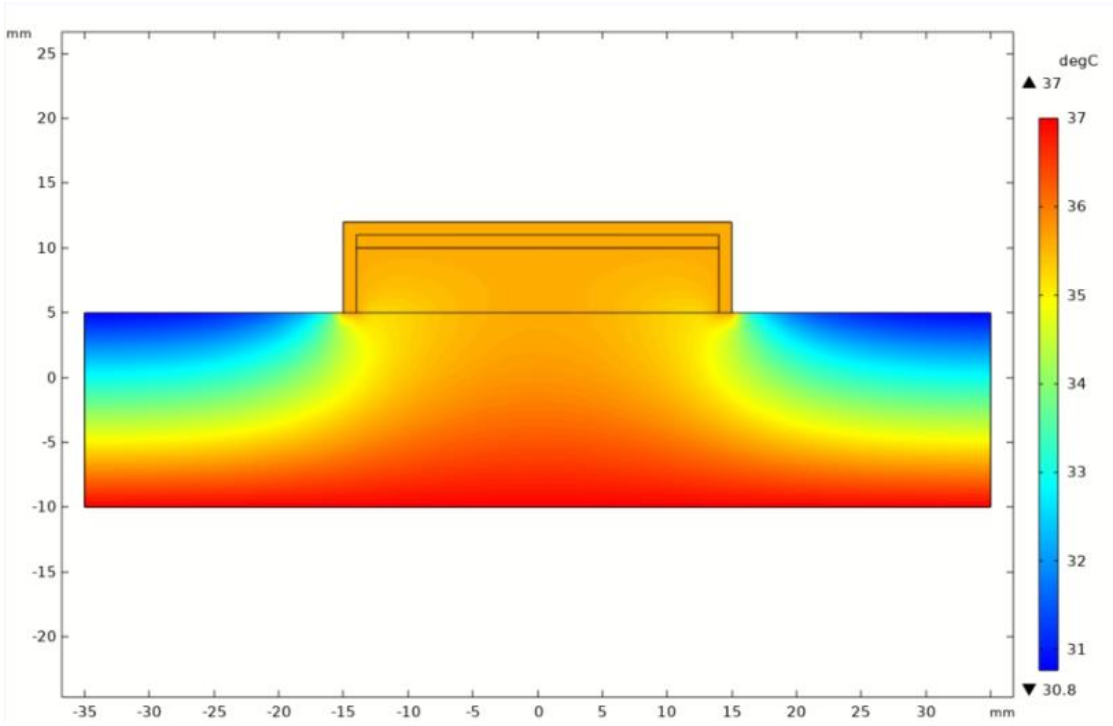

(d)

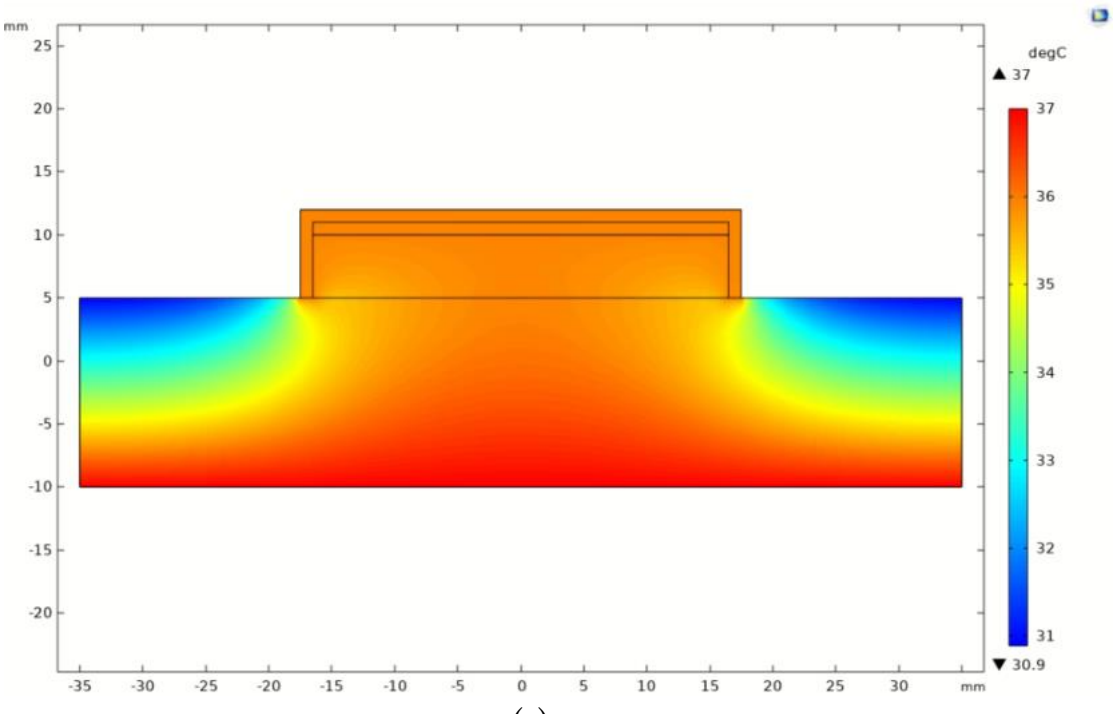

(e)

Figure 6-8 The 2Dtemperature results of different Diameter D of the ZHF probe. (Tair=25℃, Thickness of the skin d=15mm) (a) D=15mm (b) D=20mm (c) D=25mm(d) D=30mm (e) D=35mm

The relationship between the probe radius and the measurement results is shown in Figures 6-9. It can be seen that for thicker subcutaneous tissues, the larger the probe radius, the closer the measured results are to the true actual temperature.

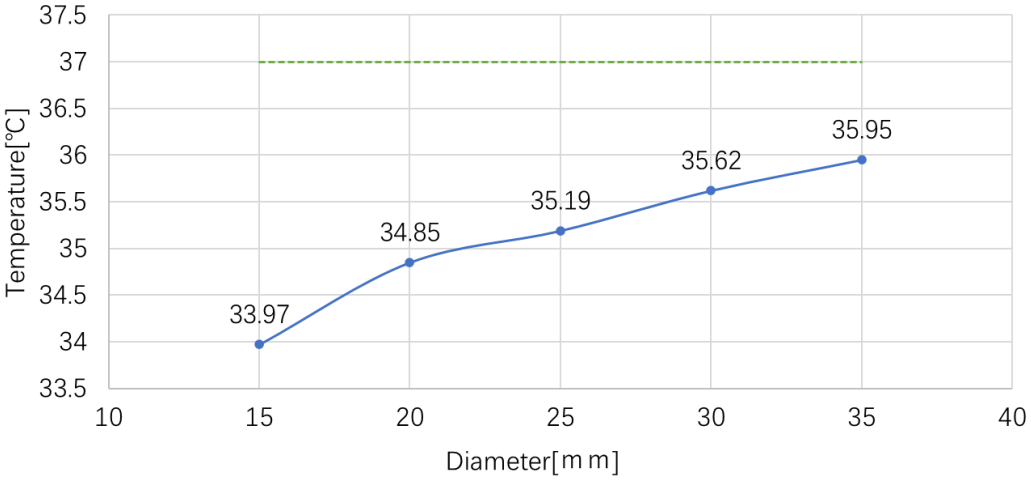

Figure 6-9 The relationship between the radius of the ZHF probe and the measured temperature

Therefore, it is highly important to choose the right probe radius. A probe radius that is too small will make it easier to wear, but will result in measured temperature results that are highly influenced by the thickness of the subcutaneous tissue. A larger probe radius will bring the results closer to the true temperature, but will tend to impede movement.

6.6. Analysis with different thicknesses of the tissues

To investigate the effect of skin thickness under the probe on the measurement results of the two probes, we did simulation experiments in two environments at high temperature (42°C) and low temperature (25°C) to simulate the equilibrium state temperature results of the two probes (ZHF probe and prototype probe) at different skin thicknesses (5-40 mm).

Figures 6-10 through 6-13 show the results of these simulations.

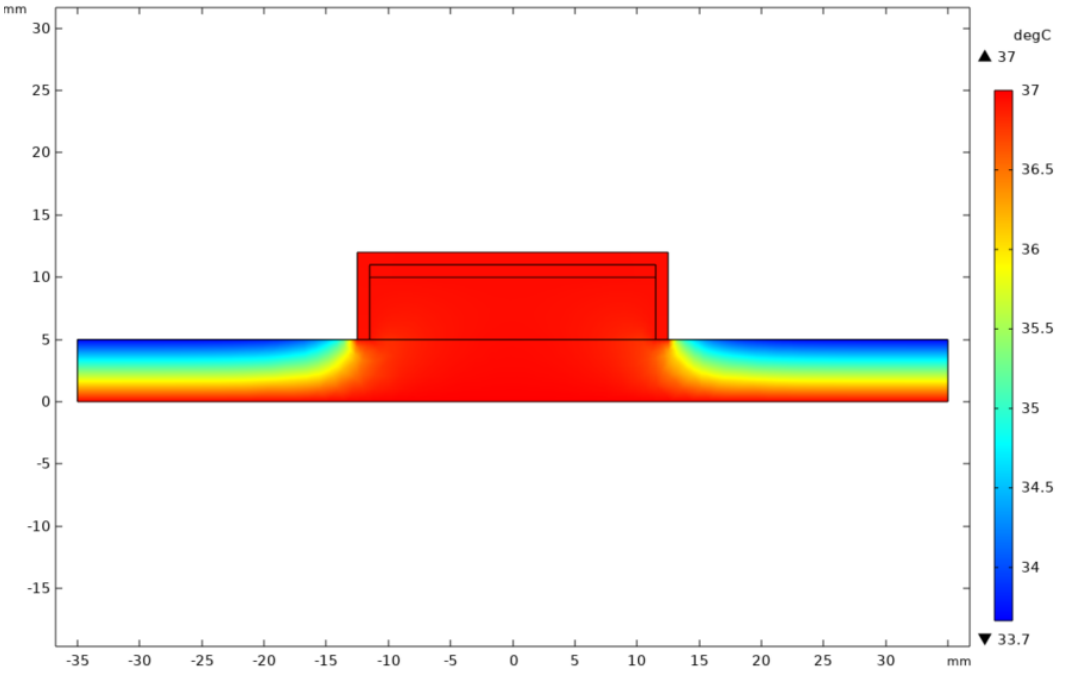
mm
30
25
20
15
10
5
0
-5
-10
-15
-35
-30
-25
-20
-15
-10
-5
0
5
10
15
20
25
30
mm
degC
▲ 37
37
36.5
36
35.5
35
34.5
34
▼ 33.7

(a)

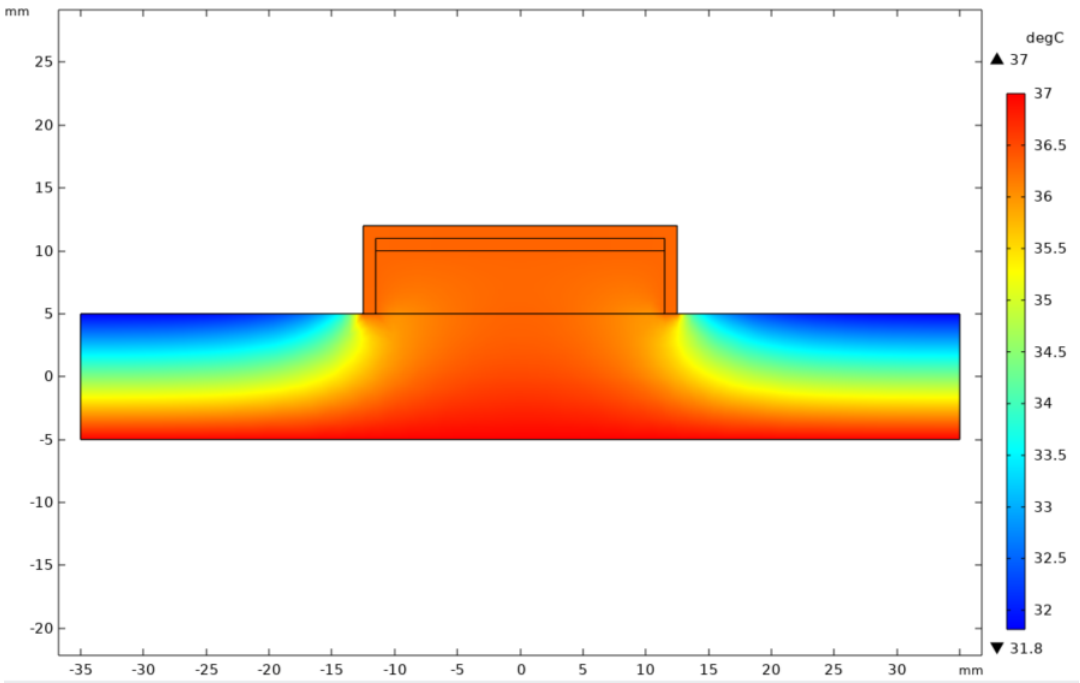
mm
25
20
15
10
5
0
-5
-10
-15
-20
-35
-30
-25
-20
-15
-10
-5
0
5
10
15
20
25
30
mm
degC
▲ 37
37
36.5
36
35.5
35
34.5
34
33.5
33
32.5
32
▼ 31.8

(b)

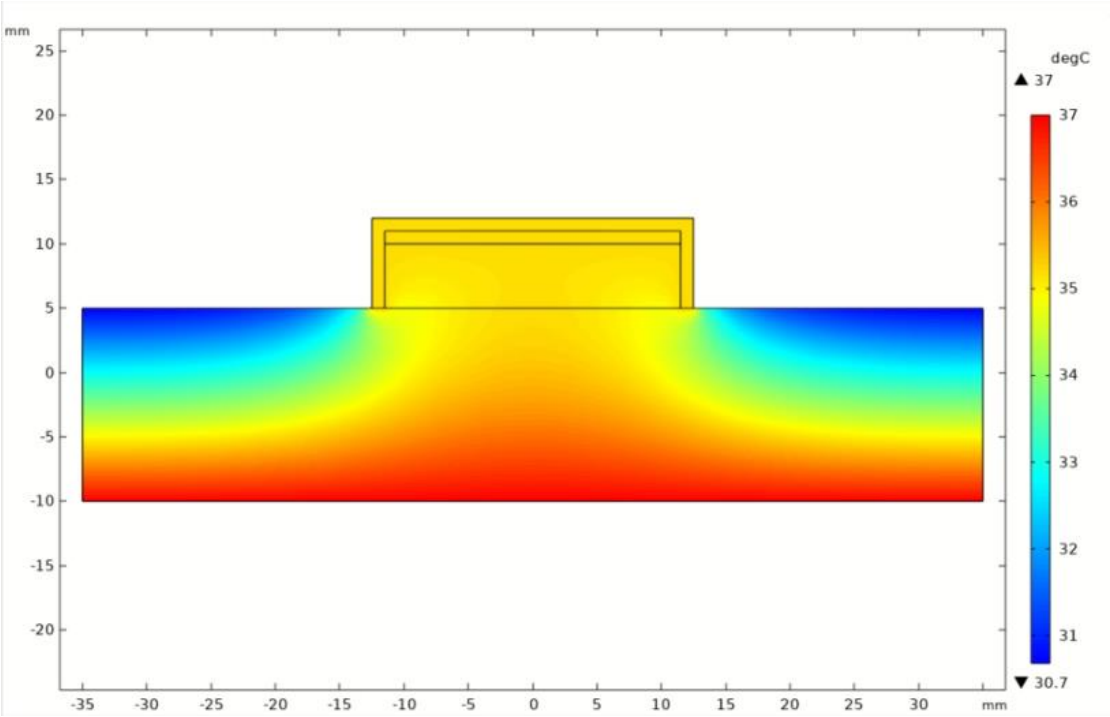
mm
25
20
15
10
5
0
-5
-10
-15
-20
-35 -30 -25 -20 -15 -10 -5 0 5 10 15 20 25 30 mm
degC
▲ 37
37
36
35
34
33
32
31
▼ 30.7

(c)

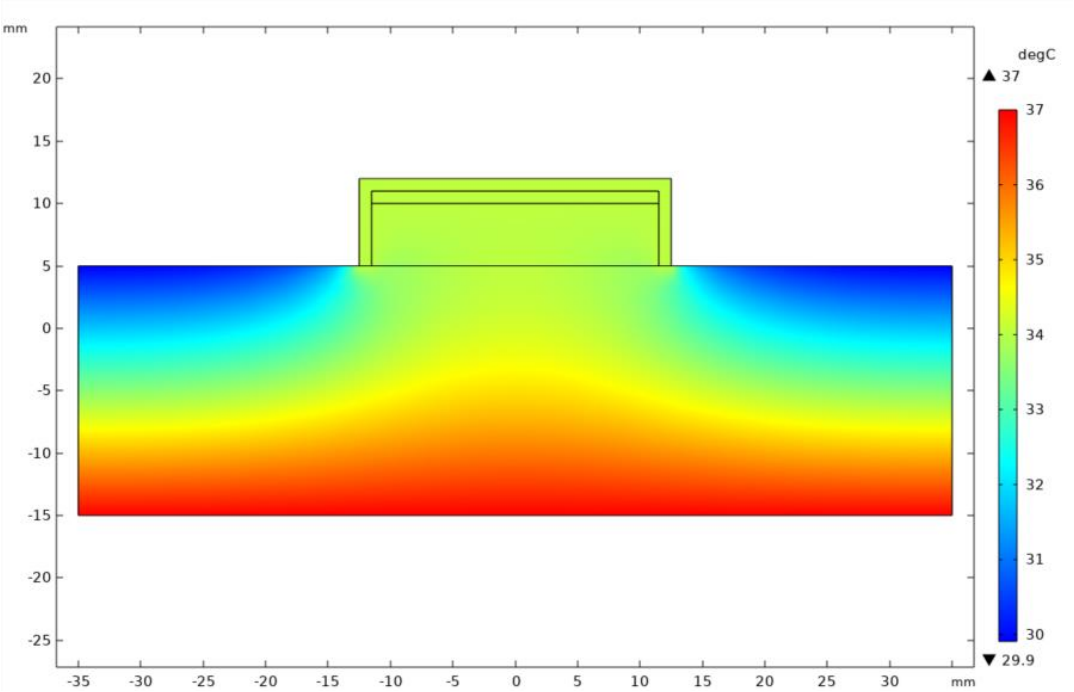
mm
20
15
10
5
0
-5
-10
-15
-20
-25
-35 -30 -25 -20 -15 -10 -5 0 5 10 15 20 25 30 mm
degC
▲ 37
37
36
35
34
33
32
31
30
▼ 29.9

(d)

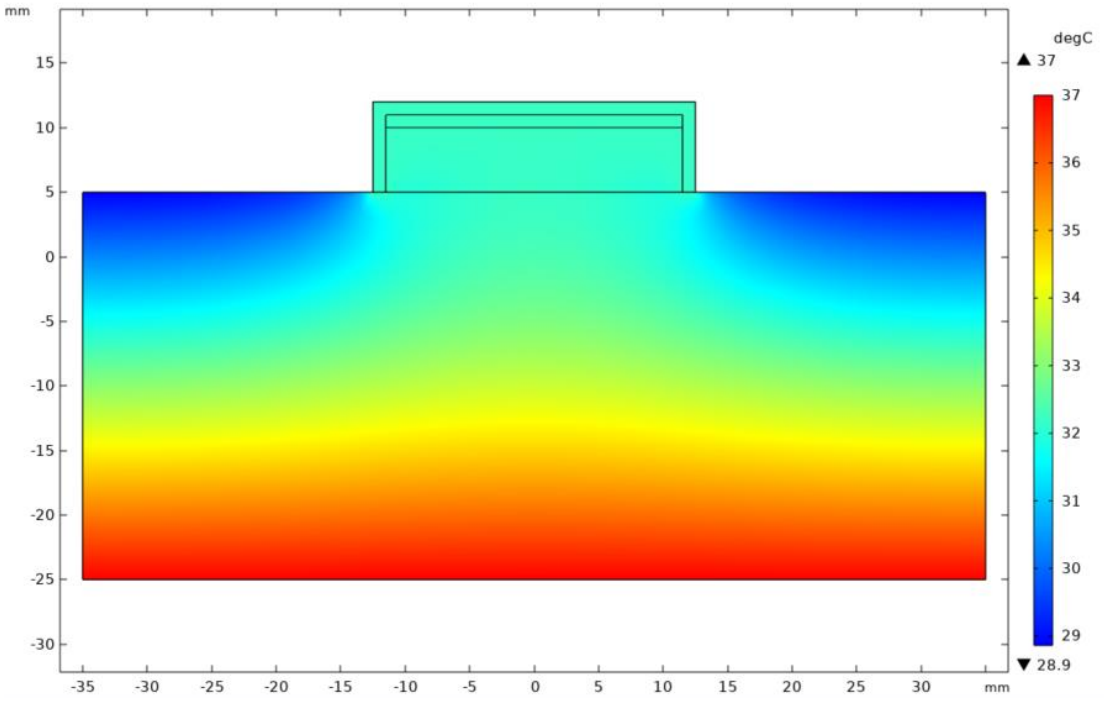

(e)

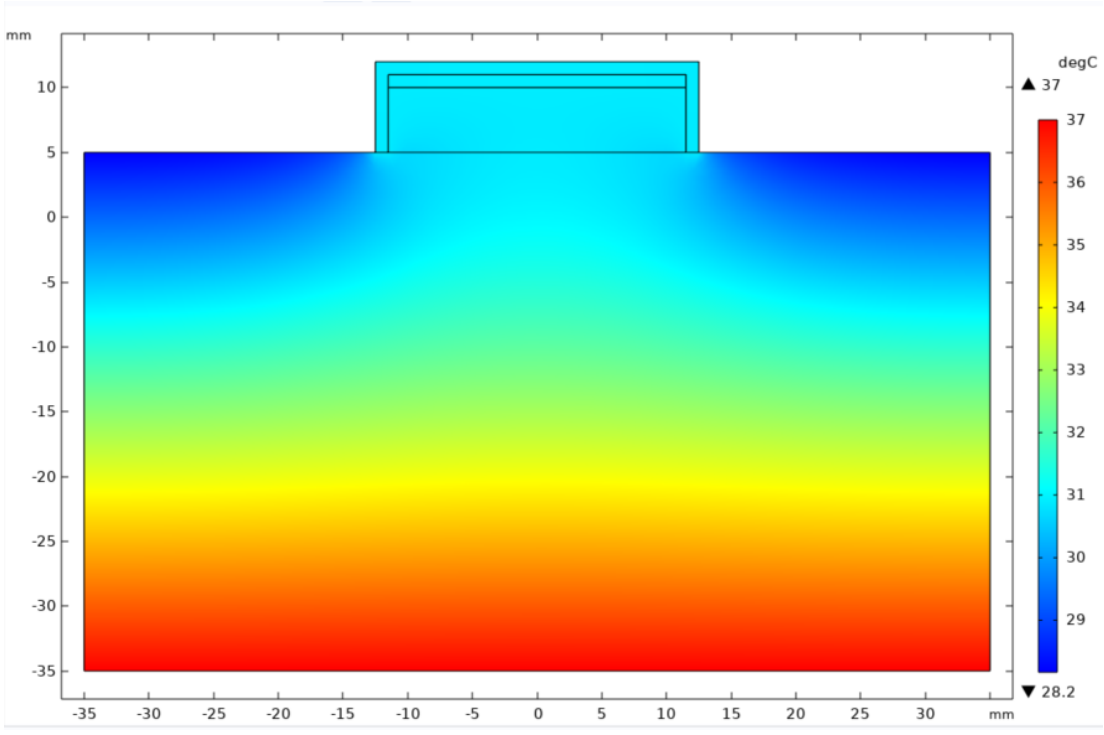

(f)

Figure 6-10 Relationship between different thicknesses d of subcutaneous tissue of ZHF probe and 2D measurement results (Tair=25℃, h=28W/(m2-K), probe diameter D=20mm). (a)d=5mm; (b)d=10mm; (c)d=15mm; (d)d=20mm; (e)d=30mm; (f)d=40mm;

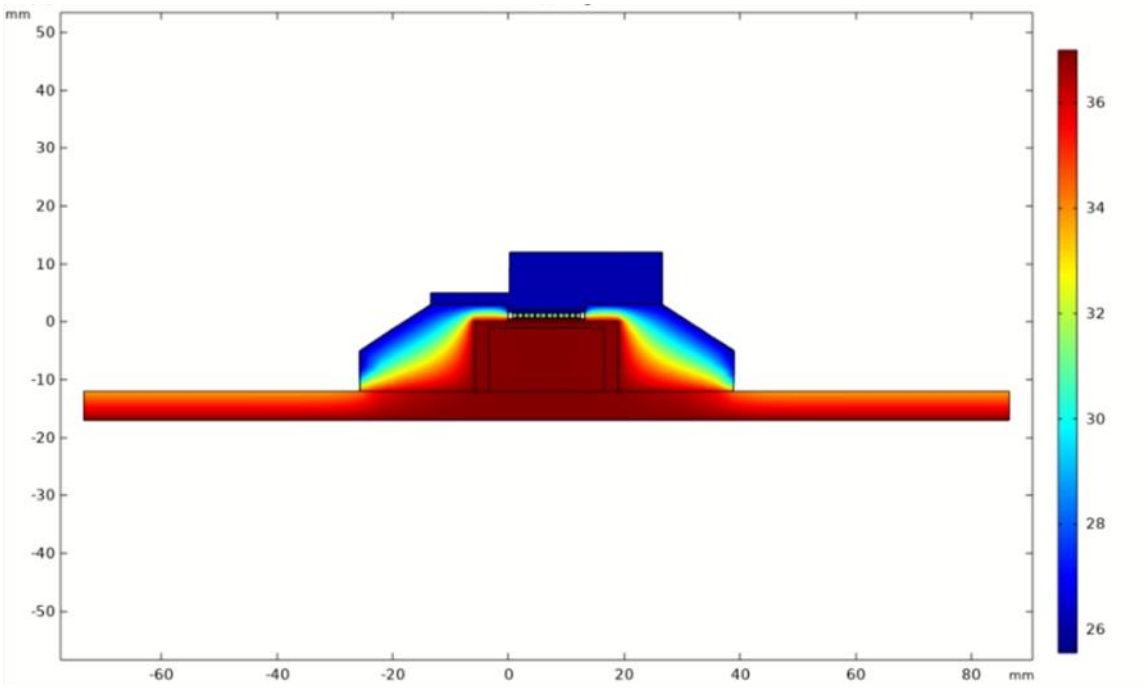
mm
50
40
30
20
10
0
-10
-20
-30
-40
-50
-60
-40
-20
0
20
40
60
80
mm
36
34
32
30
28
26

(a)

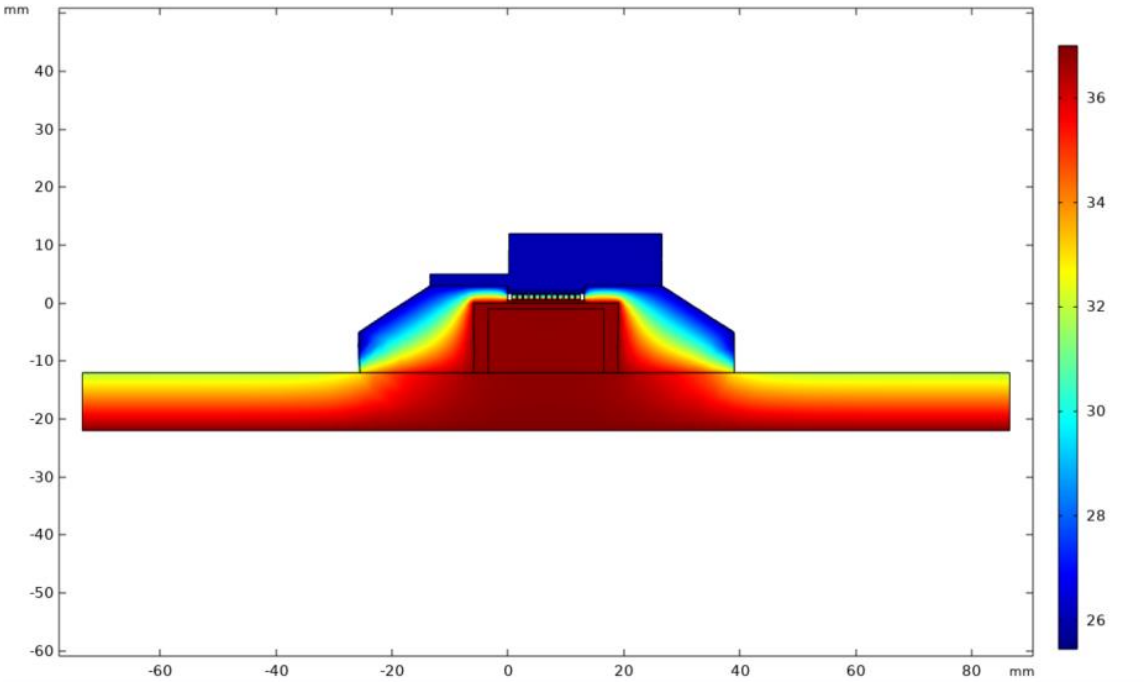
mm
40
30
20
10
0
-10
-20
-30
-40
-50
-60
-60
-40
-20
0
20
40
60
80
mm
36
34
32
30
28
26

(b)

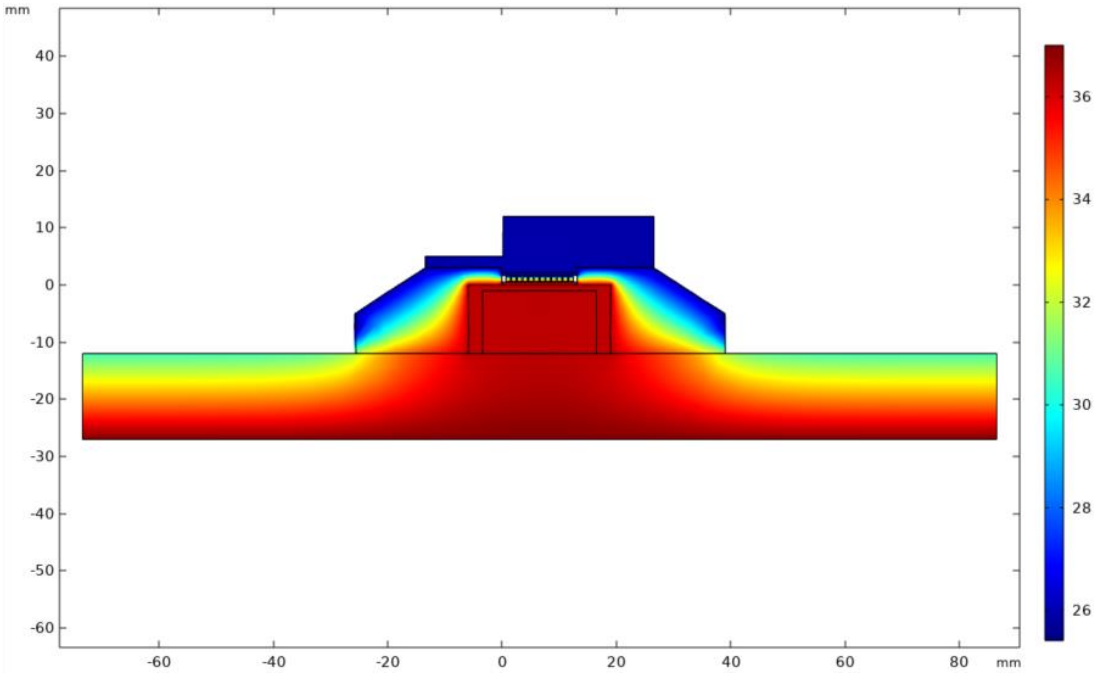
mm
40
30
20
10
0
-10
-20
-30
-40
-50
-60
-60
-40
-20
0
20
40
60
80
mm
36
34
32
30
28
26

(c)

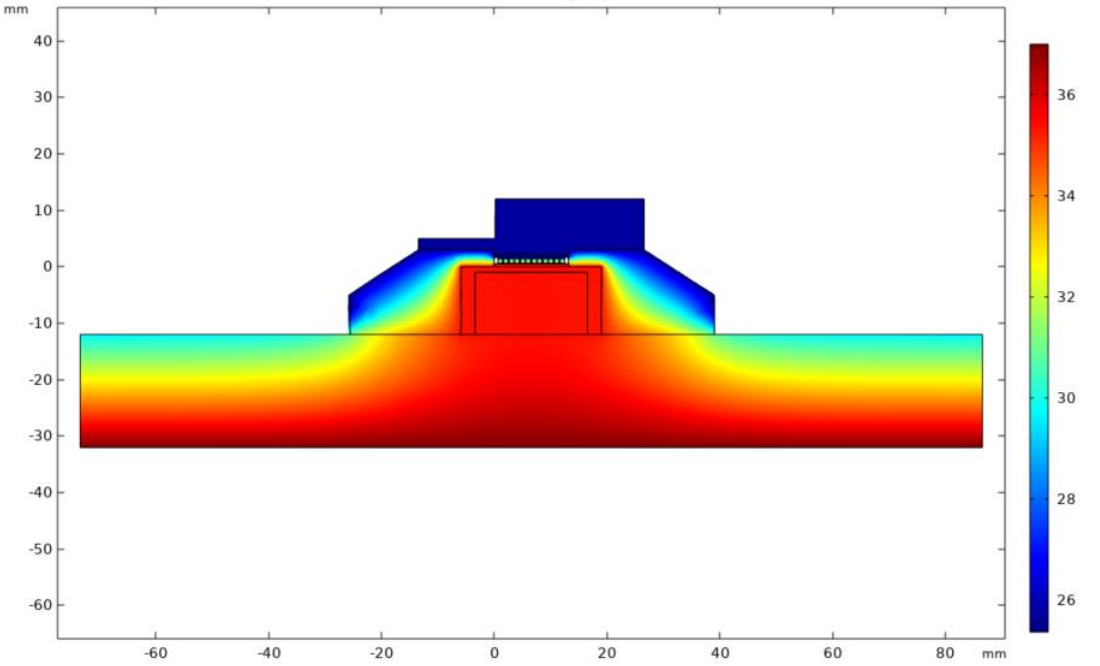
mm
40
30
20
10
0
-10
-20
-30
-40
-50
-60
-60
-40
-20
0
20
40
60
80
mm
36
34
32
30
28
26

(d)

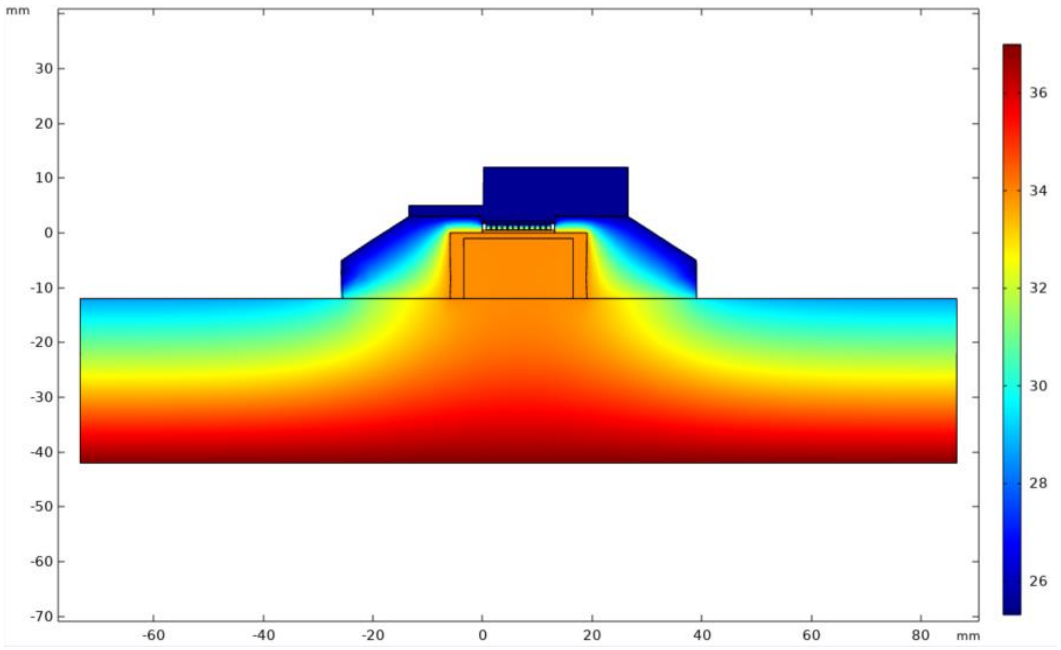

(e)

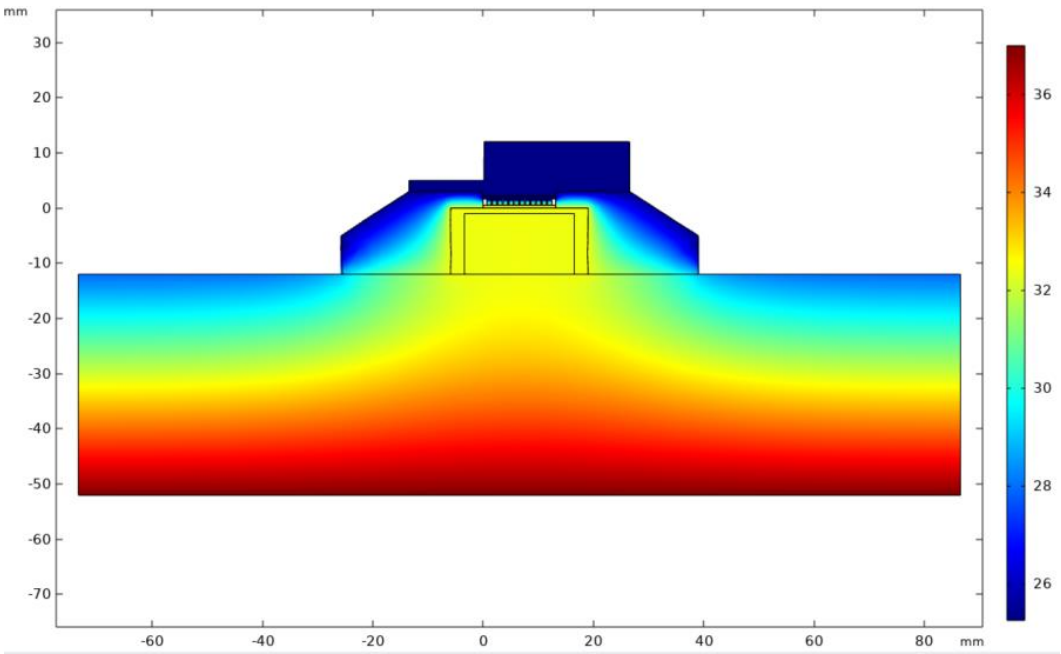

(f)

Figure 6-11 Relationship between different thicknesses of subcutaneous tissue of the prototype probe and 2D measurement results (Tair=25°C, h=28W/(m2-K)) (a)d=5mm; (b)d=10mm; (c)d=15mm; (d)d=20mm; (e)d=30mm; (f)d=40mm;

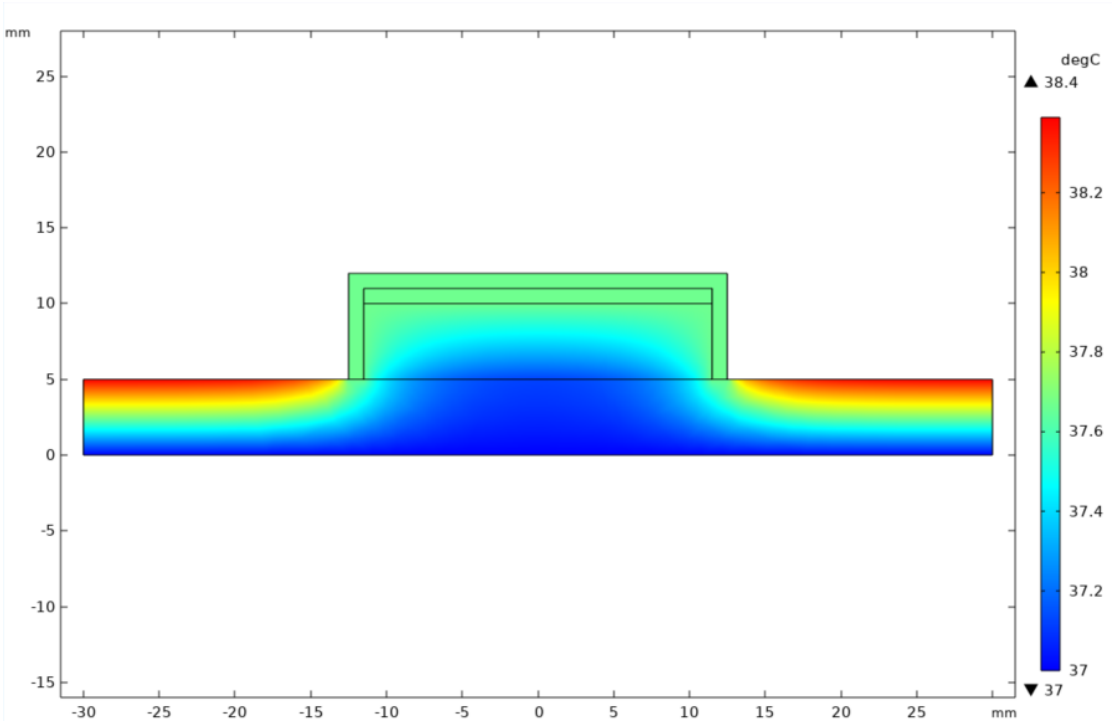
mm
25
20
15
10
5
0
-5
-10
-15
-30
-25
-20
-15
-10
-5
0
5
10
15
20
25
mm
degC
▲ 38.4
38.2
38
37.8
37.6
37.4
37.2
37
▼ 37

(a)

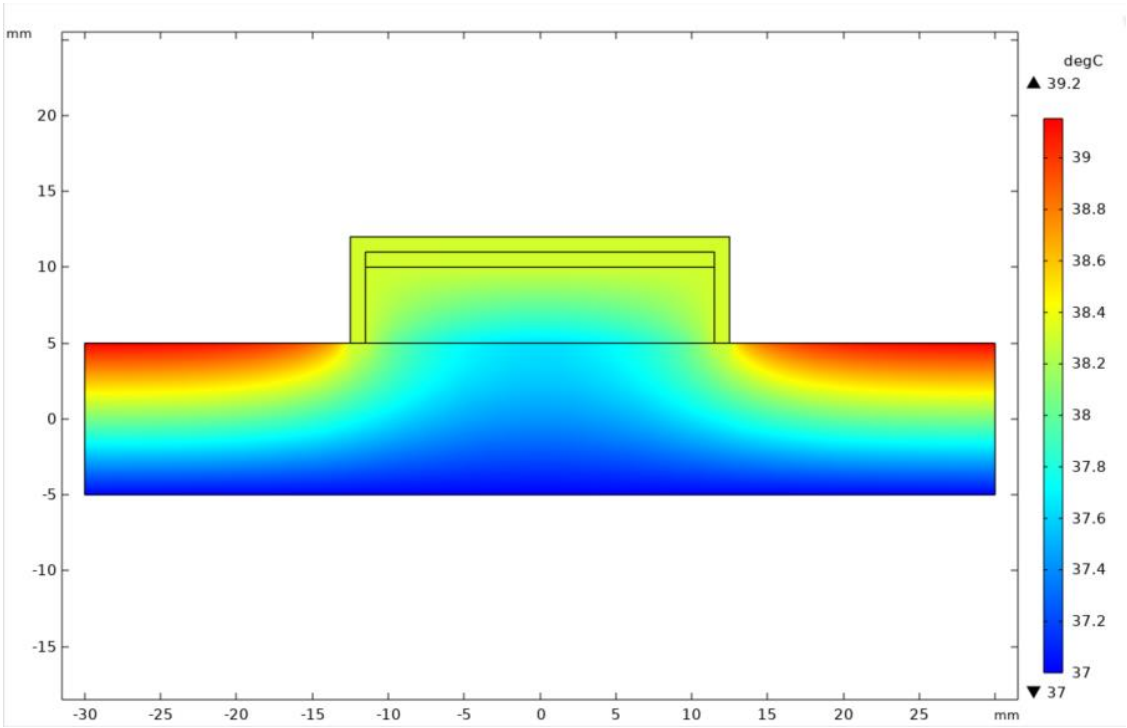
mm
20
15
10
5
0
-5
-10
-15
-30
-25
-20
-15
-10
-5
0
5
10
15
20
25
mm
degC
▲ 39.2
39
38.8
38.6
38.4
38.2
38
37.8
37.6
37.4
37.2
37
▼ 37

(b)

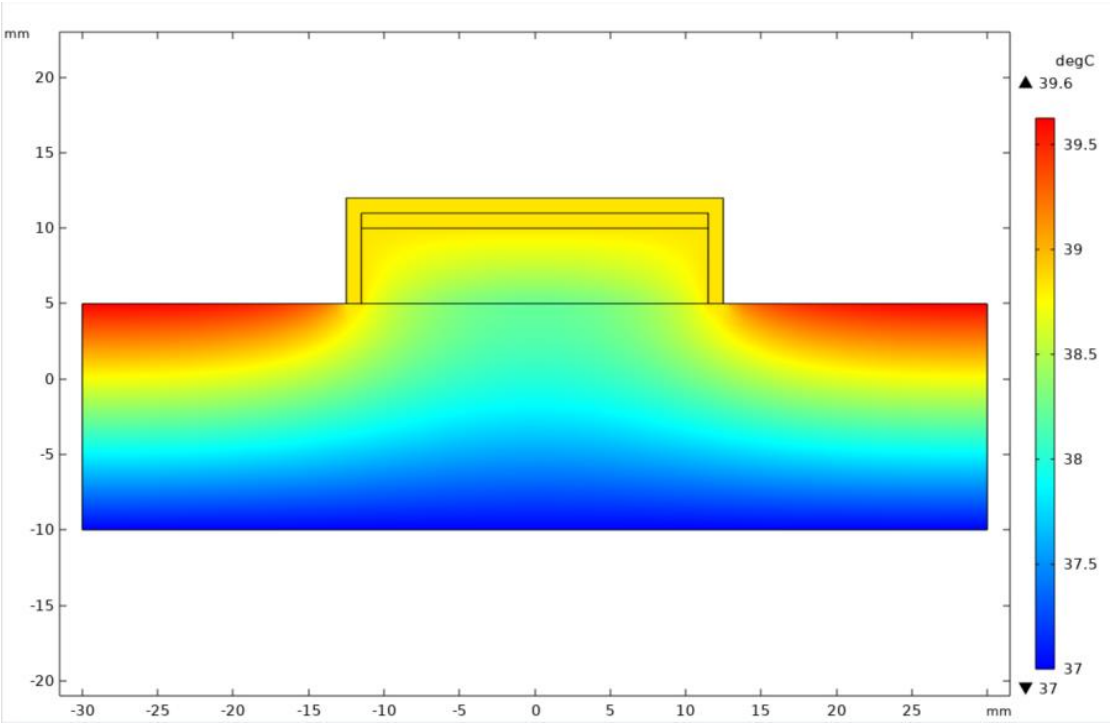
mm
20
15
10
5
0
-5
-10
-15
-20
-30
-25
-20
-15
-10
-5
0
5
10
15
20
25
mm
degC
▲ 39.6
39.5
39
38.5
38
37.5
37
▼ 37

(c)

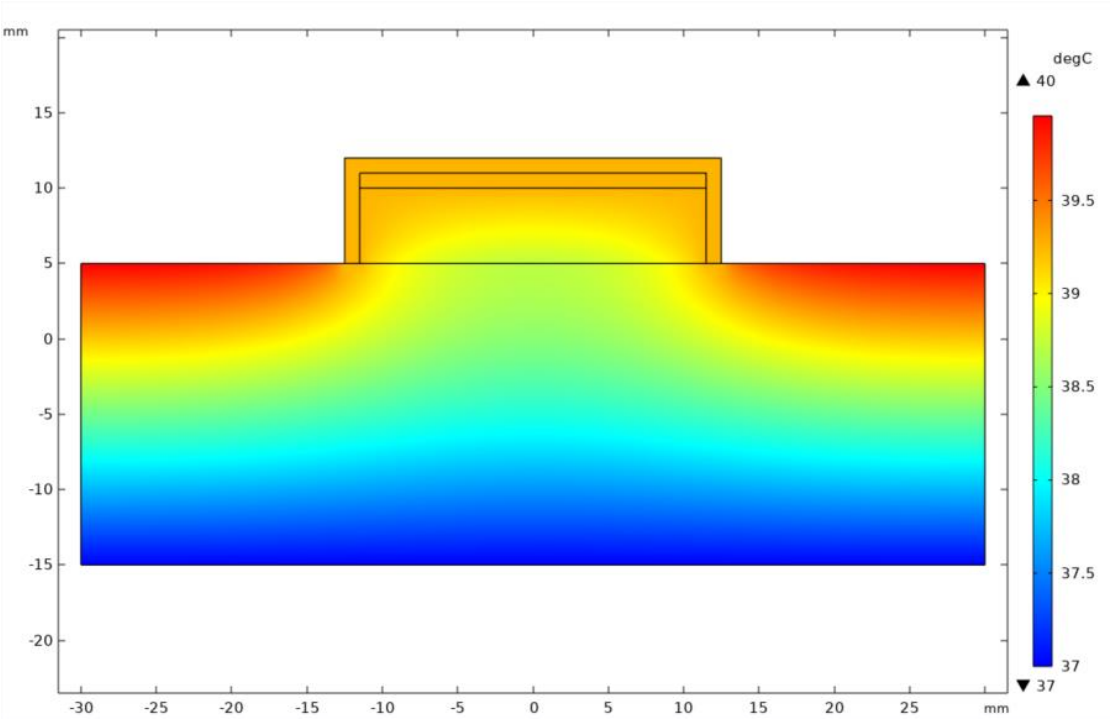
mm
15
10
5
0
-5
-10
-15
-20
-30
-25
-20
-15
-10
-5
0
5
10
15
20
25
mm
degC
▲ 40
39.5
39
38.5
38
37.5
37
▼ 37

(d)

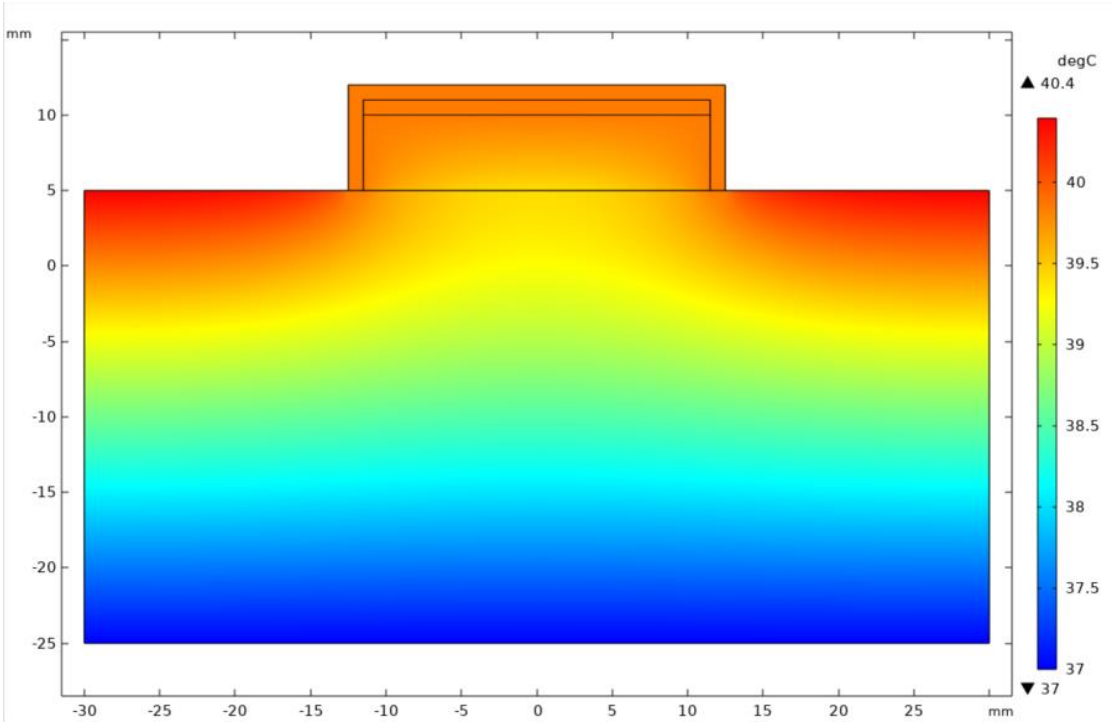

(e)

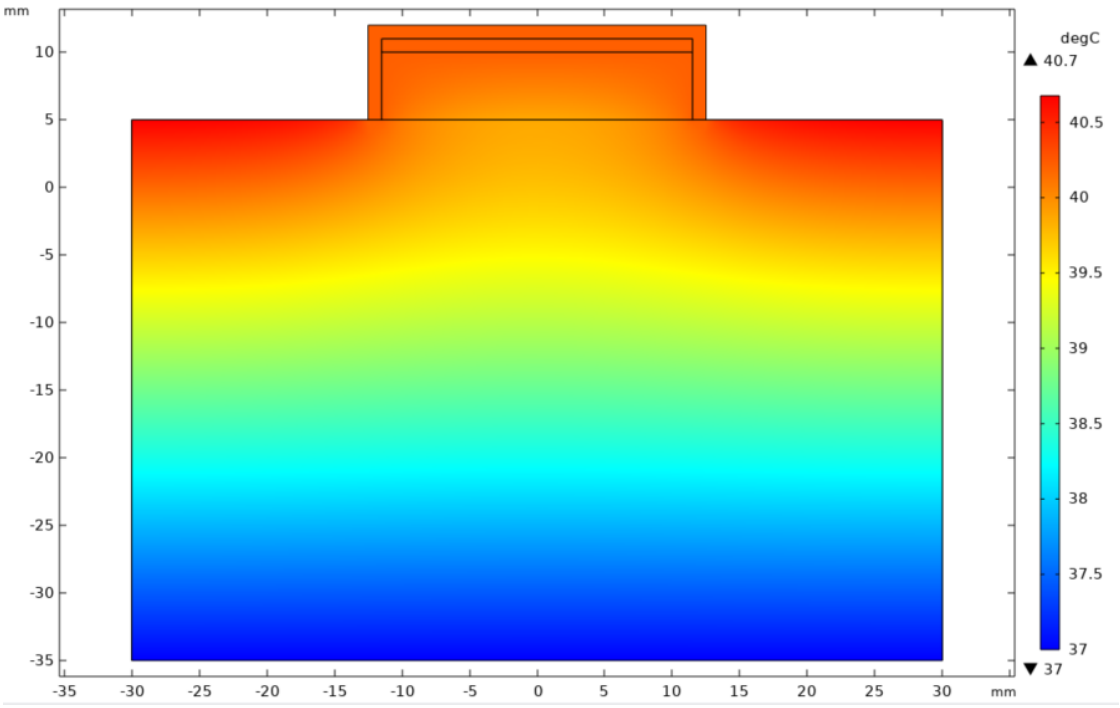

(f)

Figure 6-12 Relationship between different thicknesses of subcutaneous tissue of the ZHF probe and 2D measurement results (Tair=42°C, h=28.5W/(m2-K), probe diameter D=20mm) (a)d=5mm; (b)d=10mm; (c)d=15mm; (d)d=20mm; (e)d=30mm; (f)d=40mm;

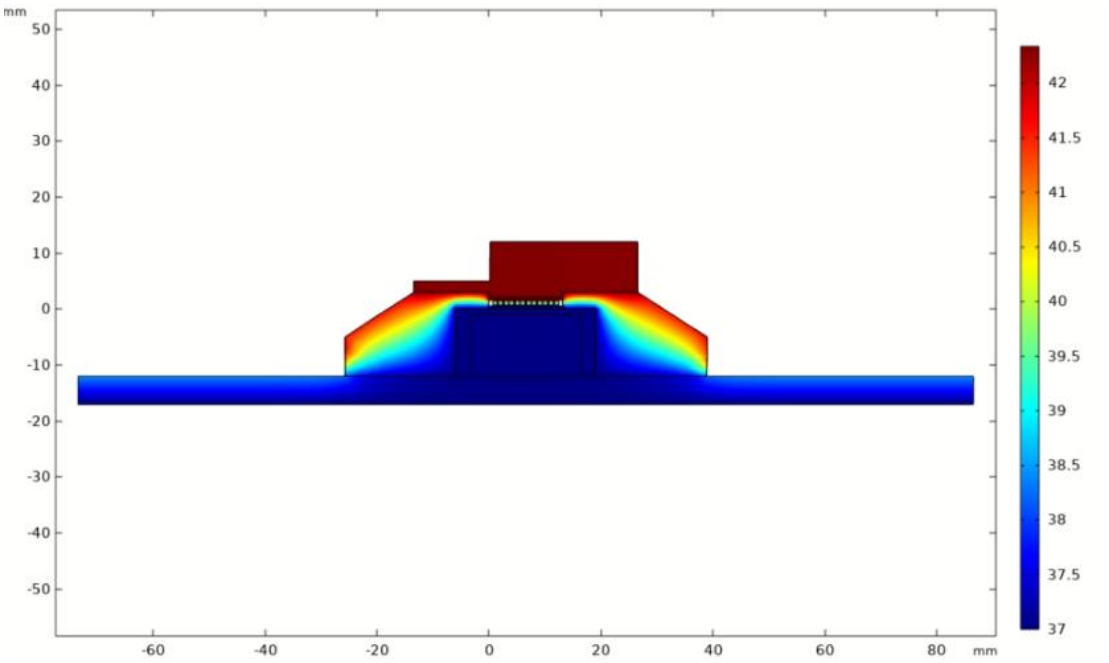
mm
50
40
30
20
10
0
-10
-20
-30
-40
-50
-60
-40
-20
0
20
40
60
80
mm
42
41.5
41
40.5
40
39.5
39
38.5
38
37.5
37

(a)

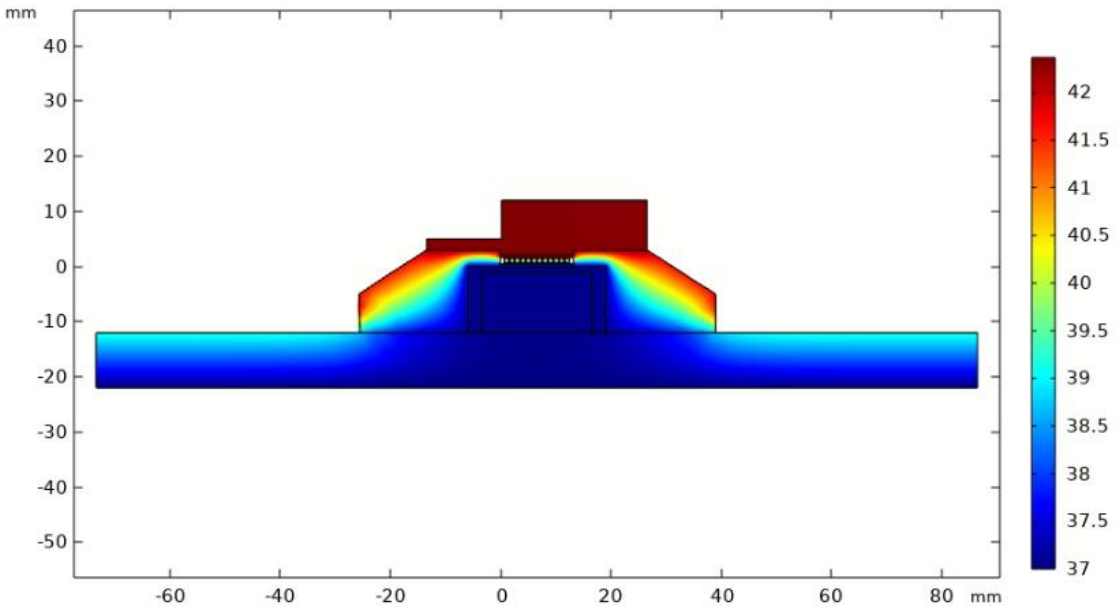
mm
40
30
20
10
0
-10
-20
-30
-40
-50
-60
-40
-20
0
20
40
60
80
mm
42
41.5
41
40.5
40
39.5
39
38.5
38
37.5
37

(b)

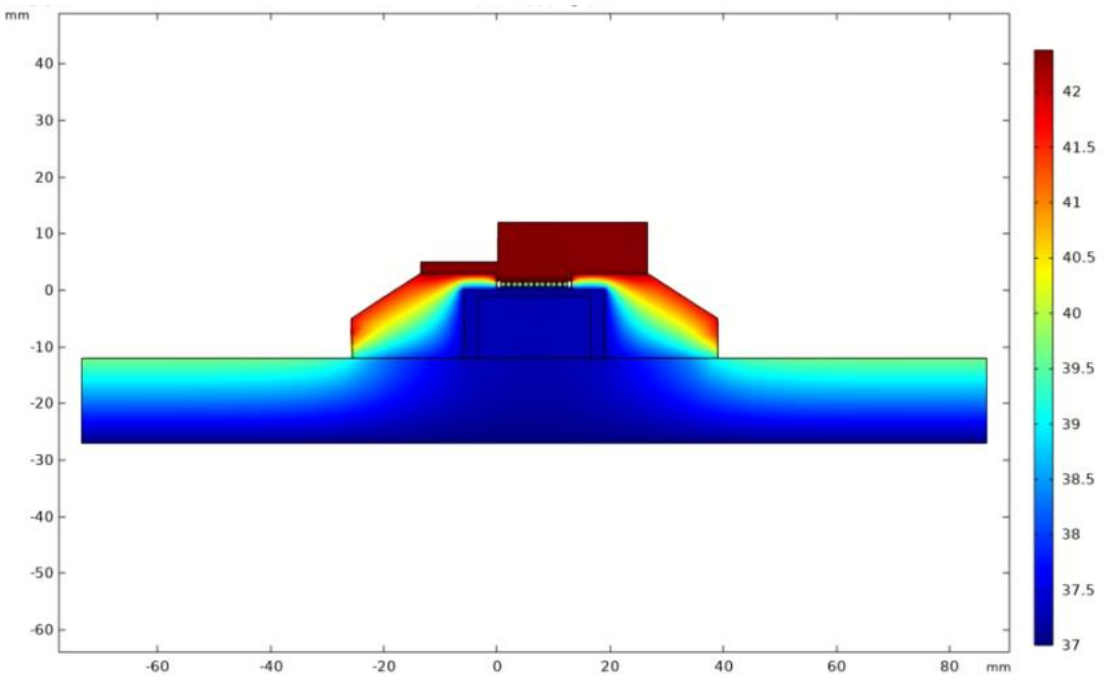
mm
40
30
20
10
0
-10
-20
-30
-40
-50
-60
-60
-40
-20
0
20
40
60
80
mm
42
41.5
41
40.5
40
39.5
39
38.5
38
37.5
37

(c)

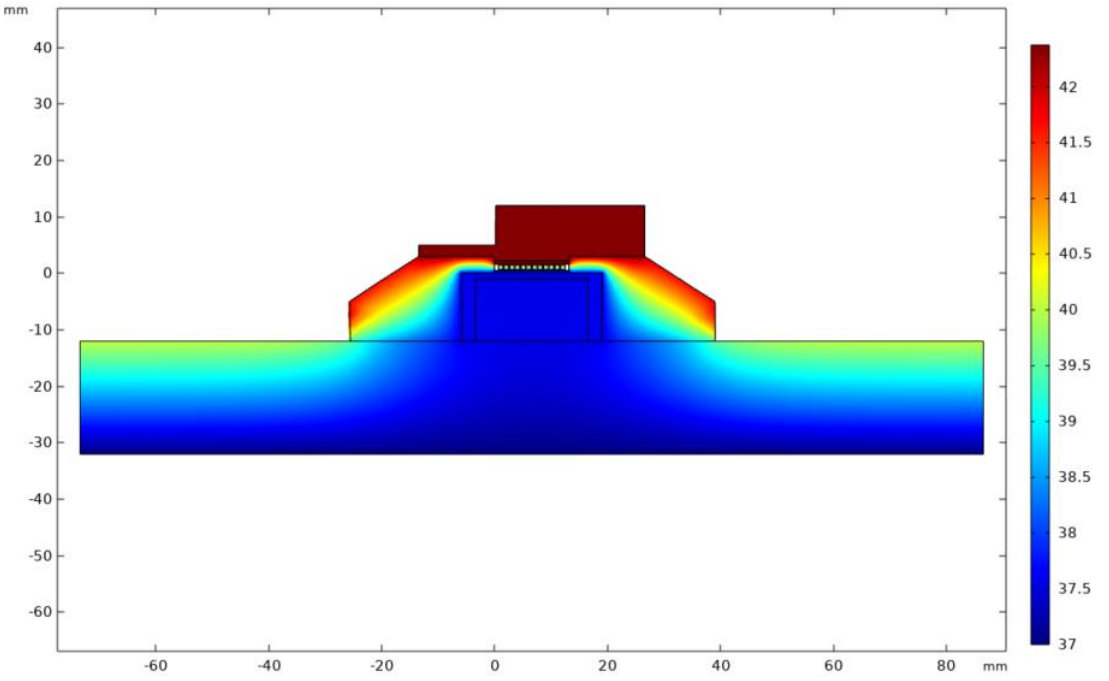
mm
40
30
20
10
0
-10
-20
-30
-40
-50
-60
-60
-40
-20
0
20
40
60
80
mm
42
41.5
41
40.5
40
39.5
39
38.5
38
37.5
37

(d)

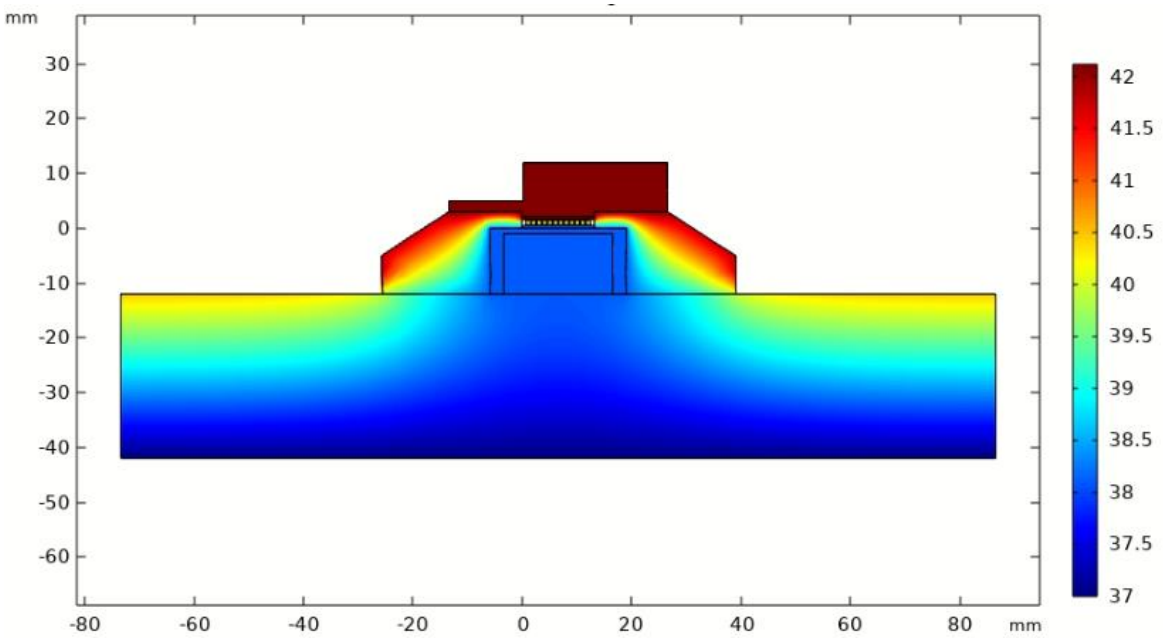

(e)

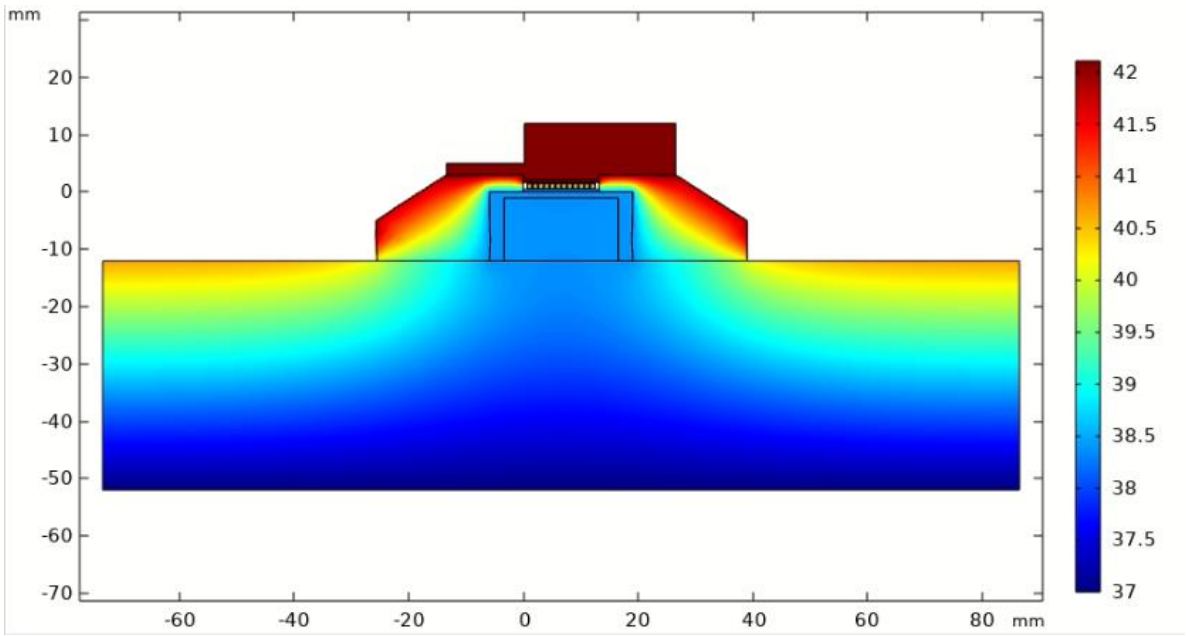

(f)

Figure 6-13 Relationship between different thicknesses of subcutaneous tissue of the prototype probe and 2D measurement results (Tair=42°C, h=28W/(m2·K)) (a)d=5mm; (b)d=10mm; (c)d=15mm; (d)d=20mm; (e)d=30mm; (f)d=40mm;

Figure 6-14 summarizes the effect of skin thickness on the temperature results of the two probes. It was also found that the thicker the subcutaneous tissue, or the higher the thermal conductivity of the same thickness, the smaller the maximum depth that can be measured

within the margin of error. Moreover, due to the larger radius of the prototype probe, its measurement error under various temperature conditions is smaller than that of the smaller radius ZHF probe.

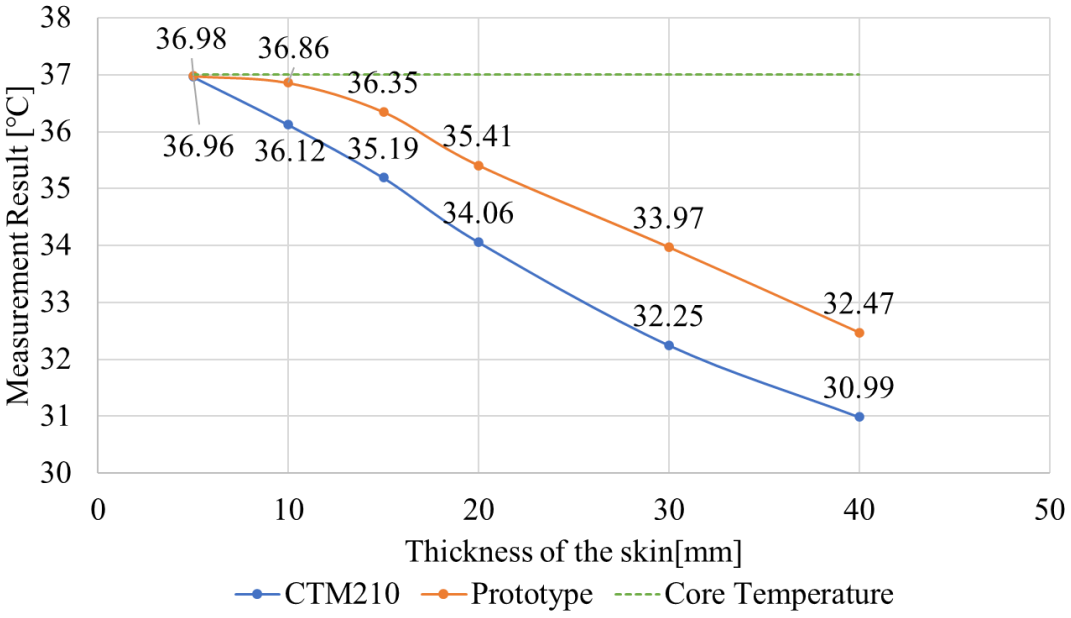

(a)

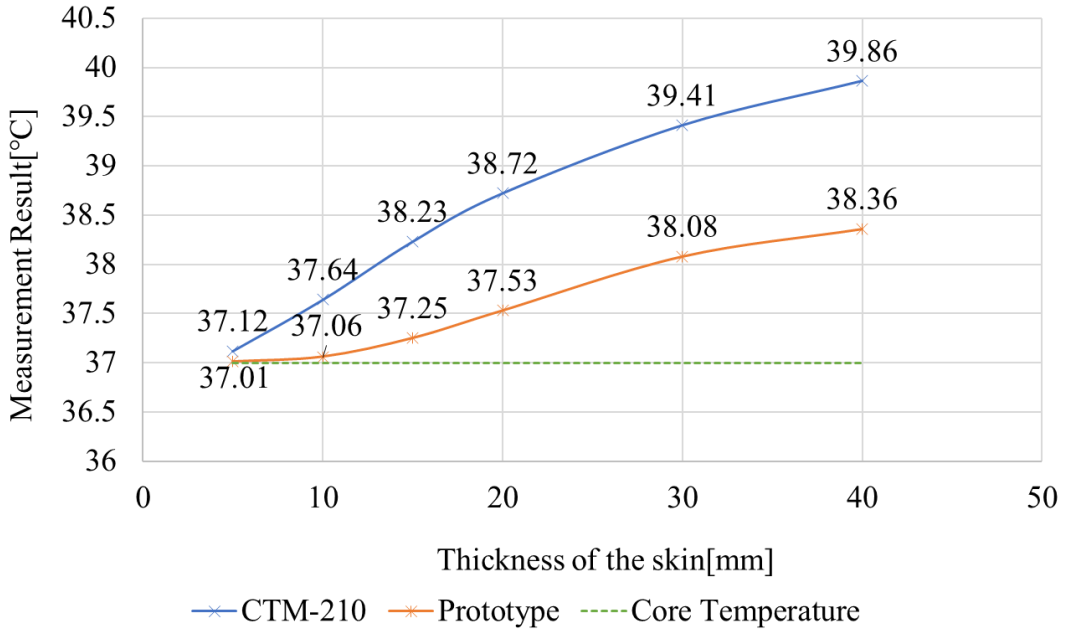

(b)

Figure 6-14 Final temperature results when the ZHF probe (blue line) and Prototype probe (orange line) are placed on different thicknesses of skin (a) at room temperature (Tair=25°C) (b) at high temperature (Tair=42°C)

The finite element analysis confirms that the probe can measure at high temperatures with the current design. The main focus was on the measurements at the end of temperature equilibration and the initial time before reaching equilibrium.

In the study of subcutaneous tissue thickness, we found that the thickness of the subcutaneous tissue at the measurement site affects the measurement results. Therefore, it is recommended to use the forehead as the measurement site because the brain under the forehead is a vital core body temperature organ whose structure hardly changes with movement. On the other hand, the solar plexus under the sternum can also be considered a measurement site. Still, the effect of motion on the contact surface of the upper abdomen with the probe needs to be considered.

Therefore, the forehead was used as the measurement site in exercise-related experiments in subsequent human experiments. In sauna and heat therapy, the solar plexus was chosen as a safe temperature measurement site because the upper abdomen is smoother unaffected by movement.

In addition, the simulation of the probe morphology can be further utilized for wearable improvements. Appropriate flattening and enlarging the internal aluminum probe radius can yield better results and reach thermal equilibrium more quickly. It is worth mentioning that a balance needs to be struck between radius expansion and wearability, as too large a probe radius can lead to discomfort on the forehead and higher power consumption. In cases where high precision measurements are required, the radius of the aluminum housing of the probe can be expanded, sacrificing some of the wearability, while a small radius probe can be used appropriately for extended use, focusing on capturing the degree of temperature change rather than measurement accuracy.

Reference

[1] T. L. Bergman, A. S. Lavine, F. P. Incropera, and D. P. DeWitt, *Introduction to heat transfer*. John Wiley & Sons, 2011.

7. Experiments and results

7.1. Simulator Experiment

The temperature measurement accuracy of the prototype probe was evaluated in a simulator experiment using a thermostatic water bath.

7.1.1. Experiment settings

As shown in **Figure 7-1** and **Figure 7-2**, an aluminum case was immersed in the thermostatic water bath (C-650, TAIYO TAITE C, room temperature ~ 100°C, Figure 4), and a gel sheet (HTCH2-150-150, MISUMI, thickness: 6 mm) was attached to the inner bottom of the bath. The prototype probe and a probe for a commercial core body thermometer (CoreTemp CTM-210, Terumo) were set on the gel sheet. Temperature results of the prototype device T_{Proto} were recorded every 1 second, while those of the commercial device T_{CTM} were registered every 2 seconds. At the beginning of the experiment, the water temperature T_{water} was set to 37±0.5°C. T_{water} and the air temperature T_{air} were monitored by a thermistor thermometer (3312A, INSTRULAB).

(a)

(b)

Figure 7-1. (a) thermostatic water bath (b) thermostatic water bath with the heat gun and cover

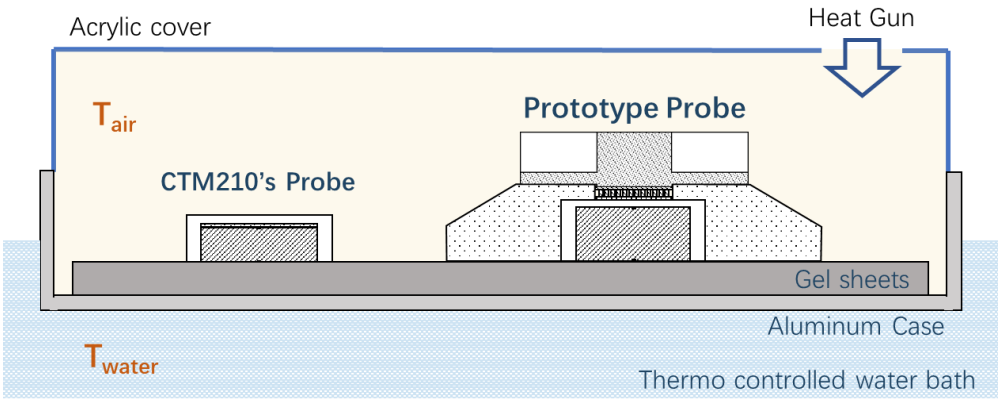

Figure 7-2. Cross-sectional view of the experimental setup

The main experimental protocol (No.1) starts with a preparatory phase (Phase I), where each probe was left open at room temperature for 40 minutes until the output stabilized. Then follows the high-temperature Phase (Phase II), where an acrylic cover covered the entire case, and a hot air gun was used to blow hot air at about 45 °C inward for 20 minutes. At the start of the recovery period (Phase III),

the acrylic cover is removed so that the temperature returns to room temperature again and holds for 20 minutes.

We also tried various combinations of water temperature variation with air temperature (Table7-1,7-2,7-3) and investigated the temperature measurement variation of both probes at different temperature combinations.

Table 7-1. Experimental protocol No.2

Time	Water temperature(℃)	Air temperature(℃)
0-20min	37	25
20-35min	37	42
35-50min	37	25
50-65min	37	42
65-80min	37	25
80-95min	37	42
95-110min	37	25

Table7-2. Experimental protocol No.3

	Water temperature	Air temperature
0-30min	37	25
30-40min	37	38.5
40-50min	37	40.5
50-60min	37	42.5
60-75min	38.6	42.5
75-85min	39.6	42.5
85-95min	39.6	25

Table 7-3. Experimental protocol No.4

	Water temperature	Air temperature
0-20min	39	26
20-40min	39	41
40-55min	37.3	41
55-70min	36.3	41

7.1.2. Results

Figure 7-3. shows an example of the results of the simulator experiment No.1. The temperature variation graph in (a) shows that the commercial probe matches the water temperature in Phase I and III. However, when the outside temperature increased during Phase II, the difference between the commercial probe measurement result T_{CTM} and the actual water temperature T_{Water} was more than 1°C at the maximum. The commercial probe cannot measure the water temperature accurately when the external temperature is higher than the water temperature.

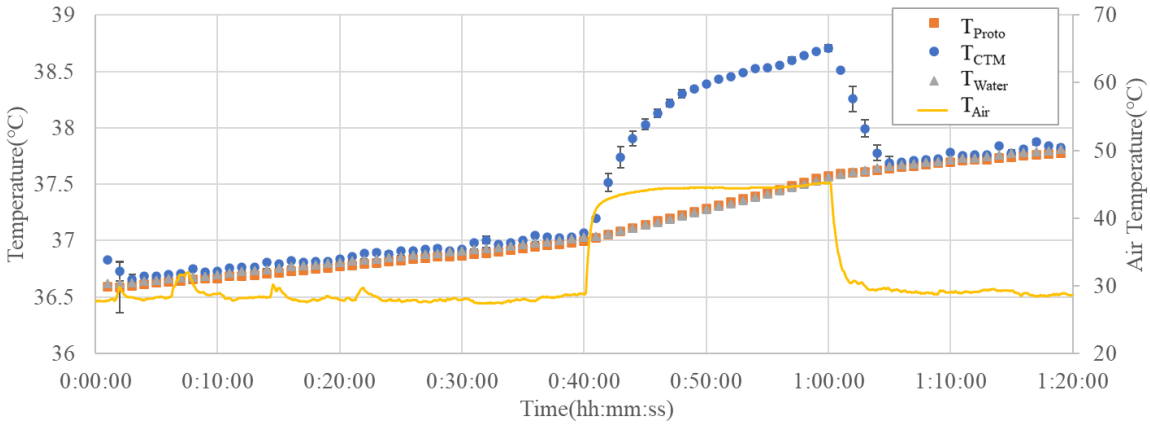

(a)

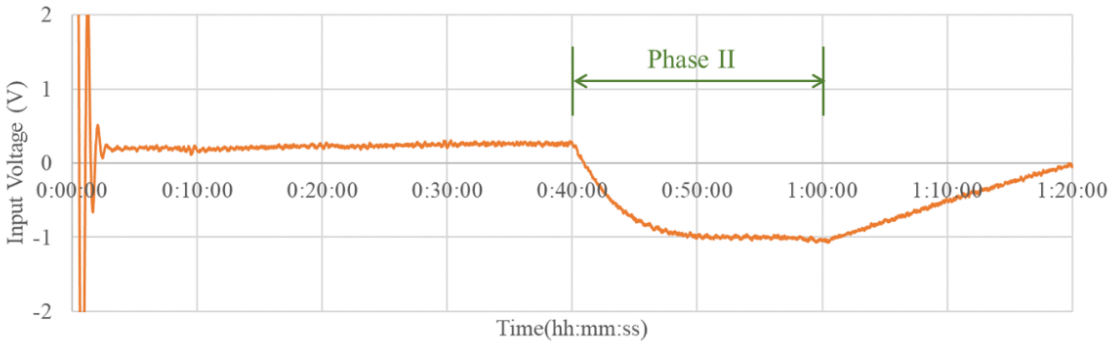

(b)

Figure 7-3. Example of the results of simulator experiment showing

the temperature change (a) and the overtime change of Peltier module input voltage (b).

On the other hand, the prototype probe showed a temperature difference with the water of less than 0.02 ± 0.021°C in all the phases, indicating that the water temperature could be measured with high accuracy even in the high-temperature period of Phase II.

The graph in **Figure 7-3 (b)** shows that the input voltage of the Peltier element V_{Input} reverses its polarity and switches the module from heating to cooling when the external temperature exceeds the water temperature, confirming that the designed control system is operating effectively.

In the test results of No.2, No.3, and No.4, we can see that the Prototype always maintains the same measurement result as the water temperature no matter how the outside air temperature changes; while the ZHF probe has a large fluctuation by the air temperature and changes with the air temperature. In terms of hysteresis, the Prototype showed a slight hysteresis, while the hysteresis of the ZHF probe was more obvious.

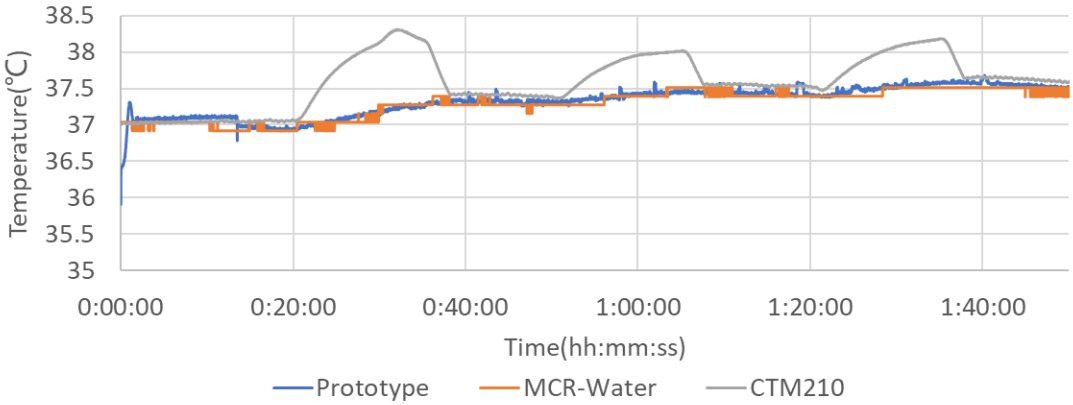

(a)

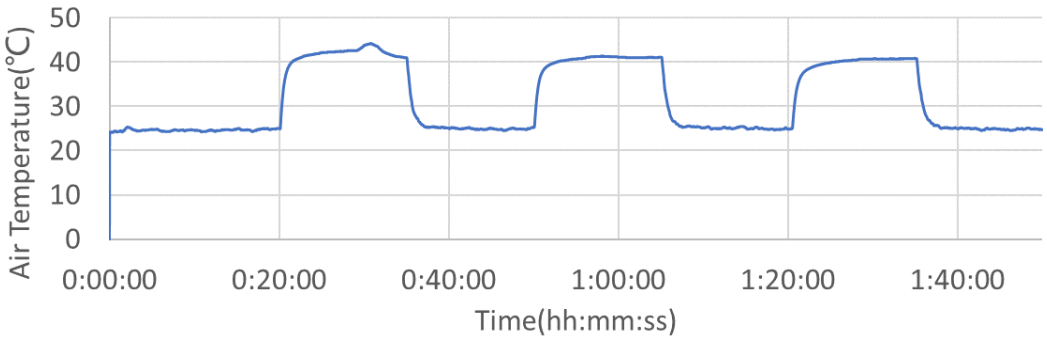

(b)

Figure 7-4 Results of simulator experiment No.2

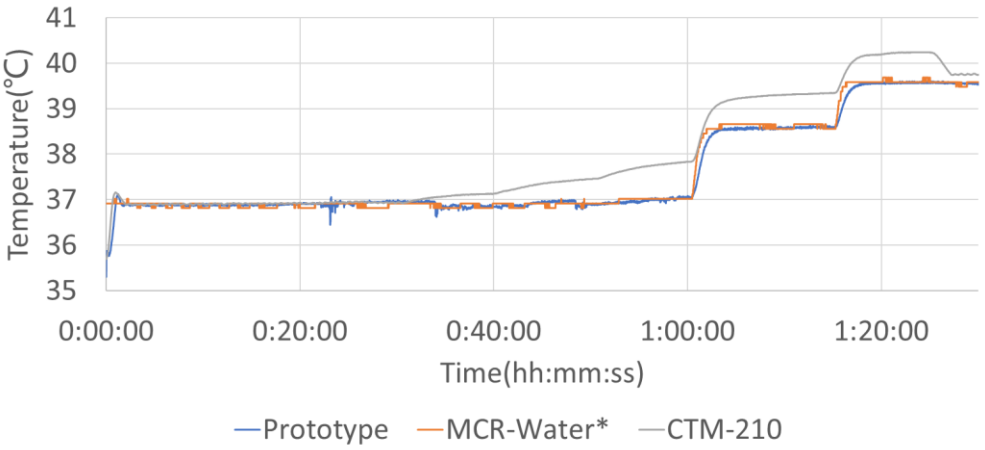

(a)

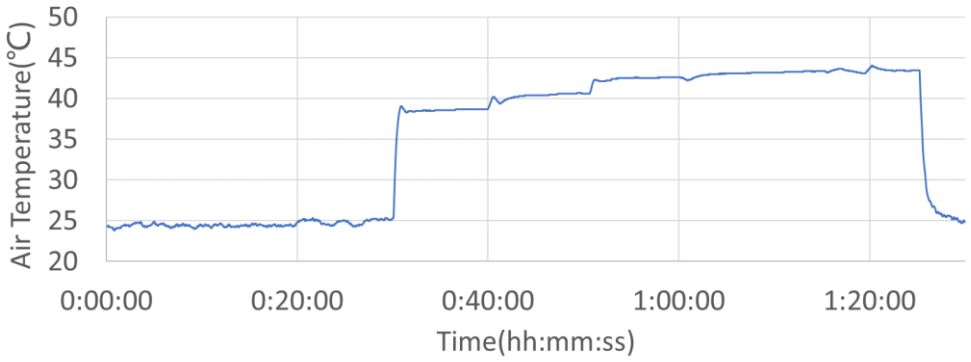

(b)

Figure 7-5 Results of simulator experiment No.3

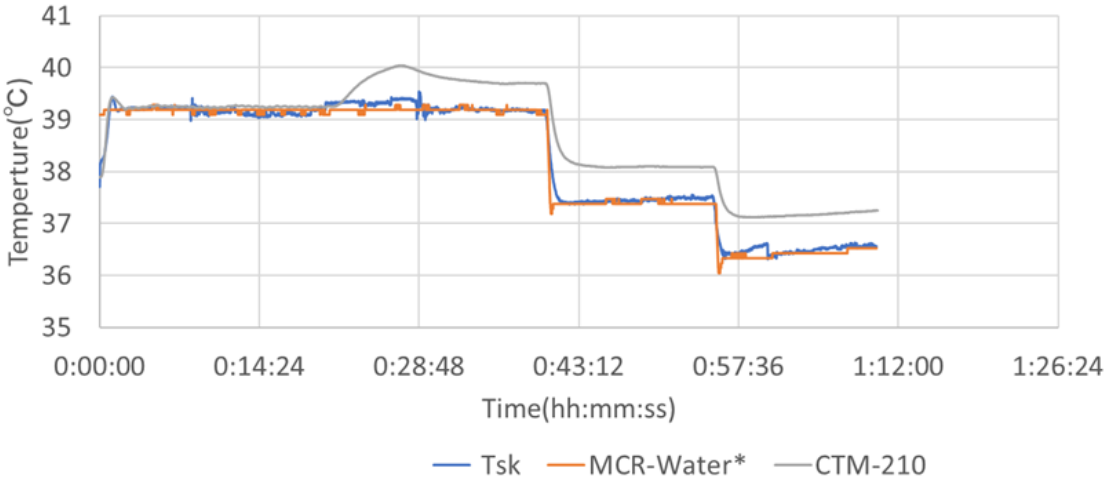

(a)

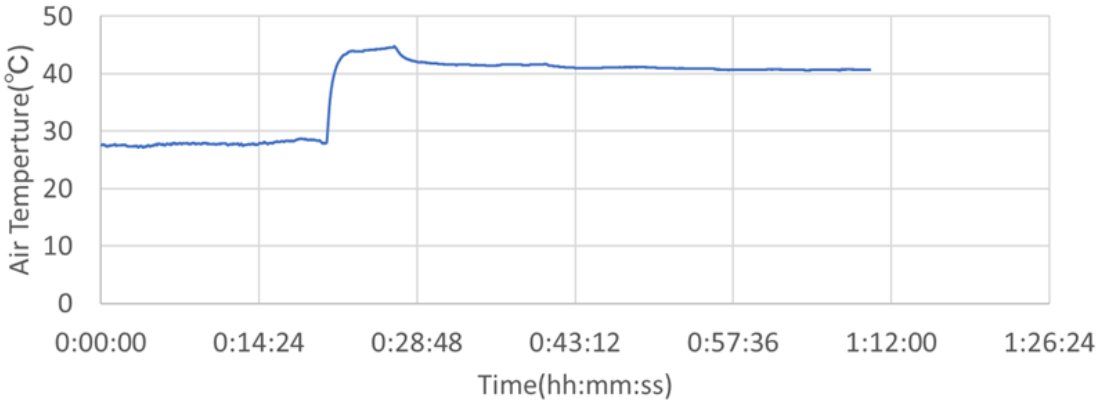

(b)

Figure 7-6 Results of simulator experiment No.4

7.2. Fast-changing measurement in room temperature

7.2.1. Experiment settings

The measurement accuracy and time delay of the prototype probe at room temperature were investigated by simultaneous measurements with a commercially available core-body thermometer (CoreTemp CTM-210, Terumo).

Four healthy male adults (22±2years) were enrolled in the experiment. The prototype and commercial probes were fixed symmetrically to the forehead using a belt. The experiments were performed at room temperature (25±1°C), and the procedure was as follows.

In Phase 1, the subject was at rest in the sitting position for 30 minutes after the fixation of the probe. In Phase 2, the subject performed 10 minutes of exercise (load intensity 75W) on the ergometer shown in **Figure 7-7** (AEROBIKE 75XLIII, Konami Sports), and Phase 3 was the sitting rest for another 20 minutes. The total duration of the whole experiment was 60 minutes. During this period, T_{Proto} and T_{CTM} were recorded at the same time described above.

Figure 7-7 Ergometer (AEROBIKE 75XLIII, Konami Sports)

7.2.2. Results

Figure 7-8 shows the results of core body temperature change during the ergometer experiments. As shown in the figures, core body temperature increased by approximately 0.6°C with the exercise load, and the prototype responded to this change almost identically to the commercial probe.

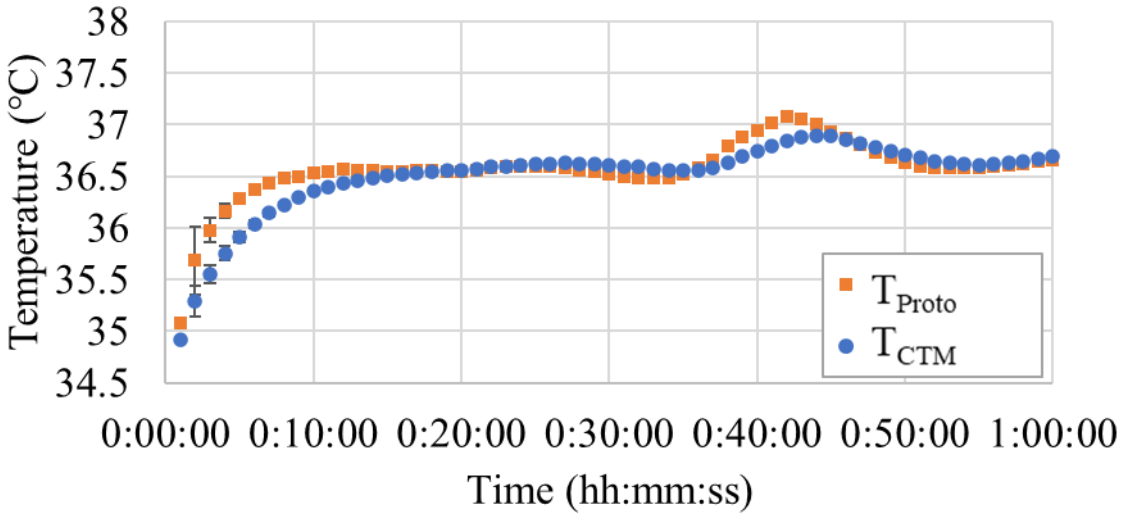
38
37.5
37
36.5
36
35.5
35
34.5
Temperature (°C)
0:00:00 0:10:00 0:20:00 0:30:00 0:40:00 0:50:00 1:00:00
Time (hh:mm:ss)
T Proto
T CTM

(a)

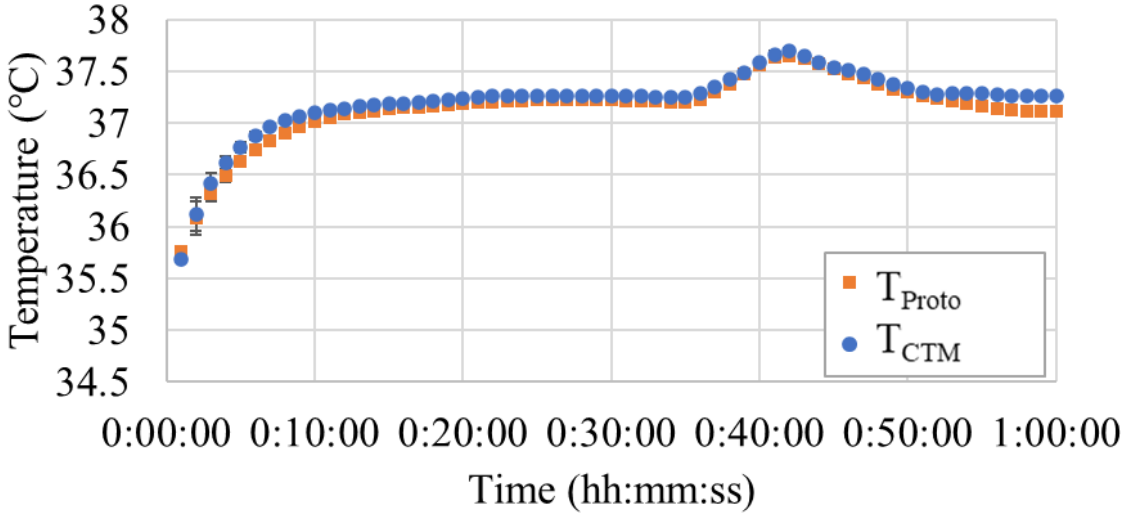
38
37.5
37
36.5
36
35.5
35
34.5
Temperature (°C)
0:00:00 0:10:00 0:20:00 0:30:00 0:40:00 0:50:00 1:00:00
Time (hh:mm:ss)
T Proto
T CTM

(b)

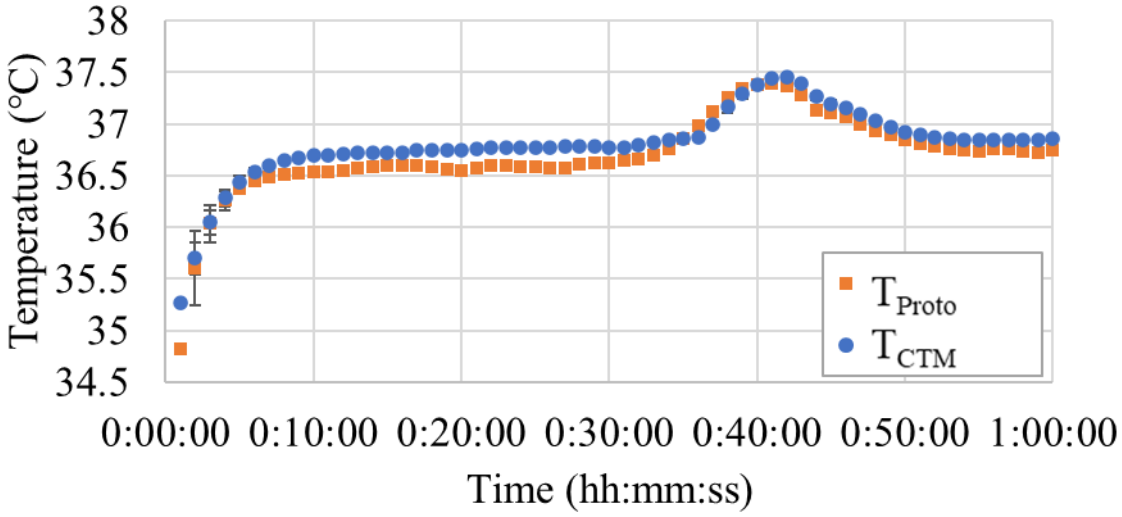
38
37.5
37
36.5
36
35.5
35
34.5
Temperature (°C)
0:00:00 0:10:00 0:20:00 0:30:00 0:40:00 0:50:00 1:00:00
Time (hh:mm:ss)
T Proto
T CTM

(c)

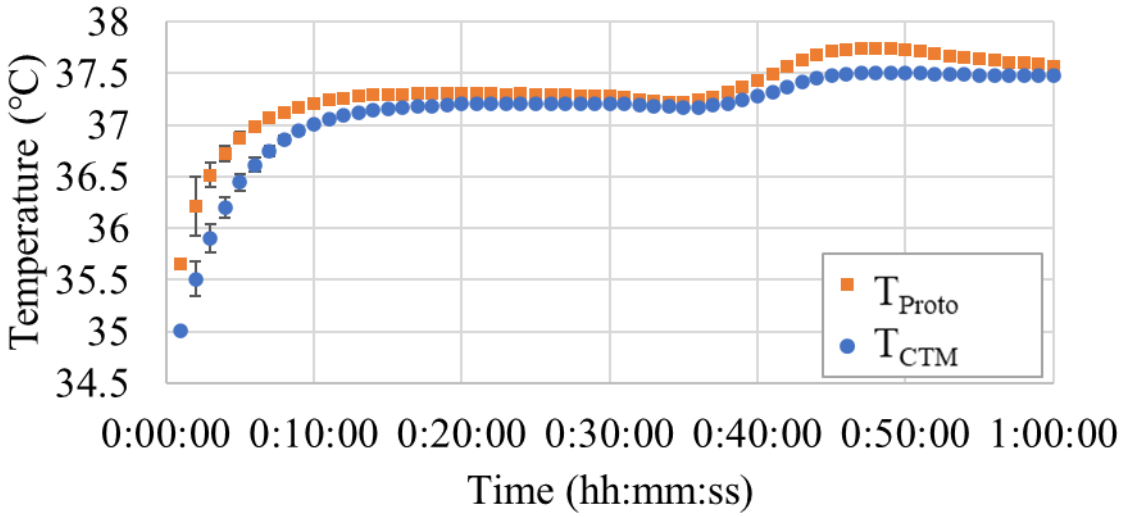

(d)

Figure 7-8 (a)~(d) Measurement results of the exercise experiment showing the core body temperature change of the four subjects (one-minute average and SD)

Cross-correlation analysis of the data from the four cases, focusing on the period of the shift in core body temperature induced by exercise load, showed a time lag in the narrow range of -1.5 minutes to 0.1 minutes with the CTM and an almost identical response.

Bland-Altman analysis of data (**Figure 7-9**) from all four subjects showed a deviation of -0.01°C and ±1.96 SD values of +0.21°C and -0.23°C, confirming the agreement between the commercial and prototype probes.

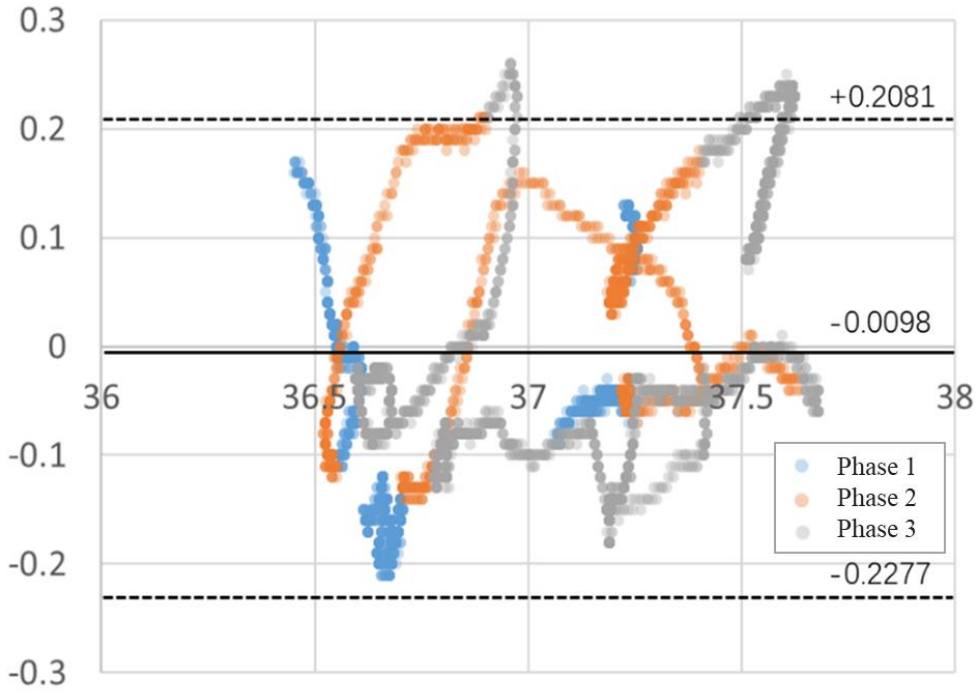

Figure 7-9 Bland-Altman Plot of the four subjects.

7.3. Simultaneous experiments with domed sauna

7.3.1. Experiment settings

The effect of changes in ambient temperature on the measurement accuracy of the prototype and commercial probes was studied in the following manner.

Referring to Sawatari et al.'s study [1], a domed sauna (KMC DOME SAUNA Professional, Kobe Medi-care Co. Ltd) was used to raise the external temperature of the subjects below the neck. Seven healthy male adults (23±2 years old) were involved in the following experiment in the supine position, wearing shorts and T-shirts with their upper abdomen exposed.

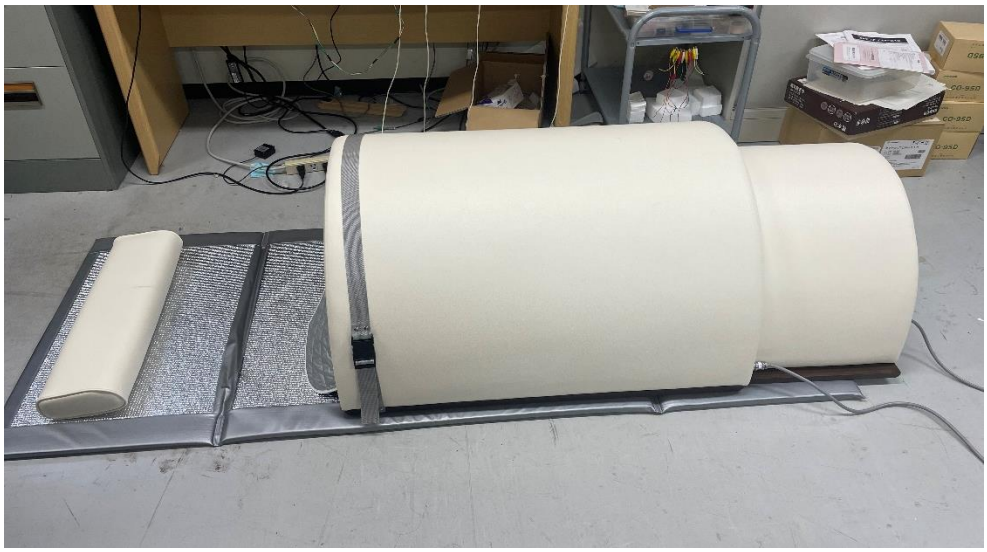

(a)

(b)

Figure 7-10 Domed sauna (a) and its controller (b)

A prototype probe and a probe of CTM-210 were placed side-by-side near the midline of the upper abdomen, and the values of T_{Proto} and T_{CTM} were sampled in the above-mentioned timing. In addition, another probe of CTM-210 was attached to the forehead area to simultaneously measure the core body temperature in the head (T_{Head}) as a reference value.

The ambient temperature Tair was measured by a digital thermometer (CENTER 376, MK Scientific, Inc) with a dedicated sensor (Precision Pt100 Probe) fixed around the abdominal probe.

Figure 7-11 Digital thermometer for air temperature measurement

As shown in the **Figure 7-12**, after each probe was secured, the subject was at rest in a supine position at room temperature (24±1°C) for 30-40 minutes (phase a). In phase b, a preheated domed sauna was placed over the subject's body to raise its perimeter temperature from the feet to the neck up to 43°C for 20 minutes. The sauna was then removed, and the surrounding temperature of the body was allowed to return to room temperature for 20 minutes (phase c).

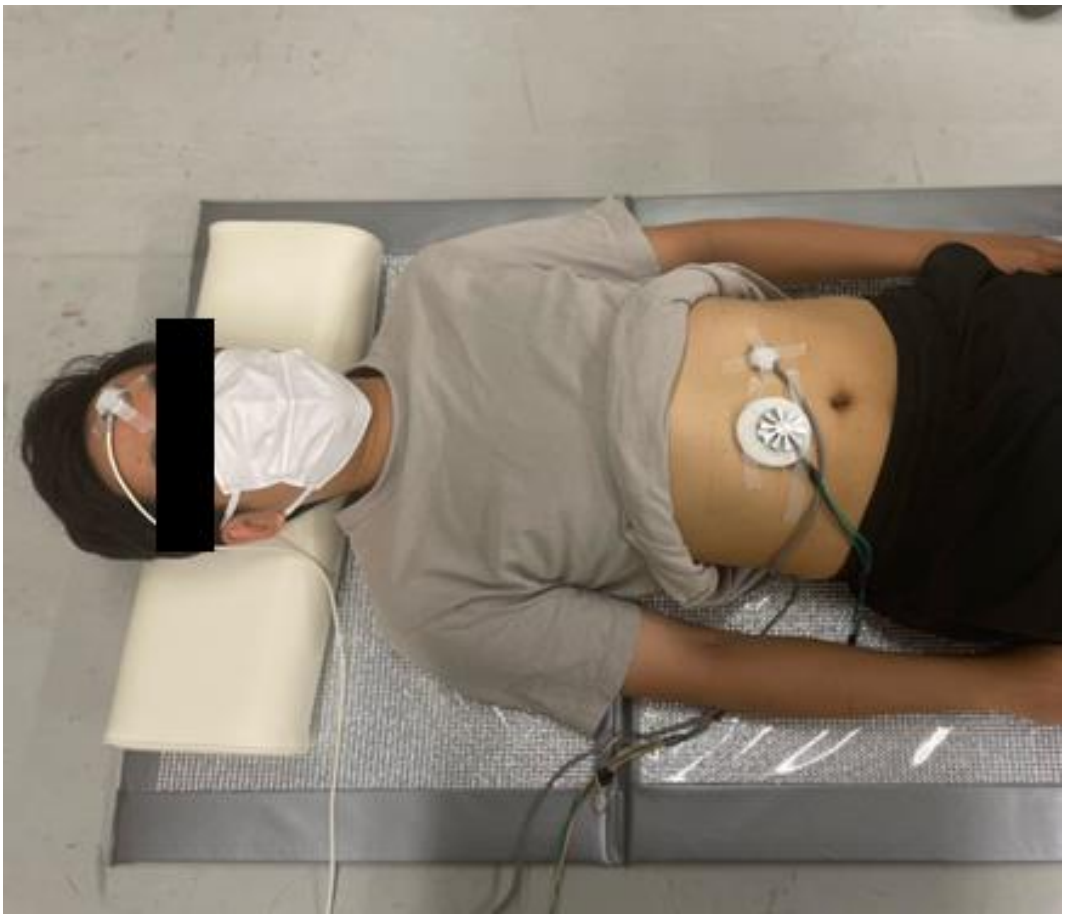

(a)

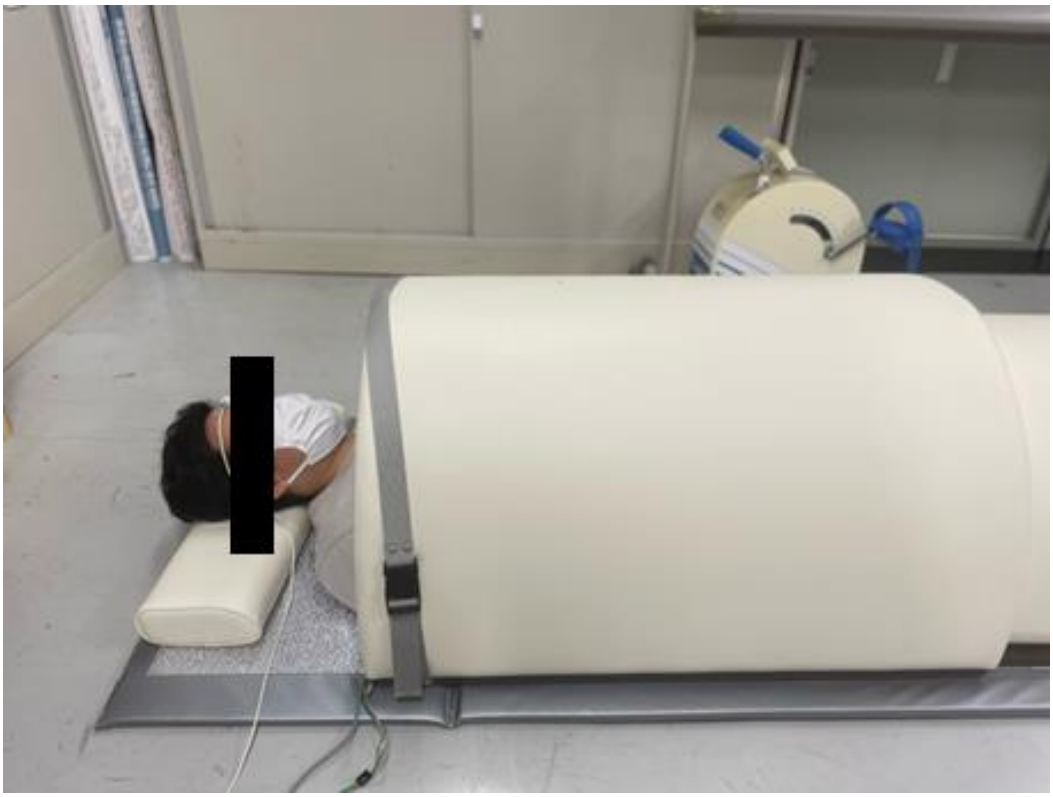

(b)

Figure 7-12 (a) Phase a and Phase c (b) Phase b

These experiments on humans were conducted with the approval of the Medical Ethics Committee of Kanazawa University (Approval number: 2020-236(087)).

7.3.2. Results

Figure 7-13 (a) to (g) show the temperature results from all seven subject. In the first phase, T_{head} tended to be greater than or equal to those measured by the two probes in the abdomen. T_{Proto} also tended to be greater than or equal to T_{CTM} in the two probes in the abdomen. In the second and third phases, T_{CTM} showed significant changes with external temperature changes; T_{Proto}, except for (b), was almost unaffected by external temperature changes.

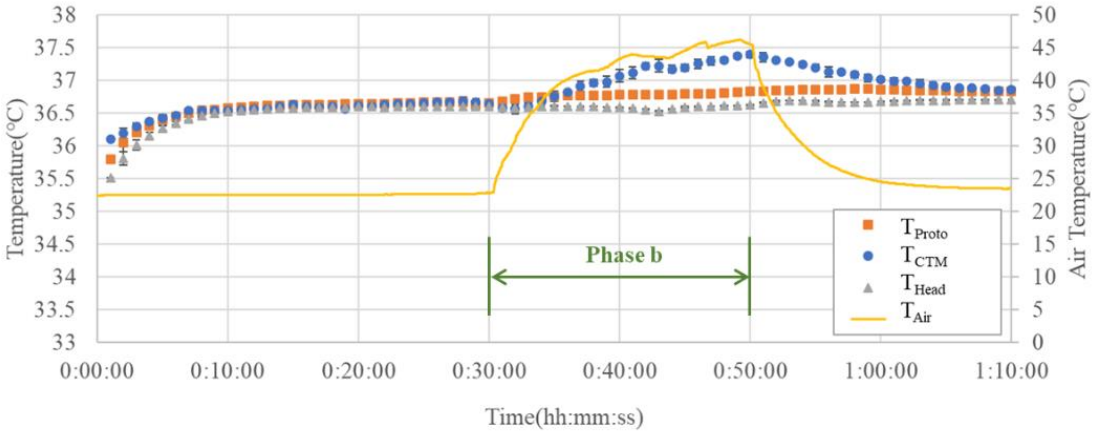

(a)

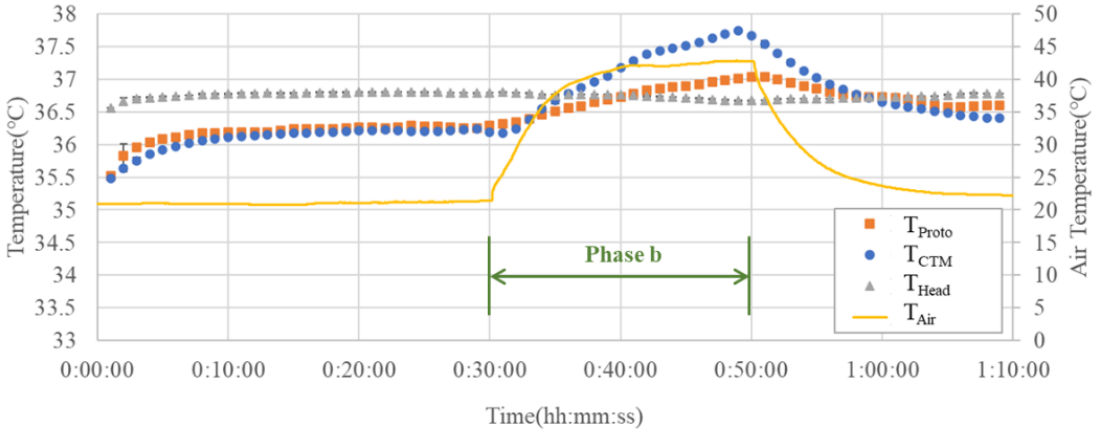

(b)

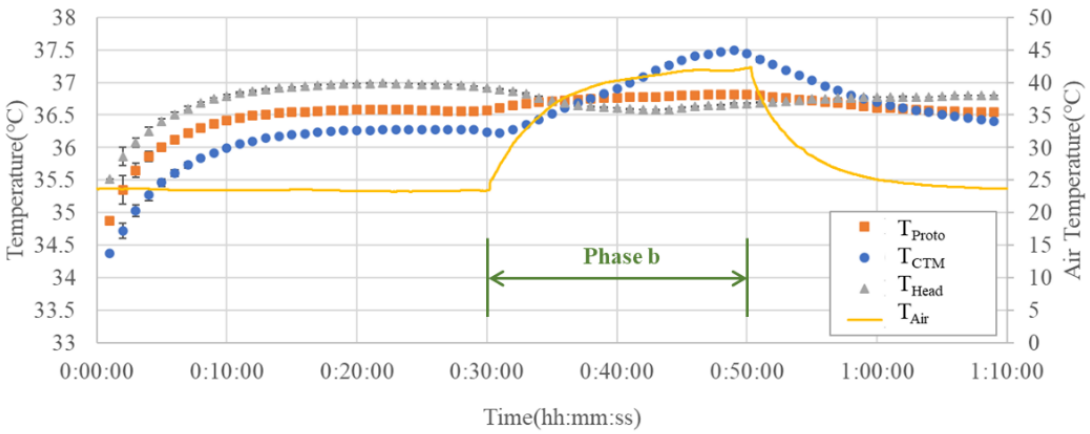
Temperature(°C)
Air Temperature(°C)
Time(hh:mm:ss)
Phase b
T Proto
T CTM
T Head
T Air

(c)

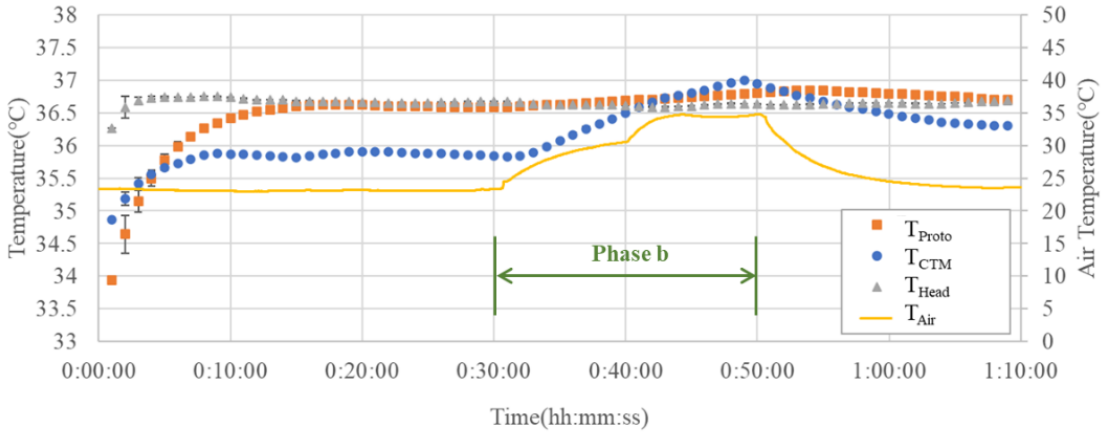
Temperature(°C)
Air Temperature(°C)
Time(hh:mm:ss)
Phase b
T Proto
T CTM
T Head
T Air

(d)

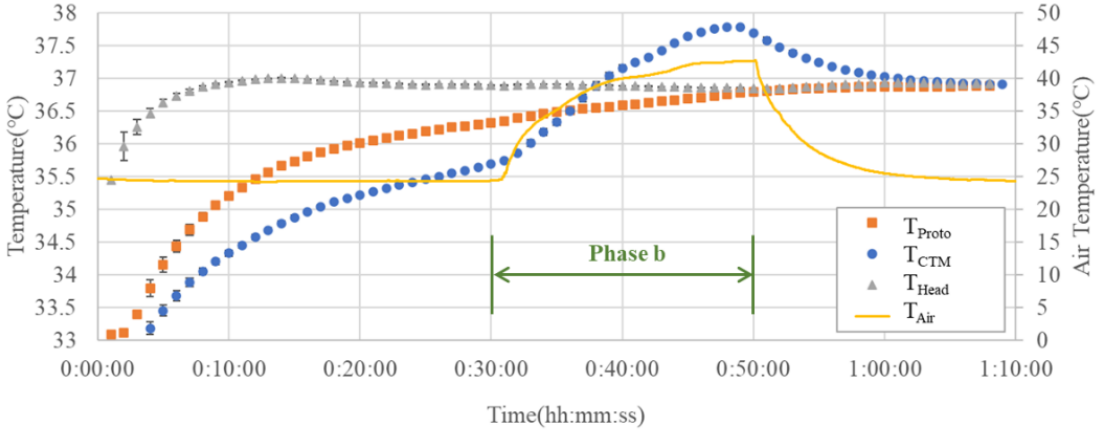
Temperature(°C)
Air Temperature(°C)
Time(hh:mm:ss)
Phase b
T Proto
T CTM
T Head
T Air

(e)

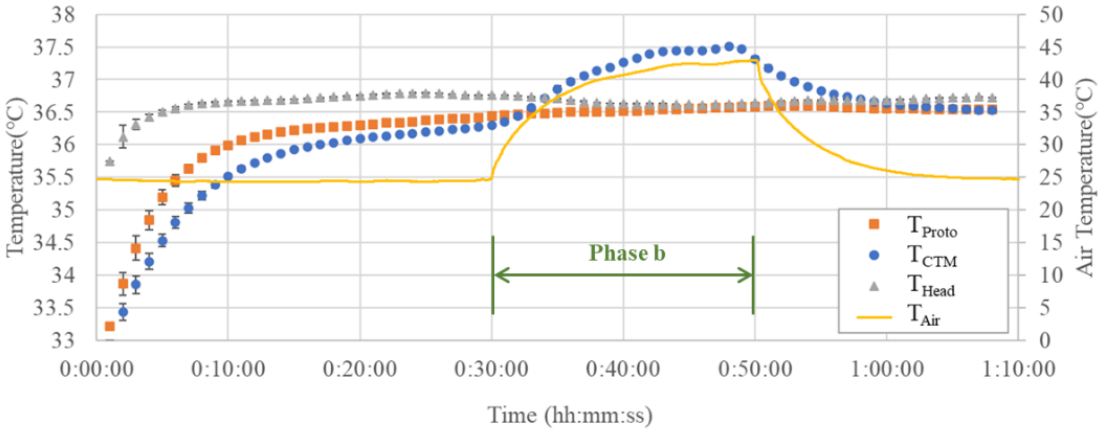

(f)

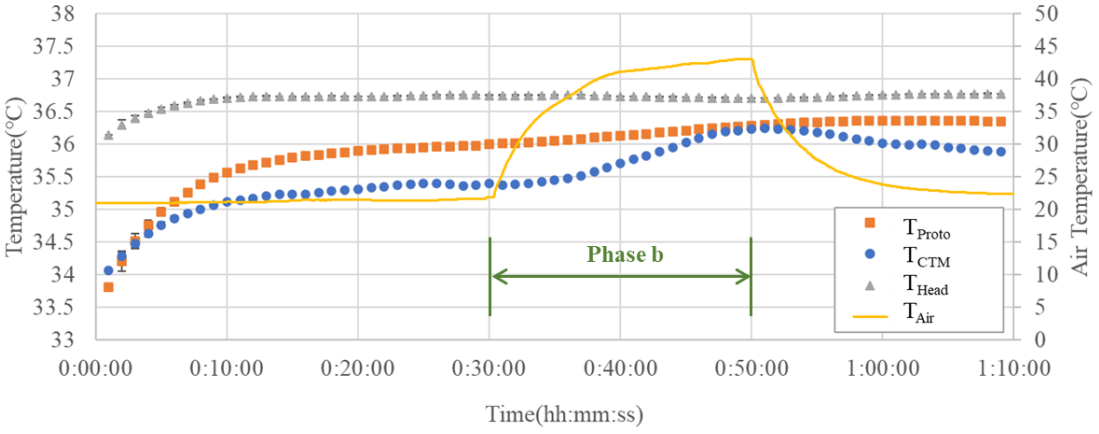

(g)

Figure 7-13. (a) ~(g)Measurement results of the sauna experiments showing the core body temperature change of seven subjects

Figure 7-14 (a) shows the mean and standard deviation error bands for each minute for all seven subjects. In Phase a, the temperature measured on the forehead T_{Head} was significantly greater than that measured on the abdomen; and the abdominal CTM210 probe T_{CTM} measured lower results than the prototype probe T_{Proto}. In Phase b, there was no significant change in T_{Head}, while T_{CTM} showed a significant increase up to 1.3°C. The results of T_{Proto} showed a minor addition but were comparable to T_{Head}. In the third phase, T_{CTM} showed a significant downward trend with air temperature, while T_{Head} and T_{Proto} showed almost no change.

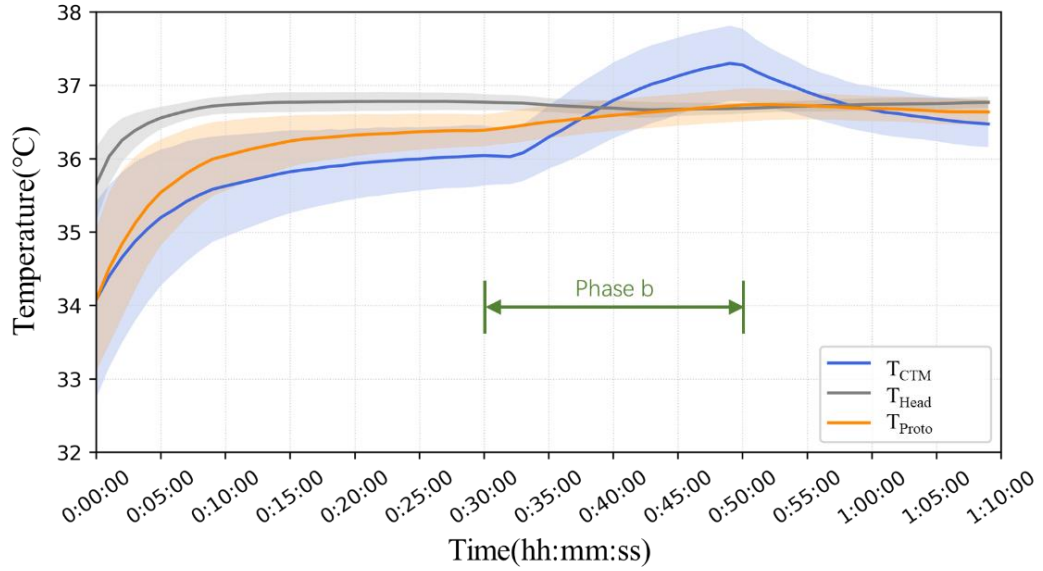

(a)

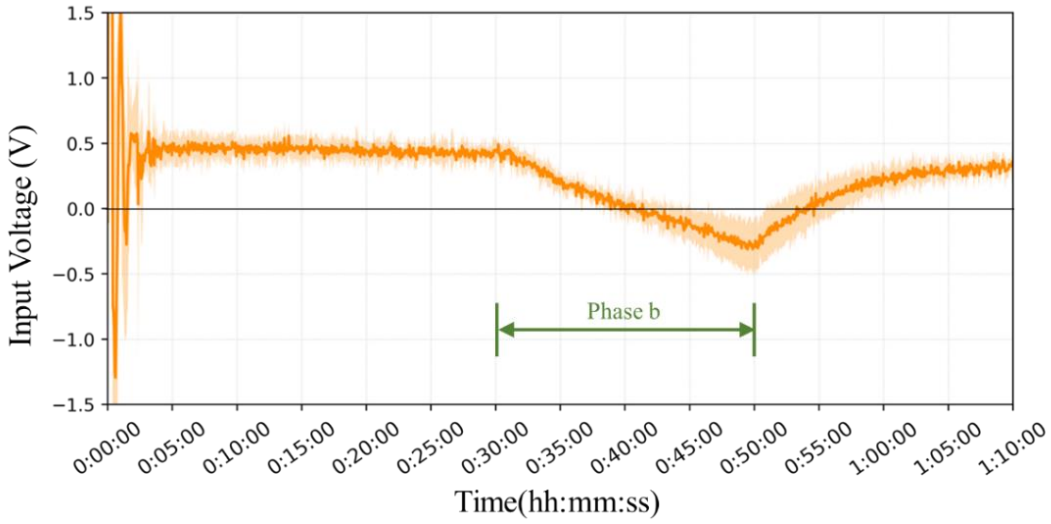

(b)

Figure 7-14. (a) The means and error bands of the measurement results of all seven subjects. (b) The average input voltage V_{input} of the Peltier module with the error band of the seven subjects

Figure 7-14(b) shows the output of the PID under the influence of temperature. It can be seen that after the initial oscillation of the PID regulation, the V_{input} stabilizes at about 0.5V and continues to heat the probe interior to maintain the internal thermal equilibrium; in the second stage, the V_{input} starts to gradually decrease and flip the current direction to start cooling the probe interior. After the external temperature returns to room temperature conditions, its current gradually shifts back to heating mode.

Reference

1. Sawatari, H.; Chishaki, A.; Miyazono, M.; Hashiguchi, N.; Maeno, Y.; Chishaki, H.; Tochihara, Y. Different Physiological and Subjective Responses to the Hyperthermia between Young and Older Adults: Basic Study for Thermal Therapy in Cardiovascular Diseases. *Journals Gerontol. - Ser. A Biol. Sci. Med. Sci.* **2014**, *70*, 912–916, doi:10.1093/gerona/glu224.

8. Discussion

8.1. FEA Experiment

The finite element analysis confirms that the probe can measure at high temperatures with the current design. The main focus was on the measurements at the end of temperature equilibration and the initial time before reaching equilibrium.

In the study of subcutaneous tissue thickness, we found that the thickness of the subcutaneous tissue at the measurement site affects the measurement results. Therefore, it is recommended to use the forehead as the measurement site because the brain under the forehead is a vital core body temperature organ whose structure hardly changes with movement. On the other hand, the solar plexus under the sternum can also be considered a measurement site. Still, the effect of motion on the contact surface of the upper abdomen with the probe needs to be considered.

Therefore, the forehead was used as the measurement site in exercise-related and subsequent human experiments. In sauna and heat therapy, the solar plexus was chosen as a safe temperature measurement site because the upper abdomen is smoother and unaffected by movement.

In addition, the simulation of the probe morphology can be further utilized for wearable improvements. Appropriate flattening and enlarging of the internal aluminum probe radius can yield better results and reach thermal equilibrium more quickly. It is worth mentioning that a balance needs to be struck between radius expansion and wearability, as too large a probe radius can lead to discomfort on the forehead and higher power consumption. In cases where high-precision measurements are required, the radius of the aluminum housing of the probe can be expanded, sacrificing some of the wearability. In contrast, a small radius probe can be used appropriately for extended use, focusing on capturing the degree of temperature change rather than measurement accuracy.

8.2. Simulator Experiment

The simulator experiments showed a significant increase in the water temperature during the second stage. The water temperature change may be because the hot air continuously heats the aluminum tray and indirectly heats the water in the narrow tank. The prototype

probe still recorded the temperature change accurately under hot strong wind.

Compared to the room temperature environment, where the temperature difference between the inside and outside of the probe is tremendous, the absolute value of Vinput is greater in the high-temperature environment. This may be due to the higher wind speed around the radiator, which brings more heat to the interior by thermal convection, and the Peltier element transmits more heat to counter the effect of thermal convection when it is operating.

8.3. Fast-changing measurement in room temperature

The prototype showed a response rate comparable to or better than that of the conventional ZHF probe to temperature changes induced by motion at room temperature, confirming the sensitivity of the measurements.

The dual heat flow method of Ming H. et al. [1]removed the heater and used changes in heat flow to monitor core body temperature. In a similar cycling exercise experiment, the time delays of its two probes (Fit and Standard type) were 0 min and 3 min, respectively, relative to the CTM-210 probe, which was also the reference. With their results of Bland-Altman analysis done with the CTM-210 probe, the mean difference was -0.07°C, - 0.07°C, and 95% confidence interval of the differences were (0.26°C, -0.40°C) and (0.12°C, -0.27°C).

In comparison, our prototype probe has a lower time delay (-1.2 min-0 min) and higher accuracy (mean difference = 0.01 °C, 95% confidence interval of the differences = (0.21 °C, -0.23 ℃) than the fit type relative to the two probes of the DHF method

8.4. Simultaneous experiments with a domed sauna

In the first phase, the results of T_{head} are often greater than or equal to those obtained from abdominal measurements (T_{Proto} and T_{CTM}). Due to the different measurement sites, the difference between abdominal temperatures and T_{head} cannot be used as an indicator of the accuracy of the measured temperature. However, it can be used as a reference value, as the change in CBT can be estimated as the change in Thead.

The results obtained with T_{Proto} are often greater than those obtained with T_{CTM}, confirming the FEA view that the thickness of the subcutaneous tissue and the thermal conductivity of the tissue influence the results, and a larger radius probe gives values closer to the deep

temperature being measured. For subjects with less body fat, there was less fat in the upper abdomen, and the viscera were closer to the probe, so the results from the abdominal probe were less different from those from the forehead (e.g., Figure 7(a)). For subjects with thicker abdominal fat, the time to reach thermal equilibrium was longer, and the temperature measured by the smaller radius probe was lower (e.g., Figure 7(e)). Thus, after reaching thermal equilibrium during the first phase of the sauna experiment, the temperature measured by the larger radius prototype probe tended to be closer to the reference forehead temperature than the smaller radius commercial probe. This result is consistent with the results of the performance analysis of the zero-heat-flux type thermometer by TOGAWA[2].

In six of the seven subjects, the T_{Proto} was virtually unaffected by changes in T_{Air} compared to the drastically changing T_{CTM}. The difference is also consistent with the results of the finite element analysis, i.e., confirming the validity of the Peltier element.

We believe that in Figure 7 (b), the deep temperature below the probe was influenced by the blood from the surrounding body surface, leading to the change of the T_{Proto}.

Therefore, due to subcutaneous tissue thickness, thermal conductivity, and the effect of subcutaneous peripheral blood, we recommend using the forehead as a site for CBT measurements in a practical sauna or sports workplace setting, as opposed to the abdominal solar plexus.

Table 8-1 shows the temperature changes in the human body under the influence of heating (water bath[3][4], sauna[4], dry sauna[5], or domed sauna[6][7]). The rate of temperature change for most of the test examples is less than 0.03, and our prototype probe results (0.02 ± 0.012℃ /min) align with the temperature change pattern in previous tests measured by the invasive method.

Table 8-1. Changes in human body temperature under high-temperature thermal load

BCT Measurement Site	Method of Heat Load	Thermal-load Temperature [℃]	Target CBT [℃]	Time of Thermal Load [min]	CBT Rise Value [℃]	CBT Rise Rate [℃/min]	Reference
Rectal	Hot water bath	40.5	38.5	60	1.50	0.025	M. A. Francisco, 2021
Esophageal	Sauna	46±3	<40	-	2.65	0.023	T. D. Gibbons et al., 2021
Esophageal	Hot water bath	40	<40	-	2.60	0.023	T. D. Gibbons et al., 2021
Rectal	Domed sauna	57.2	38.5	82.11±11.3	1.50	0.018	A. E. Mason et al., 2021
Sublingual	Dry sauna	60	-	35～45	1.00	0.022 ～0.029	J. Iiyama et al., 2008
Rectal	Domed sauna	70	-	60～90	0.6±0.2	0.007 ～0.015	H. Sawatari et al., 2014
Upper abdomen	Domed sauna	40-45	-	20	0.50±0.25	0.02±0.012	Prototype

Our PID control system design accomplishes the desired control objectives regarding input voltage variation. Using the PID system gives us more accurate temperature control with less temperature fluctuation and helps reduce power wastage due to overshoot, which helps further wearability.

In the second phase, the maximum average voltage achieved by the Peltier module in the cooled condition (0.31 V) was smaller than the maximum voltage in the water bath test (about 1.07 V). This difference may be due to the higher hot air wind speed in the simulator experiment, which is strong convection, while in the domed sauna, there is almost natural thermal convection. At higher wind speeds and larger temperature differences between the inside and outside of the probe, the V_{input} will be correspondingly larger.

8.5. Limitation

Brain temperatures differ from internal organs, but for the subject's safety, the heads were not placed in the sauna dome. The core body temperature from the forehead was recorded as a reference value. Consider using a capsule thermometer that can be referenced as

esophageal temperature.

The measurement time in a high-temperature environment is only 20 minutes due to the safety considerations of the subjects. The accuracy of measurement by humans over a longer time is not yet known.

In addition, a domed sauna mainly provides a temperature increase due to thermal radiation without the occurrence of strong convection conditions. In practical applications, if the probe is placed on the forehead and exposed to outside air, a strong convection environment may arise due to motion and other actions. This experiment initially verifies the performance in a high-temperature natural convection environment. In contrast, the performance of this device on the human body in a strong convection environment needs to be further explored.

8.6. Future work

Building on the current design, future work could focus on improving the wearability of the probe.

The current design may not be sufficient for extended measurements over 24 hours because strong winds and lower outside temperatures can cause a greater voltage to be applied to the Peltier when achieving temperature equilibrium, thereby increasing power consumption. A combination of a heater and a Peltier element will be considered to reduce the power consumption of the prototype probe. The Peltier element can maintain thermal equilibrium at high temperatures, but its conversion efficiency is lower than that of a heater at room temperature. More power can be utilized according to the Peltier element operating to cool when the ambient temperature is higher than the core body temperature and using the heater to heat the inside of the probe at room temperature.

Regarding the current design, there have been many requests to improve its fitness for measurement sites. We believe the current size is too large for a head-mounted device and has harder edges that do not fit very well to the forehead. In the simulator experiment, the current heat sink is sufficient to support heat dissipation in strong convection conditions of up to 65 degrees. Actual use may not reach such extreme environmental conditions. Therefore, we believe the size of the radiator could be appropriately reduced. In addition, it is possible to improve the edge fit and reduce the overall size of the probe appropriately by replacing it with a softer, better insulating material.

Reference

1. Huang, M.; Tamura, T.; Tang, Z.; Chen, W.; Kanaya, S. A Wearable Thermometry for Core Body Temperature Measurement and Its Experimental Verification. *IEEE J. Biomed. Heal. Informatics* **2017**, *21*, 708–714, doi:10.1109/JBHI.2016.2532933.

2. Togawa，Tatsuo; Nemoto，Toshio; Tetsu，Kobayashi An

   Experimental Analysis of Characteristics of the Deep Body Thermometer. *Japanese J. Med. Electron. Biol. Eng.* **1973**, *11*, 414–417.

3. Francisco, M.A.; Colbert, C.; Larson, E.A.; Sieck, D.C.; Halliwill, J.R.; Minson, C.T. Hemodynamics of Postexercise versus Post-Hot Water Immersion Recovery. *J. Appl. Physiol.* **2021**, *130*, 1362–1372, doi:10.1152/japplphysiol.00260.2020.

4. Gibbons, T.D.; Ainslie, P.N.; Thomas, K.N.; Wilson, L.C.; Akerman, A.P.; Donnelly, J.; Campbell, H.A.; Cotter, J.D. Influence of the Mode of Heating on Cerebral Blood Flow, Non-Invasive Intracranial Pressure and Thermal Tolerance in Humans. *J. Physiol.* **2021**, *599*, 1977–1996, doi:10.1113/JP280970.

5. Iiyama, J.; Matsushita, K.; Tanaka, N.; Kawahira, K. Effects of Single Low-Temperature Sauna Bathing in Patients with Severe Motor and Intellectual Disabilities. *Int. J. Biometeorol.* **2008**, *52*, 431–437, doi:10.1007/s00484-007-0137-0.

6. Sawatari, H.; Chishaki, A.; Miyazono, M.; Hashiguchi, N.; Maeno, Y.; Chishaki, H.; Tochihara, Y. Different Physiological and Subjective Responses to the Hyperthermia between Young and Older Adults: Basic Study for Thermal Therapy in Cardiovascular Diseases. *Journals Gerontol. - Ser. A Biol. Sci. Med. Sci.* **2014**, *70*, 912–916, doi:10.1093/gerona/glu224.

7. Mason, A.E.; Fisher, S.M.; Chowdhary, A.; Guvva, E.; Veasna, D.; Floyd, E.; Fender, S.B.; Raison, C. Feasibility and Acceptability of a Whole-Body Hyperthermia (WBH) Protocol. *Int. J. Hyperth.* **2021**, *38*, 1529–1535, doi:10.1080/02656736.2021.1991010.

9. Conclusion

In this study, we focused on improving two major problems of ZHF-type deep thermometers in complex environmental applications, the high power consumption and the inability to be used in high-temperature environments.

We found that the power consumption of the ZHF type of thermometer can be reduced by adding thermal insulation around the probe and skin through simulation experiments. Subsequently, we made probes of different sizes and shapes and verified their measurement accuracy by a rapid change test; and verified their performance in a long-term daily measurement by a long-term test.

We designed a ZHF probe that can be monitored in a high-temperature environment based on the improvement of the previous probes for use in high-temperature environments. We verified its performance through simulation experiments, simulator tests, and experiments on the human body. Experiments have shown that the prototype can accurately track rapid changes in core body temperature at room and in high-temperature environments that cannot be measured by the conventional ZHF method.

Since the improved ZHF method can be used even in high-temperature environments, it is expected to contribute to monitoring body temperature in high-temperature environments for athletes, outdoor workers, and firefighters.

ACKNOWLEDGEMENT

I would first like to thank my thesis advisor *Prof. Shinobu Tanaka* of the Institute of Science and Engineering at Kanazawa University. The door to Prof. Tanaka's office was always open whenever I encountered trouble or had questions about my research or writing. He consistently allowed this paper to be my work but steered me in the right direction whenever he thought I needed it.

Also, I would like to give special thanks to *Prof.* Tatsu*o Togawa* from the Advanced Research Center for Human Sciences, Waseda University, who put a lot of effort in the paper submission phase of this study and contributed a lot to the revision and direction of the paper.

I would also like to thank the experts who were involved in the validation survey for this research project:

- *Associate Prof. Masamichi Nogawa*, Faculty of Health Sciences, Komatsu University;
- *Associate Prof. Hisashi Naito*, Institute of Science and Engineering, Kanazawa University;
- *Prof. Tetsu Nemoto*, Institute of Medical, Pharmaceutical and Health Sciences, Kanazawa University;

The validation survey could not have been successfully conducted without their passionate participation and input.

Also, I would like to thank *Prof. Jiro Sakamoto, Prof. Shigeo Tanaka, Associate Prof. Michio Murakoshi, Associate Prof. Hisashi Naito*, as reviewers of this thesis for their comments on the thesis.

I would also like to acknowledge *Shun Aratake*, *Takeru Kato*, *Shohei Muto, Hao Shen, and Aqilah Ardini Binti Azmi,* for their valuable work on this thesis.

I would also like to thank *Ziyan Gao* for his excellent help with the Python code and research ideas for the data processing part of this study and his psychological and life support during my Ph.D.

Finally, I must express my profound gratitude to *Weiming Lu* and *Sumei Zhang* for providing unfailing support and continuous encouragement throughout my years of study and researching and writing this thesis. This accomplishment would not have been possible without them.

Thank you.

Author
Hanzi Lu